Relaxation moduli of glass-forming systems: temperature effects and fluctuations

L. Klochko, J. Baschnagel, J. Wittmer, Alexander Semenov

▶ **To cite this version:**

L. Klochko, J. Baschnagel, J. Wittmer, Alexander Semenov. Relaxation moduli of glass-forming systems: temperature effects and fluctuations. Soft Matter, In press, 10.1039/D1SM00778E . hal-03320069

HAL Id: hal-03320069
https://hal.science/hal-03320069

Submitted on 13 Aug 2021

HAL is a multi-disciplinary open access archive for the deposit and dissemination of scientific research documents, whether they are published or not. The documents may come from teaching and research institutions in France or abroad, or from public or private research centers.

L'archive ouverte pluridisciplinaire **HAL**, est destinée au dépôt et à la diffusion de documents scientifiques de niveau recherche, publiés ou non, émanant des établissements d'enseignement et de recherche français ou étrangers, des laboratoires publics ou privés.

Relaxation moduli of glass-forming systems: temperature effects and fluctuations

L.Klochko, J.Baschnagel, J.P.Wittmer, A.N.Semenov*
Institut Charles Sadron, CNRS - UPR 22, Université de Strasbourg, 23 rue du Loess, BP 84047, 67034 Strasbourg Cedex 2, France
(July 7, 2021)

Abstract

Equilibrium and dynamical properties of a two-dimensional polydisperse colloidal model system are characterized by means of molecular dynamics (MD) and Monte Carlo (MC) simulations. We employed several methods to prepare quasi-equilibrated systems: in particular, by slow cooling and tempering with MD (method SC-MD), and by tempering with MC dynamics involving swaps of particle diameters (methods Sw-MD, Sw-MC). It is revealed that the Sw-methods are much more efficient for equilibration below the glass transition temperature T_g leading to denser and more rigid systems which show much slower self-diffusion and shear-stress relaxation than their counterparts prepared with the SC-MD method. The shear-stress relaxation modulus $G(t)$ is obtained based on the classical stress-fluctuation relation. We demonstrate that the α-relaxation time τ_α obtained using a time-temperature superposition of $G(t)$ shows a super-Arrhenius behavior with the VFT temperature T_0 well below T_g. We also derive novel rigorous fluctuation relations providing isothermic and adiabatic compression relaxation moduli in the whole time range (including the short-time inertial regime) based on correlation data for thermostatted systems. It is also shown that: (i) The assumption of Gaussian statistics for stress fluctuations leads to accurate predictions of the variances of the fluctuation moduli for both shear (μ_F) and compression (η_F) at $T \gtrsim T_g$. (ii) The long-time (quasi-static) isothermic and adiabatic moduli increase on cooling faster than the affine compression modulus η_A, and this leads to a monotonic temperature dependence of η_F which is qualitatively different from $\mu_F(T)$ showing a maximum near T_g.

Typeset using REVTEX

1. Introduction

Rheological properties of complex and glass-forming fluids are largely defined by their dynamical relaxation viscoelastic moduli, namely the shear relaxation modulus $G(t)$ and the bulk compression modulus $K(t)$ [1]. The $G(t)$ memory function can be defined in terms of the transient shear stress response to a small shear deformation [2]. Similarly, $K(t)$ provides the mean pressure increment $\Delta p(t)$ at time t after a small uniform compression of the system whose volume V decreased to $V(1-\epsilon)$:

$$\Delta p(t) \simeq \epsilon K(t) \text{ for } \epsilon \ll 1$$

The shear modulus $G(t)$ of a liquid rapidly decays with t at high temperatures, but it develops a long-time plateau in the supercooled regime. [3,4] Thus, $G(t)$ can be used to characterize vitrification of a supercooled liquid and to identify its glass transition temperature T_g, as demonstrated in numerous simulation studies. [5–10] However, the relaxation compression modulus $K(t)$ of glass-forming liquids was much less investigated. [8,9,14,15] In the present paper we tried to reduce this gap.

To obtain the relaxation moduli, $G(t)$ and $K(t)$, a fluctuation-dissipation formalism relating them to stress-correlation functions is often used. [6,7,10–12] Recently, we demonstrated that the standard approach to get response functions based on correlation functions obtained with thermostatted MD simulations is insufficient in the general case and, in particular, for a precise calculation of the dynamical heat capacity. [13] The problem arises due to an imperfect temperature control in thermostatted simulations; it affects those variables (whose response we consider) that are coupled with temperature fluctuations. This problem concerns the pressure, but not the shear stress, so the fluctuation equations for $G(t)$ stay intact. By contrast, the standard scheme to obtain $K(t)$ based on the fluctuation-dissipation theorem (FDT; cf., eg., eq. 48 of ref. [14]) does not yield a proper isothermic compression modulus, but rather a mixture of isothermic and adiabatic responses.

In the present paper we develop and employ a rigorous formalism, generalizing the ideas presented in ref. [13], to calculate both isothermic ($K_T(t)$) and adiabatic ($K_A(t)$) compression moduli using the correlation functions obtained in thermostatted simulations. The theory is based on a number of novel FDT relations derived and discussed in Appendices A, B, C, D.

The main questions addressed in this paper are:

(i) What are the effects of the equilibration method (in particular, using non-local swaps of particle diameters) on dynamical and static properties of the studied two-dimensional (2D) colloidal model system?

(ii) Is it possible and how to fully characterize the linear viscoelastic response of a molecular system based on correlation functions of shear stress, pressure, energy, etc.?

(iii) What are the effects of temperature on both short- and long-time viscoelastic relaxation dynamics characterized by the isothermic and adiabatic bulk compression relaxation moduli and the shear stress response?

(iv) How do the static moduli of the 2D supercooled liquid (both for shear and compression) and their variances depend on temperature, in particular, near the glass transition?

The importance of these questions stems from the previous simulation results [9,6,5,10,13] and the ongoing theoretical discussion on the nature of solidification in amorphous materials [36,37,41–43].

The paper is organized as follows: In the next section we describe the two-dimensional Lennard-Jones polydisperse (2D pLJ) colloidal system and the computational approach to study it. The simulation results are presented and discussed in sections 3, 4, 5 and 6. In particular, the effects of the system quench/tempering method on the radial distribution function, mean-square displacement $h_0(t)$ and shear relaxation modulus $G(t)$ are discussed in sections 3 and 4, the relaxation compression moduli are considered in sect. 5, while the static moduli and their standard deviations are analyzed in sect. 6. The paper is summarized in sect. 7, and the key results are highlighted in sect. 8.

2. The model and simulation details

We consider a model colloidal system of polydisperse Lennard-Jones (pLJ) particles in two dimensions [16,17,8,9,21,22]. The particle diameters are uniformly distributed between $0.8\bar{\sigma}$ and $1.2\bar{\sigma}$ with $\bar{\sigma}$, the mean diameter. The interaction range of a pair ($l = ij$) of 2 particles i and j is defined by the Lorentz rule [24]: $\sigma_l = (\sigma_i + \sigma_j)/2$. The LJ interaction potential is

$$u_{LJ}(r, \sigma_l) = 4\epsilon \left(s^{-12} - s^{-6} \right) \tag{1}$$

where $s = r/\sigma_l$ is truncated at $s_{cut} = 2^{7/6}$ (so that $u_{LJ} = 0$ for $s > s_{cut}$) and shifted to avoid discontinuity at $s = s_{cut}$. The particles have identical mass which is set to unity (together with $\bar{\sigma}$ and ϵ) by using the LJ units.[1] The number of particles is $N = 10^4$.

We employed different approaches to quench and equilibrate the systems. In the first approach (method SC-MD) the standard molecular dynamics (MD) simulations with periodic boundary conditions were performed as implemented in the LAMMPS code [25] (velocity-Verlet algorithm with MD time-step $t_{MD} = 0.005$). The system was first tempered at the initial temperature $T = 1$ (where the system is well in the liquid regime with short α-relaxation time $\tau_\alpha \lesssim 1$) to prepare $m = 100$ independent well-equilibrated configurations. The Nosé-Hoover (NH) thermostat and barostat were used to impose the desired temperature and the external pressure $p_0 = 2$. The obtained configurations were then slowly cooled with rate $\Gamma \equiv -\mathrm{d}T/\mathrm{d}t = 10^{-5}$ keeping the same pressure and allowing the system volume to fluctuate. This way we produced m initial configurations at ~ 30 specific working temperatures. At each working temperature the system was tempered at constant pressure ($p_0 = 2$) over a time $\Delta t_{max} = 10^5$ (in LJ units). At $t = \Delta t_{max}$ the instantaneous volume $V(t)$ was fixed and the system was further tempered in the canonical NVT ensemble over the same time Δt_{max}. Starting from the final configuration of this NVT tempering we performed NVT production runs over a 'sampling time' of $\Delta t = 10^5$.

---

[1] Here and below we use LJ units by considering ϵ, $\bar{\sigma}$ and particle mass m_p as physical units. The LJ unit of time is therefore $\tau_{LJ} = \bar{\sigma}\sqrt{m_p/\epsilon}$.

An alternative way to equilibrate the quenched configurations is to perform tempering via a hybrid MC/MD approach (method Sw-MD). The MC part comprises a combination of local moves (local displacements of single particles) and particle swaps (exchanging the diameters of two randomly chosen particles) [23]. In addition, we allow for volume fluctuations of the system controlled by an MC barostat [39] to impose the constant pressure $p_0 = 2$. Local moves, particle swaps and volume fluctuations are accepted according to the Metropolis criterion to ensure detailed balance [39]. Time in these MC simulations is measured in units of MC steps (MCS) where we define an MC step as an attempt to displace randomly each particle by a local move [9]. [2] An ensemble of m independent configurations ($m = 100$ for $0.2 \leq T \leq 0.3$, $m = 50$ for $T > 0.3$, and $m = 20$ for $T < 0.2$) was tempered over $\Delta t_{\max} = 10^7$ MCS (local, swap and volume moves) at constant pressure. At $t = \Delta t_{\max}$ the instantaneous volume $V(t)$ was fixed and the system further equilibrated over 10^7 MCS (local and swap moves) at constant volume, and then over the same time again with local moves only. As discussed in [17], this MC approach is successful in equilibrating the pLJ system at much lower temperatures than the MD tempering discussed above. Equilibration is achieved down to $T_{\mathrm{f}} = 0.16$ ($< T_{\mathrm{g}} \approx 0.26$) below which fractionation of particles of different sizes occurs. The final configurations of the MC simulations for $T \geq T_{\mathrm{f}}$ were further tempered with MD Nosé-Hoover dynamics to equilibrate the velocities: first, at constant pressure $p_0 = 2$ over a time of $2 \cdot 10^5$ (in LJ units) and then over the same time at constant V equal to the volume of the final configuration of the preceding NPT run.

After tempering by either method SC-MD or Sw-MD all production runs are then done with MD at $V = \mathrm{const}$. The instantaneous energy, pressure, shear stress (averaged over the system volume) and other parameters were recorded during the sampling time $\Delta t = 10^5$ (LJ units) with time spacing of $\delta t = 0.05$ or smaller between successive data entries. In addition, we also used 2 similar approaches (SC-MC and Sw-MC) where the standard MC dynamics (with local moves only) was used instead of MD for ultimate tempering and production runs.

3. The RDF, structure factor and MSD

The system volumes $V(T)$ have been recorded for the configurations prepared by 3 quench methods (Sw-MC, SC-MC and SC-MD) at all temperatures; the corresponding densities $\rho = N/V$ are shown in Fig. 1. The SC-MC and SC-MD results are almost identical. Moreover, at high temperatures the densities for all the 3 cases coincide. However, the Sw-MC curve parts from the SC-curves at low temperatures. The $\rho(T)$ curves for the SC-systems thus reveal two distinct linear slopes, while $\rho(T)$ for the Sw-MC case does not show any slope change except for very low temperatures $T \lesssim 0.16$. All the linear branches of $\rho(T)$ intersect at roughly

[2] A particle displacement vector $\delta \underline{r}$ for a local move is chosen randomly within a disk $\delta r < \delta r_{max}$ with $\delta r_{max} = 0.1$. For a swap move we attempt to cycle $N/2$ randomly chosen pairs of particles.

the same point defining the dilatometric glass-transition temperature $T_g \approx 0.26$. [3] The obtained T_g is in agreement with that estimated previously [9,17].

The radial distribution (Kirkwood) functions (RDFs) $g(r)$ for configurations equilibrated using particle swaps (method Sw-MD) at different T's are shown as black curves in Fig. 2. The $g(r)$ functions reveal decaying oscillations whose period is roughly equal to the mean particle diameter. The obtained RDFs also show a rather weak T-dependence. These features point to a liquid-like amorphous structure both above and below T_g (for $T \geq T_f \approx 0.16$). Fig. 2 also includes the $g(r)$ data for configurations obtained by slow cooling with the realistic MD (method SC-MD). A similar comparison was performed in ref. [16] for $T \geq 0.24$. The data reveal no dependence of this static property on the equilibration/tempering method (SC-MD or Sw-MD, cf. sect. 2) for $T > 0.16$ (within the statistical error). This feature is non-trivial since the SC- and Sw-equilibrated systems have different densities at $T < T_g \approx 0.26$, so we can conclude that $g(r)$ is much less sensitive to the equilibration method than the density.

At $T = 0.16$ a tiny deviation (between the $g(r)$ results obtained with the two methods) can be observed near the extrema. By contrast, the deviation is rather considerable at $T = 0.15$. The RDFs for swap-tempered configurations (method Sw-MD) start to show the secondary incommensurate oscillation mode, which apparently signals the onset of a fractionation (phase separation) at $T < 0.16$. By comparison, no signs of fractionation are observed down to $T = 0.15$ for configurations prepared by method SC-MD, which means that particle demixing is a very slow (interdiffusion) process inaccessible on the time-scales furnished by the SC-MD tempering protocol. On the other hand, with the Sw-MD equilibration method the (artificial) particle exchanges of the swap algorithm circumvent the physical dynamics, thereby revealing the tendency of the studied system to fractionation/crystallization at $T \ll T_g$.

Qualitatively, the presence of a structural transition at $T \approx T_f$ is also evident in Fig. 3 showing snapshots of configurations obtained from method Sw-MD. The snapshots illustrate that the system becomes phase-separated below $T_f \approx 0.16$. Moreover, even for $T_f \leq T \lesssim 0.2$ the structure gradually gets locally heterogeneous on cooling due to the formation of small clusters of particles of similar size. Note that the clustering effect is enhanced due to preparation with swap moves (as compared with the standard slow cooling preparation protocols). The enhancement is moderate at $T > 0.17$, but becomes more dramatic at low temperatures $T \lesssim T_f \approx 0.16$. However, all the systems (both SC- and Sw-based) remain homogeneous and isotropic at $T > T_f$ on scales beyond the cluster size ($\lesssim 4\bar{\sigma}$). These qualitative observations suggest that a quantitative analysis of the ordering tendency, e.g. via the local bond order parameters [18–20], would be rewarding.

The structure factor $S(q)$ of the system, where q is the wavenumber ($q = \left|\underline{q}\right|$), is shown in Fig. 4 for a wide range of temperatures ($0.16 \leq T \leq 0.5$ in part (a), $0.15 \leq T \leq 1$ in part (b)). All data refer to the hybrid MC/MD equilibration (method Sw-MD). The main peak of $S(q)$ is located at $q = q_{max} \approx 6.3$ corresponding to the mean particle size; its height somewhat increases at low T together with the

---

[3] Thus obtained T_g depends on the total time ($\sim \Delta t_{max} = 10^5$) the system spent at a given T during NPT cooling and tempering.

amplitudes of the secondary minima and maxima at higher q's. This T-dependence of $S(q)$ for $q \gtrsim q_{max}$ reflects a short-range packing in neighbor shells around a particle, which becomes tighter on cooling. Interestingly, the zero-q limit of $S(q)$, $S_0 \equiv \lim_{q\to 0} S(q)$, first slightly decreases on cooling down to T_g, but then increases significantly below T_g. Moreover, $S(q)$ shows a dip at $q_{dip} \sim 3$ corresponding to about 2 particle diameters ($2\pi/q_{dip} \sim 2$). The dip gets more pronounced at low temperatures. It can be explained by local clustering of similar particles which is visible in the snapshots of Fig. 3 at $T \geq T_f$. [4] The increase of S_0 on cooling towards T_f is apparently due to the same clustering effect (a tendency for demixing of larger and smaller particles) which may be considered as a precursor of fractionation and/or crystallization. Note an additional secondary peak (see arrows in Fig. 4b) that appears to the right of the maximum for temperatures below T_f. This peak is consistent with the secondary oscillation feature in the RDF at $T = 0.15$ (cf. Fig. 2). Possibly it originates from sufficiently large clusters of smaller particles.

The mean-square particle displacement (MSD) as a function of time, $h_0(t)$, is shown in Fig. 5. Here again we compare the results obtained from the (initial) configurations prepared using particle swaps (method Sw-MD) and slow MD cooling (method SC-MD). It is clear that for $T > T_g \approx 0.26$ the particle dynamics is independent of the tempering procedure. Besides, it is obvious that for liquid systems ($T > T_g$) the MSD always enters the purely diffusive regime, $h_0(t) \simeq 4D_s t$, at long enough times $t \gg \tau_d$. Here $D_s = D_s(T)$ is the (mean) self-diffusion constant and $\tau_d = \tau_d(T)$ is defined by the condition $D_s\tau_d \sim \bar{\sigma}^2 = 1$ (it is expected that $\tau_d \lesssim \tau_\alpha$ in the supercooled regime since a full structural relaxation associated with τ_α could hardly be achieved before the particles move on their own size). By contrast, below the glass transition, $T < T_g$, the linear Fickian diffusion regime is not accessible. In this low-T range the MSD develops a transient plateau which sets in at $t \sim 1$. Furthermore, at $T \lesssim T_g$ the long-time MSD for the MD-tempered configurations (method SC-MD) gets significantly larger than that for the configurations equilibrated with the Sw-MD method. The latter feature suggests that the particle self-diffusion for $T < T_g$ is much faster for less equilibrated (and, therefore, less dense, cf. Fig. 1 and ref. [17]) configurations obtained by method SC-MD.

These results can be explained in the following way: First, we note that the Sw-MD approach involving particle swaps is much more efficient for equilibration than just MD tempering (method SC-MD), so that an arguably full equilibrium is achieved with the Sw-MD approach in the studied T-range [17,23]. By contrast, only partial equilibration can be achieved by MD tempering (method SC-MD) at $T \lesssim T_g$. Therefore, in 'cooled' systems some structural order parameters may remain closer to their higher-temperature levels, and this out-of-equilibrium effect (leading, in particular, to a lower mean density) may result in faster local

---

[4] A similar, but less significant dip was observed for a 3D glass-forming system [10] (unpublished result). Moreover, a dip in $S(q)$ for $0 < q < q_{\max}$ is not uncommon in binary mixtures, the simplest representative of multicomponent systems. For binary mixtures the dip can be understood by decomposing $S(q)$ into its contributions stemming from the partial static structure factors of like and unlike particles (see e.g. [40]).

rearrangements of particles and their higher D_s. As the Sw-MD approach allows to equilibrate the system also below $T_g \approx 0.26$, the differences between the MSD for two methods (SC-MD and Sw-MD) at $T \leq 0.26$, illustrated in Fig. 5, reflect the degree of deviation from equilibrium for the configurations obtained by standard MD tempering (method SC-MD).

All in all, the results discussed above show that the system remains macroscopically homogeneous and amorphous also below $T_g \approx 0.26$, so long as $T > T_f \approx 0.16$. Only for $T < T_f$ does demixing, possibly followed by crystallization [17], occur at the scale of the system size. An analysis of the dynamics in terms of the shear relaxation and bulk relaxation moduli is carried out in the next sections. The definitions of these moduli are based on the assumption of spatially isotropic and homogeneous systems. This is pertinent in the regime $T > T_f$, which is the focus of the following analysis.

4. Shear relaxation modulus

The shear-stress relaxation modulus $G(t)$ defines the mean shear stress at time t, $\sigma(t)$, generated by a small step γ_0 of the shear strain at $t = 0$:

$$G(t) = \lim_{\gamma_0 \to 0} \sigma(t)/\gamma_0$$

The response function $G(t)$ can be obtained using the stress-fluctuation equation [5,9,10]:

$$G(t) = \frac{T}{\rho}\left[C_\sigma(t) - C_\sigma(0)\right] + \mu_A \tag{2}$$

where $\rho = N/V$ is the mean concentration of particles,

$$C_\sigma(t) = \frac{N}{T^2}\left\langle \delta\sigma(t+t')\delta\sigma(t')\right\rangle \tag{3}$$

$\delta\sigma(t) = \sigma(t) - \langle\sigma\rangle$, $\sigma(t) = \sigma_{xy}(t)$ is the shear stress (xy-component of the stress tensor), $\langle ... \rangle$ in eq. (3) mean averaging over the ensemble of m independent configurations and the gliding averaging over t', and $\langle\sigma\rangle$ is the ensemble- and time-averaged stress. Note that $\langle\sigma\rangle$ typically vanishes in the liquid regime. Eq. (2) is applicable to well-tempered/equilibrated systems that do not show any aging effects up to the longest sampling time Δt [10], which is the case for our systems (prepared with either SC- or Sw-methods described in sect. 2).

In eq. (2) $\mu_A = G(0)$ is the affine shear modulus [9,10] defining the instant response of shear stress after a small shear deformation. It is defined by both ensemble- and time-averagings of the instantaneous shear modulus $\mu_A(t)$ calculated using eq. (1) of ref. [10], $\mu_A = \langle\mu_A(t)\rangle$. Thus defined μ_A slightly depends on the orientation of the coordinate frame (i.e., of the shear direction) [10]; the affine modulus for the natural coordinate frame (with x,y axes along the sides of the simulation box) is denoted here as μ_A^0. To improve its precision we pre-averaged μ_A with respect to all orientations of the coordinate frame. [5] This is equivalent

[5] This idea was proposed in ref. [10] where it was shown that such preaveraging leads to a significant reduction of the standard deviation of μ_A.

to averaging over all orientations $\underline{n}$ of the bond vector $\underline{r}_l$ connecting a pair of interacting particles, leading to the following instantaneous modulus [10,5] [6]

$$\mu_A^{\rm or}(t) = \rho T + \frac{1}{V}\frac{1}{d(d+2)}\sum_l \Big[s^2 u''(s) + (d+1)s u'(s)\Big]_{s=s_l} \qquad (4)$$

The corresponding average affine modulus is $\mu_A^{\rm or} \equiv \langle \mu_A^{\rm or}(t)\rangle$. Here $d=2$ is the space dimension, l is a pair of interacting particles, r_l is the distance between their centers, σ_l is their interaction range, $s_l = r_l/\sigma_l$, $u(s)$ is the interaction potential defined in the r.h.s. of eq. (1), u' and u'' are its first and second derivatives with respect to s, $s < s_{cut}$. [7] An additional preaveraging over the equilibrium (Maxwellian) distribution of particle velocities is also implied here. Further technical details concerning calculation of μ_A are delegated to Appendix E.

Comparison of μ_A^0 (or μ_A for any fixed coordinate frame) with μ_A^{or} drives us to conclude that the system is macroscopically isotropic: the deviation $|\mu_A^0 - \mu_A^{or}|$ is random and small, it amounts to about 0.001% above T_g, while well below T_g it increases to just $\sim 0.1\%$ (essentially due to an insufficient, i.e. effectively more poor, statistics in the glassy regime).

The temperature dependence of μ_A for the 'swapped' configurations (method Sw-MD) is shown in Fig. 6(a) (black curve). [8] The function $\mu_A(T)$ is almost linear, apart from the low-T region, $T < 0.16$, where a weak but well-resolved deviation from the linear behavior is observed. Such deviation points to a structural change which we tend to associate with fractionation of particles at $T < T_f = 0.16$. By contrast $\mu_A(T)$ does not show any anomaly in the vicinity of the glass transition, $T \approx T_g$. This feature emphasizes once again the apparently dynamical nature of vitrification: the static properties like density $\rho = N/V$, or μ_A, or $g(r)$ do not change at the glass transition provided that the system is well-equilibrated both above and below T_g. The latter condition is satisfied for the 'swapped' configurations, but not for the 'cooled' configurations. As a result, the equilibrium properties (like ρ or μ_A) of 'cooled' systems (prepared with method SC-MD) show a cusp at $T \approx T_g$ (cf. red curve in Fig. 6(a)).

Above T_g the shear modulus $G(t)$ vanishes at long time (the static modulus $G(\infty) = 0$), and the same is true for the shear stress correlations, $C_\sigma(\infty) = 0$. Hence, by virtue of eq. (2)

---

[6] Note that the general fluctuation-dissipation relation for $G(t)$, eq. (2), involves $\mu_A = G(0)$ which can be calculated by time-averaging of eq. (4). This equation is based on the classical definition of μ_A as a linear coefficient between the shear stress increment generated instantly by a small shear strain and the magnitude of the latter. It comes from and agrees with the well-established theoretical framework [14,37,54].

[7] It would be better to use a smooth interaction potential with continuous $u'(s)$. [38] In the present study, however, we used eq. (1) for consistency and better comparison with the previous results on the same system.

[8] In fact this curve shows $\mu_A = \mu_A^{\rm or*}$ calculated using the procedure to eliminate the effect of mean pressure variations between the configurations as described in Appendix F.

$$\mu_A = \mu_0 \equiv \frac{T}{\rho} C_\sigma(0), \quad T > T_g \tag{5}$$

Note that eqs. (2), (5) lead to a simple well-known relation [5,11,24]

$$G(t) = \frac{T}{\rho} C_\sigma(t), \;\; T > T_g \tag{6}$$

The relation, eq. (5), is verified in Fig. 6(b), which shows, in addition, that for the swap-equilibrated systems $\mu_A \approx \mu_0$ not only in the liquid regime, but also in a temperature range, $T_g > T > T_f$, below the glass transition. Noteworthily, however, the scattering of the μ_0 data obtained in the glassy regime, $T_f < T \lesssim T_g$, with production runs involving realistic local MC moves only (cf. open circles in Fig. 6(b)) is much stronger than that for μ_A. Besides, the data scattering for μ_0 obtained with local MC moves is much stronger than the one obtained for MC dynamics involving also swap moves (cf. filled circles in Fig. 6(b)).

The time-dependent shear moduli $G(t)$ for 'swapped' configurations (prepared with method Sw-MD) are shown in Fig. 7. At all temperatures one can observe two relaxation stages: a fast process (presumably related to particles collisions and vibrations) with characteristic time $\tau_f \sim 0.1$, and a much slower structural relaxation process with terminal time $\tau_\alpha \gtrsim 1$. The gap between the two times strongly increases on cooling leading to the emergence of an intermediate shoulder gradually turning into a glassy plateau at $T \lesssim 0.2$. Qualitatively the same T dependence of $G(t)$ was also observed in other simulations of glass-forming 2D systems [41,46–48]. The plateau corresponds to the quasi-static elastic shear modulus $\mu \approx \mu_{sf}$ of the glassy system (cf. sect. 6.1), which increases at low T.

Interestingly, $G(t)$ also develops short-time oscillations for $T < T_g \approx 0.26$ leading to short-time minima at $T \leq 0.24$. This feature is an inertial effect since in overdamped systems (without inertia) $G(t)$ must be equal to a sum of decaying exponentials with positive amplitudes (generalized Maxwell model) [1], hence $G(t)$ must monotonically decay together with all its time-derivatives. This interpretation is also supported by the MC results for $G(t)$ (obtained with local MC moves only during production runs) which are exempt of inertial effects by construction and decrease monotonically with increasing t (cf. Fig. 11). Apparently, the oscillation features are due to short-time particle vibrations with frequency $\omega_v \sim 20$rad/s (this frequency corresponds to the period $2\pi/\omega_v \sim 0.3$ which can be read off from the $G(t)$ curves).

The shear relaxation curves for the systems prepared with particle swapping (Sw-MD) and continuous MD cooling (SC-MD) protocols are shown in Fig. 8. The results are qualitatively similar to those for the MSD (cf. Fig. 5). One can observe almost no difference between $G(t)$ for the two types of systems above T_g. By contrast, as T decreases below the glass transition (at $T \leq T_g$) the Sw-MD based relaxations get increasingly slower than those for the SC-MD systems. The difference becomes really dramatic at $T \leq 0.21$: while $G(t)$ for Sw-MD based configurations develops a long-time plateau, the SC-MD systems show only a transient shoulder. In other words, well below T_g the 'swapped' systems (prepared with method Sw-MD) show a persistent long-time elasticity, in contrast to 'cooled' systems (method SC-MD) which exhibit a creep-like complex-fluid behavior.

The two types of viscoelastic response of the two systems are apparently due to a wide spectrum of relaxation times which spans over almost the whole run-time

window (from 1 to 10^5 LJ time-units) in the 'cooled' case (SC-MD), but is mostly outside this time-window (shifted to longer times) in the 'swapped' case (Sw-MD).

We suggest the following criterion to get the structural relaxation time τ_α based on a relaxation function like $G(t)$:

$$-\partial \ln G(t)/\partial \ln t = 1 \quad \text{at} \quad t = \tau_\alpha \tag{7}$$

where one should seek for the longest t satisfying the equation above. Indeed, with single exponential $G(t) = \text{const} \exp(-t/\tau)$ one gets $\tau_\alpha = \tau$ using eq. (7), while for multi-exponential function with well-separated relaxation times the above operational criterion gives the time of the slowest mode. Clearly, the criterion for τ_α based on eq. (7) (with any constant in the r.h.s.) is in harmony with (and comes from) the time-temperature superposition (TTS) principle. Indeed, this principle says that relaxation functions at different T's can be superimposed by shifting them both vertically and horizontally in log-log plots. This means that the points (on $G(t)$ curves at two T's) with the same log-derivative $\partial \ln G(t)/\partial \ln t$ must correspond to the same t/τ_α. To further support this idea we attempted a direct TTS of $G(t)$ functions. The result shown in Fig. 9 reveal a reasonable collapse of $G(t)$ curves onto a master curve.

The T-dependence of τ_α obtained using the criterion of eq. (7) is shown in Fig. 10. The relaxation times τ_α for different tempering methods (SC-MD and Sw-MD) coincide for $T > T_g$, however τ_α for the 'swapped' systems (method Sw-MD) gets longer (than for configurations prepared with method SC-MD) for $T \leq T_g$. The $\tau_\alpha(T)$ dependence for 'swapped' configurations is fitted with the Vogel-Fulcher-Tammann (VFT) law

$$\tau_\alpha = \tau_0 \exp(E_0/(T - T_0)) \tag{8}$$

with $E_0 = 1.21$, $T_0 = 0.162$. Note that the fitted T_0 is remarkably close to the fractionation temperature $T_f \approx 0.16$. This fit suggests that the activation energy E_a for the structural relaxation is increasing on cooling in a super-Arrhenius fashion:

$$E_a = E_0 T/(T - T_0) \tag{9}$$

Starting from similar configurations equilibrated with the tempering method Sw-MC involving particle swaps, $G(t)$ was also obtained via eq. (2) based on production runs with pure MC dynamics using local moves only [17]. The MD results (cf. Fig. 7) are compared with the MC data (cf. Fig. 13 of ref. [17]) in Fig. 11. In order to superimpose the MD and MC curves the MC time was rescaled: 1 LJ time unit was identified with k MCS. Obviously, the data cannot overlap in the short-time regime where the stochastic MC dynamics cannot replicate the deterministic MD dynamics (accounting for the inertial effects), so we used the long-time behavior to determine the shift factor $k(T)$. Noteworthily, for the three-dimensional Kob–Andersen mixture it has been shown in ref. [49] that MC with local moves and (microcanonical) MD yield identical long-time behavior for the average dynamics (incoherent scattering function, MSD) and dynamic fluctuations (four-point susceptibility) upon rescaling the time axis so as to optimize the overlap in the late-time regime. Here we make a similar observation: A reasonable superposition of MC and MD curves for $G(t)$ is obtained over a broad range of temperatures at times t outside the inertial regime, for $t > \tau_{\min}$, where $\tau_{\min}$

somewhat increases at low T ($\tau_{\min} \sim 0.3$ for $T \geq 0.3$ roughly corresponds to the period of short-time oscillations; $\tau_{\min} \sim 3$ for $T \leq 0.24$, with time in LJ units). The agreement is very good for $T \geq 0.3$, above the glass transition, but it is less perfect in the vicinity of T_g. Moreover, it turns out that the time-scaling factor $k = k(T)$ depends on temperature, for example $k(0.3) \sim 600$, $k(0.24) \sim 300$.

Discussion:

MC vs. MD production runs. An imperfect superposition of MD and MC relaxation curves at low temperatures may be due to stronger variations of $G(t)$ between individual members of the ensemble (with $m = 100$ systems) at $T < 0.3$. Future more precise simulations on larger ensembles may help to better characterize the origin of these deviations. We also believe that there is a more general reason for small deviations between MD and MC relaxation curves: the two dynamics are not entirely equivalent even for long time-scales. Indeed, the true MD transition rates (between the inherent states) are generally different from the MC rates (even with time-rescaling) due to different dependencies of these rates on the potential energy barrier width. While this effect leads to some difference between MD and MC relaxation functions, it is unclear if it is ever significant. Note that at very low T's well inside the glassy regime the relaxation spectrum is very wide, but falls mainly outside the accessible time-window, so the relaxation functions exhibit a plateau at $t \gg \tau_{\min}$ and a difference between MC and MD time-dependencies becomes invisible in this regime. To some extent, an imperfect superposition at $T < 0.3$ may be also related to the system polydispersity which leads to a broader distribution of the energy barrier width.

Swap-MC vs. MD-cooling preparation protocols. We propose the following qualitative argument to account for different $G(t)$ relaxation functions for the two types of configurations: Consider a system cooled by MD down to the target temperature $T = T_1 < T_g$. After the cooling stage the kinetic temperature T_{kin} becomes close to T_1, yet the system configurational state remains rather similar to the equilibrium configuration at T_g (apart from a small density change and minor local differences) since a structural relaxation at any $T < T_g$ takes longer than the cooling stage time (which is comparable to the sampling time $\Delta t = 10^5$). The configurational temperature is therefore $T_x \approx T_g$; it corresponds to the configuration entropy $S_{conf} = S_{conf}(T_x)$ and the configurational energy $E_{conf} = E_{conf}(T_x)$ defined as the mean of the nearest local energy minimum of the potential energy landscape. Note that the total energy $E = E_{conf} + E_{vib}$, where E_{vib} is the energy of vibrations near a local potential minimum (E_{vib} includes both potential and kinetic parts), and, in a similar way, the total entropy $S = S_{conf} + S_{vib}$, where S_{vib} is the vibrational contribution to entropy. The general thermodynamic relation $T\mathrm{d}S = \mathrm{d}E$ (here for simplicity of the argument we neglect compressibility assuming that $V = \mathrm{const}$) now splits in two:

$$T_{kin}\mathrm{d}S_{vib} = \mathrm{d}E_{vib}, \quad T_x\mathrm{d}S_{conf} = \mathrm{d}E_{conf}$$

The energy barrier E_a for the cooperative structural relaxation of a 'cooled' configuration must correspond to $E_a = E_a(T_x) \approx \frac{E_0 T_x}{T_x - T_0}$ (cf. eq. (9)). The relevant structural time $\tau_{\alpha c}$ (the apparent α-relaxation time for the 'cooled' system) is defined by the activation energy E_a for $T_x \approx T_g$ and the kinetic temperature $T_{kin} \approx T_1$:

$$\tau_{\alpha c} \approx \tau_0 \exp(E_a/T_{kin}) \approx \tau_0 \exp\left(\frac{E_0 T_g}{(T_g - T_0)\, T_1}\right) \tag{10}$$

At low T_1 this time gets much shorter than the equilibrium relaxation time relevant for the 'swap-based' configurations (cf. eq. (8)),

$$\tau_\alpha \approx \tau_0 \exp\left(\frac{E_0}{T_1 - T_0}\right) \tag{11}$$

Moreover, the ratio $\tau_\alpha/\tau_{\alpha c}$ diverges as T_1 approaches the VFT temperature T_0. Therefore $\tau_{\alpha c}$ can stay inside the sampling time-window (or near it), while τ_α grows well beyond Δt, thus explaining a dramatic difference of $G(t)$ relaxation behaviors for the 'swap-based' (tempering method Sw-MD) and 'MD-cooled' (method SC-MD) systems at low temperatures, cf. Fig. 8. [9]

5. Bulk compression moduli

In this section we present the results on the instantaneous (affine) compression modulus and both the isothermic and adiabatic compression relaxation moduli.

5.1. Affine compression modulus

The affine compression modulus η_A is defined by the instantaneous pressure response, $\Delta p \simeq \eta_A \epsilon$, to a canonic affine compression of the system (at $t = 0$)

$$\underline{x} \to \underline{x}(1 - \epsilon/d), \quad \underline{v} \to \underline{v}/(1 - \epsilon/d) \tag{12}$$

where $\epsilon \ll 1$ defines the relative decrease of the total volume. Here $\underline{x}$ stands for all coordinates of all particles, $\underline{v}$ for their velocity components, d is the space dimension, and $\Delta p = \langle p(0^+) - p(0^-) \rangle$, where $p(t)$ is the pressure. The affine modulus is a sum of the excess and ideal-gas parts (which are due to, respectively, particle interactions and their momenta):

$$\eta_A = \eta_A^{ex} + \frac{d+2}{d}\rho T \tag{13}$$

For a system of particles with pairwise interactions the excess part is [9]

$$\eta_A^{ex} = \frac{1}{V d^2} \left\langle \sum_l \left[s u'(s) + s^2 u''(s) \right]_{s=s_l} \right\rangle + p_{ex} \tag{14}$$

where $p_{ex} = p - \rho T$ is the excess pressure. As before (cf. sect. 4) l is a pair of interacting particles, $s_l = r_l/\sigma_l$, r_l is the distance between their centers, σ_l is their interaction range, $u(s)$ is the interaction potential defined in the r.h.s. of eq. (1), u' and u'' are its first and second derivatives with respect to s. Using the equations

---

[9] This argument also explains a similar difference in the MSD, $h_0(t)$, for the two ensembles, cf. Fig. 5.

above and the microscopic definition of the instantaneous shear modulus [10] we arrive at a rigorous relation between shear and compression affine moduli:

$$\eta_A = \frac{d+2}{d}\mu_A^{or} + 2p_0 - 2\rho T \tag{15}$$

where μ_A^{or} can be calculated for each independent system by time-averaging of eq. (4) (cf. sect. 4). A similar relation for $d = 3$ was obtained long ago in ref. [51] where it was called 'the generalized Cauchy identity'. Using eq. (15) we obtained η_A for ensembles of pLJ systems at each temperature, and then calculated the corrected ensemble average, η_A^*, as explained in Appendix F. The obtained T-dependence of η_A^* is shown in Fig. 17. As the ideal-gas term $-2\rho T$ in eq. (15) only represents a small correction to μ_A^{or}, $\eta_A^*(T)$ behaves essentially as $\mu_A^{or}(T)$ (cf. Fig. 6): The affine compression modulus increases monotonically on cooling, showing a small feature (change of slope) at $T \approx 0.16$ corresponding to the fractionation effect (cf. sect. 4).

5.2. Bulk relaxation moduli

The bulk relaxation compression modulus $K(t)$ of a liquid (or of any macroscopically homogeneous isotropic molecular system like an amorphous solid) can be defined in terms of the response of the total mean pressure (averaged over the whole system of volume V) to a small uniform compression, $V \to V(1-\epsilon)$: $K(t) = \Delta p(t)/\epsilon$, where $\Delta p(t) = \langle p(t) - p(0^-)\rangle$ is the pressure increment due to an instant affine step deformation (with $\epsilon \to 0$) occurred at $t = 0$. [10]

To complete the definition of K one has to specify what happens with temperature T (or energy) of the system after the deformation. If no heat is transferred to/from the system (or the *total* heat current is always zero), the energy is conserved leading to the adiabatic response characterized by the relaxation modulus $K_A(t)$. By contrast, in the case of an ideal temperature control ($T = \text{const}$) we arrive at the isothermic relaxation modulus $K_T(t)$. The properly defined bulk moduli $K_A(t)$ and $K_T(t)$ [11] are different, and are both universal: they must not depend on the statistical ensemble, nor on the thermostat properties (in the case of

---

[10] Note that the static limits ($t \to \infty$) of $G(t)$ and $K(t)$ are related to the small-strain elasticity tensor $\mathbf{c}$ (cf. eqs. (2.196) and (2.199) of ref. [32]; in turn, $\mathbf{c}$ is related to the material and mixed elasticity tensors in a well-known way, cf. eq. (2.195) in [32]): for an isotropic material $G(\infty) = (c_{11} - c_{12})/2$, $K(\infty) = (c_{11} + (d-1)c_{12})/d$.

[11] By 'properly defined' we mean that the adiabatic or isothermic conditions ($E = \text{const}$ or $T = \text{const}$) are imposed at all times after the perturbation. Such conditions may be naturally satisfied by the dynamical system like the condition $E = \text{const}$ in the case of microcanonical simulations. Alternatively, however, the required conditions can be also kept by weak perturbations like small heat injections associated with appropriate velocity transformations (cf. eq. (B4)). The latter approach provides a way to obtain $K_T(t)$ based, for example, on microcanonical simulations. The underlying general idea here is the same as the one proposed in ref. [13] to obtain the isochoric heat capacity $c_v(t)$ from thermostatted simulations.

a 'decent' thermostat that negligibly affects the particle dynamics at the time-scale of fast collisional/vibrational relaxation; cf. ref. [13] for more details).

Most of the thermostatting approaches used in real experiments or in simulations are not ideal and allow for some systematic T-variations following the perturbative deformation (since generally the instantaneous temperature $T = T(t)$ does not coincide with the temperature T_i imposed by the thermostat). In particular, this is true for the Nosé-Hoover thermostat employed in MD simulations considered in the present paper. Note that normally by $K(t)$ we mean the relaxation modulus obtained at a constant imposed temperature, $T_i = \mathrm{const}$. The thus defined 'bare' modulus $K(t) = K_0(t)$ is *not* universal: it depends on the thermostat/system coupling parameters (a similar problem for the heat capacity is discussed in ref. [13]). However, an advantage of the $K_0(t)$ response function is that, by virtue of the FDT, it can be easily calculated based on the pressure autocorrelation function $C_p(t)$:

$$K_0(t) = \eta_A + \frac{T}{\rho}\left[C_p(t) - C_p(0)\right] \tag{16}$$

where

$$C_p(t) = \frac{N}{T^2}\left\langle \delta p(t+t')\delta p(t')\right\rangle_{NVT_i} \tag{17}$$

is the equilibrium correlation function of pressure in the canonical NVT_i ensemble, $\delta p(t) = p(t) - \langle p\rangle$, $\langle p\rangle$ is the ensemble- and time-averaged pressure p (cp. eqs. (2), (3)).

Importantly, eq. (16) also implies that the ϵ-compression at $t = 0$ is a canonical-affine transformation of coordinates (x) and velocities (v) of all particles, cf. eq. (12) (this transformation is adiabatic since it conserves the measure in the phase space). Therefore $K_0(0)$ provides the instantaneous *adiabatic* response in the case of a Nosé-Hoover or any other thermostat allowing for temperature fluctuations: $K_0(0) = \eta_A$ is both affine and adiabatic.

Noteworthily, to derive the FDT relation, eq. (16), one has to consider an extended ensemble including systems of different (but time-independent) volumes whose equilibrium distribution is defined by the imposed pressure p_0 (the effective Hamiltonian of the system therefore is $H = E + p_0V$). The finding that the FDT relation requires an extended (Np_0T_i) ensemble is consistent with other approaches [14,52]. For thermostatted (NVT_i) simulations (with the same V for all systems) $C_p(t \to \infty) = 0$ in the liquid regime, hence the equilibrium isothermal compression modulus can be defined as $K_{Te} = K_0(t \to \infty) = \eta_A - TC_p(0)/\rho$, and Eq. (16) can be rewritten as $K_0(t) = TC_p(t)/\rho + K_{Te}$. In this form, Eq. (16) agrees with eq. (48) in [14] and with the Lebowitz–Percus–Verlet transformation of fluctuations between different ensembles (here NPT and NVT) [53], allowing to identify $K_0(t)$ with $K_0(t) = (V/T)\langle\delta p(t+t')\delta p(t')\rangle_{Np_0T_i}$ for the extended ensemble where p_0 is imposed (but $V = \mathrm{const}$ for each system). [12]

---

[12] Note also that $K_0(t)$ for microcanonical simulations is equal to the adiabatic modulus $K_A(t)$ which can be defined in analogy with eq. (19) of ref. [52]: $K_A(t) = \lim_{q\to 0}(V/T)\langle\delta p(\underline{q}, t +$

5.3. Results and discussion on compression relaxation moduli

As discussed in the previous section, for thermostatted simulations the relaxation function $K_0(t)$ generally reflects an adiabatic response at short times, while its long-time behavior is isothermic. Hence we arrive at the following problem: to obtain the proper (universal) relaxation moduli $K_T(t)$ and $K_A(t)$ based on $K_0(t)$ (or based on the correlation functions measured in simulations). The solution to this problem is outlined in Appendix A based on the ideas developed in ref. [13].

The relaxation functions $K_T(t)$ for the Sw-MD systems at different temperatures, calculated as described in Appendices A, B, are plotted in Fig. 12. The compression modulus shows a minimum around $t = 0.2$ for $T \leq 0.4$ (the minimum time slightly decreases on cooling). The minimum is deeper than the similar short-time undershoots of the shear relaxation modulus $G(t)$ (cf. Fig. 8) and it gets more pronounced at lower T's. This feature points to stronger inertial effects for $K_T(t)$ than for $G(t)$. In both cases an undershoot is followed by an overshoot at longer times ($t_o \gtrsim 1$ for $K_T(t)$ at $T \lesssim 0.3$). At low temperatures, $T < 0.22$, the relaxation modulus develops a well-defined quasistatic plateau, K_{Ts}, in a wide time range (for $t > 1$). The quasistatic compression modulus K_{Ts} (cf. eq. (29)) is always much higher (by a factor of ~ 3) than the analogous quasistatic shear modulus.

The adiabatic compression modulus $K_A(t)$ for the Sw-MD systems was calculated in two ways: First, by solving the exact eq. (D7) derived in Appendix D (the numerical approach to solve it is described below eq. (B28) in Appendix B). Second, by using the approximate eq. (A5) (cf. Appendix A). The results are compared in Fig. 13 showing that the approximate equation works quite well for all times and all temperatures. There is no difference between the 'exact' and approximate $K_A(t)$ for $t \gtrsim 2$ (within the numerical precision of the data). At shorter times some minor deviations of the red (approximate) curves are detected mostly in the overshoot-undershoot region.

The functions $K_A(t)$, obtained using the 'exact' FDT relation, eq. (D7), in a wider range of temperatures and times are shown in Fig. 14. One can observe the following differences between adiabatic and isothermic relaxation functions (cf. Figs. 14, 12): $K_A(t)$ show stronger variations at short times, $t < 1$ (in particular, a deeper undershoot and a much sharper and higher overshoot). The short-time minima of $K_A(t)$ are located at $t_u \sim 0.25$ at all T's, whereas for $K_T(t)$ this time somewhat decreases down to $t_u \lesssim 0.2$ at low T's. On the other hand, the long-time relaxation (for $t > 1$) is weaker in the adiabatic case.

Noteworthily, the minima of $K_A(t)$ emerge already well above T_g, in contrast to $G(t)$ showing undershoots only below T_g. It is reasonable to attribute these undershoot/overshoot features to the effect of overstressed bonds. It is easier to understand this effect at a low T, when each particle is close to its equilibrium position. Upon a perturbative affine compression the force balance may be upset,

---

$t')\delta p(-\underline{q}, t')\rangle_{NVT}$, where $\underline{q}$ is the wave-vector and $\delta p(\underline{q}, t)$ the pressure fluctuation at $\underline{q}$ and t. As long as $\underline{q}$ is not strictly equal to 0, the thermodynamic boundary condition of fixed particle number and volume is not felt and all fluctuations are allowed. Identifying $K_0(t)$ for microcanonical simulations with the $q \to 0$ limit of the autocorrelation function of $\delta p(\underline{q}, t)$ is thus again consistent with an extended ensemble with imposed pressure.

so the particles have to move to the new equilibrium positions. The contribution of a bond to the pressure increment (due to the deformation) is proportional to the bond force increment Δf which, in turn, is proportional to the elastic constant $k \equiv r_l^2 \partial^2 U/\partial r_l^2$ of the bond (here by a bond we mean any interacting pair of particles, r_l is the bond length). A bond with higher k (than on the average) is likely to push the particle so as to increase r_l. After a half-period of the resultant oscillating motion the force Δf decreases to a minimum (which may even be opposite to the initial value Δf_0), this corresponds to the undershoot of $K_A(t)$. Waiting another half period returns the force closer to the initial value Δf_0 leading to an overshoot. The undershoots for $K_A(t)$ are located at $t_u \sim 0.25$ and the overshoots - at a twice longer time, $t_o \sim 0.5$, in agreement with the argument given above. The mean vibration frequency ω_v is therefore $\omega_v \sim \pi/t_u \sim 13$rad/s, which is in harmony with an estimate of a typical vibration frequency in a LJ liquid [26]. Interestingly, the undershoot time is somewhat shorter ($t_u \sim 0.2$) in the case of isothermic relaxation at low T, while the overshoots for $K_T(t)$ are very broad and weak.

6. Static moduli and their deviations

In this section we consider temperature dependencies of the long-time elastic moduli and their standard deviations for the systems equilibrated with particle swaps (method Sw-MD).

6.1. Shear moduli

The affine modulus μ_A shown with black solid line in Fig. 6(a) was discussed in sect. 4. We applied two different approaches to increase its precision. The first approach boils down to an isotropic averaging over all rotations of the coordinate frame (cf. sect. 4). The second approach is described in Appendix F.

To assess the efficiency of these precision-improving procedures for μ_A we applied them independently to obtain $\mu_A^{\rm or}$ (with orientational averaging), μ_A^* (with pressure correction), and $\mu_A^{\rm or*}$ (with both orientational averaging and pressure correction) in addition to μ_A^0 (cf. sect. 4). The variances of the affine moduli among the systems of an m-ensemble have been then evaluated based on these 4 sets of μ_A leading to 4 types of the corresponding standard deviations, $\delta\mu_A^0$, $\delta\mu_A^{\rm or}$, $\delta\mu_A^*$ and $\delta\mu_A^{\rm or*}$, whose temperature dependencies are shown in Fig. 15. It is clear that $\delta\mu_A^{\rm or*}$ is much smaller than $\delta\mu_A^0$, i.e., $\mu_A^{\rm or*}$ is much more precise than the raw modulus μ_A^0 obtained in the fixed coordinate frame and without the pressure correction. The deviations $\delta\mu_A^0$, $\delta\mu_A^{\rm or}$ (no pressure correction) coincide above the glass transition, and are nearly constant at lower temperatures (although the orientational preaveraging results in a slightly lower $\delta\mu_A^{\rm or}$ below T_g). This result suggests that both $\delta\mu_A^0$ and $\delta\mu_A^{\rm or}$ are mainly due to quenched variations of the total volume and the mean pressure across the ensemble. This view is supported by the observation that the pressure correction above T_g leads to a drastic decrease of the μ_A-deviation by a factor of ~ 20 from $\delta\mu_A^{\rm or} \approx \delta\mu_A^0 \sim 0.15$ to $\delta\mu_A^{\rm or*} < \delta\mu_A^* \lesssim 0.007$. The deviations $\delta\mu_A^0$, $\delta\mu_A^{\rm or}$ are therefore quite imprecise and irrelevant (reflecting mostly the volume dispersity of independent configurations). The remaining deviations, $\delta\mu_A^*$ and $\delta\mu_A^{\rm or*}$, show a

rather sharp increase on cooling near T_g; a similar behavior of $\delta\mu_A$ was already reported for another glass-forming system (a 3-dimensional oligomer liquid) [10]. The effect of orientational preaveraging is strong below T_g where $\delta\mu_A^{\mathrm{or}*} \ll \delta\mu_A^*$. Its origin was explained in ref. [10]: the preaveraging wipes out an important contribution to $\delta\mu_A$ due to fluctuations of bond orientations. Remarkably, all the deviations of μ_A show a peak slightly below the fractionation temperature T_f; it is therefore likely that the peak is kinetic in nature being associated with a phase-separation process.

The long-time shear modulus μ_{sf} is defined in terms of the relaxation modulus $G(t)$ in eq. (11) of ref. [10] which is equivalent to [17]

$$\mu_{sf}(\Delta t) = \frac{2}{(\Delta t)^2} \int_0^{\Delta t} G(t)\,(\Delta t - t)\,\mathrm{d}t \tag{18}$$

Another equivalent definition comes from eqs. (2), (3), (18):

$$\mu_{sf}(\Delta t) = \mu_A - \mu_F(\Delta t) \tag{19}$$

where the so-called fluctuation modulus is [10,17]

$$\mu_F(\Delta t) = \frac{V}{T} \left\langle (\sigma(t) - \bar{\sigma})^2 \right\rangle_{NVT} \tag{20}$$

where $\bar{\sigma}$ is the time-averaged stress (for $0 < t < \Delta t$) and $\langle ... \rangle_{NVT}$ implies both time- and ensemble-averaging. To improve the precision of both μ_F and μ_{sf} we applied the same procedures as for μ_A. The orientation average of μ_F is obtained by calculating μ_F both in the original coordinate frame with x, y axes along the box sides (yielding μ_F^0) and in the frame rotated by 45° (μ_F^{45}):

$$\mu_F^{\mathrm{or}} = \left(\mu_F^0 + \mu_F^{45}\right)/2 \tag{21}$$

(Note that eq. (21) is exactly equivalent to isotropic averaging over all rotations of the coordinate frame, as follows from the tensorial nature of the stress). Accordingly

$$\mu_{sf}^{\mathrm{or}} = \mu_A^{\mathrm{or}} - \mu_F^{\mathrm{or}} \tag{22}$$

Furthermore, in most cases we apply the pressure correction indicated by star ($*$) as before.

The temperature dependencies of the quasi-static moduli $\mu_{sf}^{\mathrm{or}*}$ and $\mu_F^{\mathrm{or}*}$ are shown in Fig. 16(a). Their behavior is similar to that revealed for another glass-forming system [10]: the glassy modulus μ_{sf} vanishes in the liquid regime, but sharply increases on cooling near T_g, while μ_F develops a maximum around T_g. The latter feature was explained [10] by faster increase of μ_A (as compared to μ_{sf}) on cooling in the liquid regime, and the opposite behavior (faster increase of μ_{sf}) below T_g. Note that at $T_g = 0.26$ the glassy modulus $\mu_{sf}^{\mathrm{or}*}$ is still small, it is roughly twice lower than its standard deviation, $\delta\mu_{sf}^{\mathrm{or}*}$. It is noteworthy that the temperature dependence of $v = \mu_F$ obtained by MC simulations using the same independent configurations as in the present study (cf. Fig. 14 of ref. [17]) agrees with our data for $\mu_F^{\mathrm{or}*}$.

The standard deviations $\delta\mu_{sf}^*$, $\delta\mu_F^*$ and $\delta\mu_{sf}^{\mathrm{or}*}$, $\delta\mu_F^{\mathrm{or}*}$ show similar T-dependencies characterized by a rather sharp peak slightly below T_g, cf. Fig. 16(b). The

peak of $\delta\mu_F$ was reported for the same system [17] and for a 3-dimensional glass-forming system [10]; it was explained based on the assumption of Gaussian stress fluctuations. [13] This 'Gaussian' theory is described in refs. [10,17]. The predicted 'Gaussian' standard deviations $\delta\mu_F^{(G)}$ (calculated at different temperatures based on the known shear relaxation function $G(t)$) are also shown in Fig. 16(b) (black curve). [14] It is clear that $\delta\mu_F^{(G)}$ quantitatively reproduces the behavior of $\delta\mu_F^*$ in liquid regime and in the glass-transition zone around T_g. By contrast, $\delta\mu_F^* \gg \delta\mu_F^{(G)}$ well below T_g due to a non-ergodic (and therefore non-Gaussian) contribution, $\delta\mu_F^{(ne)}$, related to quenched structural disorder in glassy systems:

$$(\delta\mu_F^*)^2 = \left(\delta\mu_F^{(G)}\right)^2 + \left(\delta\mu_F^{(ne)}\right)^2 \tag{23}$$

(cf. refs. [10,17,27]). It is important to note that the theory is not expected to be applicable quantitatively to the standard deviations $\delta\mu_F^{or*}$ of orientationally-averaged μ_F; $\delta\mu_F^{or*}$ is typically lower than $\delta\mu_F^*$ by a factor $\sim\sqrt{2}$.

To assess the importance of the pressure correction for μ_F and μ_{sf} we compared $\delta\mu_F^*$ with $\delta\mu_F^0$ and $\delta\mu_{sf}^*$ with $\delta\mu_{sf}^0$ (cf. Fig. 16(c)). It turns out that the pressure correction is not important for $\delta\mu_{sf}$ (apart from a weak effect at low $T \leq 0.18$, where $\delta\mu_{sf}^0$ exceeds $\delta\mu_{sf}^*$ by $\sim 10\%$). It is also negligible for $\delta\mu_F$ at $T \leq 0.28$. However, the situation is different at higher temperatures ($T > 0.28$) where $\delta\mu_F^*$ gradually becomes significantly smaller than the bare (uncorrected) deviation $\delta\mu_F^0$ (by a factor of 4 at $T = 0.5$). Why is μ_F strongly affected by pressure variations above T_g in contrast to μ_{sf}? The point is that the shear modulus μ_{sf} vanishes in the liquid regime, and thus gets uncorrelated with pressure for this simple reason. As a result $\delta\mu_{sf}^0$ becomes negligible compared to $\delta\mu_A^0$, and in view of the relation $\mu_F^0 = \mu_A^0 - \mu_{sf}^0$, the deviation $\delta\mu_F^0$ gets dominated by the deviations of μ_A^0 which strongly depend on pressure (cf. Fig. 15): $\delta\mu_F^0 \sim \delta\mu_A^0 \gg \delta\mu_{sf}^0$ in the liquid regime. Fig. 16(c) also shows that in the glass-transition region ($T \sim T_g$) the standard deviations of all the fluctuation shear moduli, $\delta\mu_F^*$, $\delta\mu_F^0$, $\delta\mu_{sf}^*$, $\delta\mu_{sf}^0$, are accurately described (are dominated) by the Gaussian contribution $\delta\mu_F^{(G)}$.

Following the approach described in Appendix F, fluctuations of any variable X can be represented as

$$(\delta X)^2 = (\delta X^*)^2 + (\delta X^p)^2 \tag{24}$$

where δX^p accounts for the variations of the mean pressure between the systems

$$(\delta X^p)^2 = \left(\frac{\partial X}{\partial p}\right)^2 \mathrm{var}(\bar{p}) \tag{25}$$

---

[13] Note that the pressure correction was not applied in ref. [17]. This difference led to larger $\delta v = \delta\mu_F$ in the high T region (cf. Fig. 15 of ref. [17]) as compared to $\delta\mu_F^*$ shown in Fig. 16(c). A part of this effect is also due to shorter sampling times used in [17].

[14] Note that the pressure correction is irrelevant for $\delta\mu_F^{(G)}$ since the latter is invariant to vertical shifts of $G(t)$, $G(t) \to G(t) + \text{const}$. [10,17]

where $\mathrm{var}(\bar{p}) \equiv (\delta\bar{p})^2 \simeq \frac{T}{V}K_{Te}$ is the mean pressure variance between the independent configurations (K_{Te} is defined below eq. (29)), and $\frac{\partial X}{\partial p}$ is the thermodynamic derivative at $T = \mathrm{const}$. Hence $\delta X^p \propto \frac{\partial X}{\partial p}\delta\bar{p}$ stems from trivial equilibrium pressure fluctuations. By contrast, δX^* reflects more important effects of structural heterogeneities. In fact, a dispersion of X^* between different parts of a supercooled liquid (which is due to its inherently heterogeneous glassy structure) must be similar to the dispersion between independent configurations considered in the present paper. Thus, a better resolution of structural heterogeneities demands lower $\delta X^p/\delta X^*$. Comparing this ratio for $X = \mu_A$, μ_F and μ_{sf} we found that μ_F is better suited than other moduli for detecting structural heterogeneities.

6.2. Compression moduli

Temperature dependence of various compression moduli is shown in Fig. 17. The instantaneous (affine) modulus η_A discussed at the end of sect. 5.1 (cf. eq. (15)) provide the upper bound for all the moduli. The isothermic quasi-static modulus η_{sf} is defined using the stress-fluctuation formula in analogy with eqs. (19), (20):

$$\eta_{sf}(\Delta t) = \eta_A - \eta_F(\Delta t) \tag{26}$$

where $\eta_F(\Delta t)$ is the fluctuation compression modulus proportional to the mean-square pressure fluctuations in the NVT_i ensemble (at constant volume [9] and imposed temperature T_i):

$$\eta_F(\Delta t) = \frac{V}{T}\left\langle (p(t) - \bar{p})^2 \right\rangle_{NVT_i} \tag{27}$$

where $\langle ... \rangle_{NVT_i}$ indicates both time- and ensemble-averaging as before. Equations equivalent to eq. (26) have been proposed/used in refs. [28,11,9,15].

Following the same approach as applied to the shear stress fluctuations in order to obtain eq. (18) [10,17], η_{sf} can be related to the relaxation modulus $K_0(t)$:

$$\eta_{sf}(\Delta t) = \frac{2}{(\Delta t)^2}\int_0^{\Delta t} K_0(t)\,(\Delta t - t)\,\mathrm{d}t \tag{28}$$

This relation shows that $\eta_{sf}(\Delta t)$ is dominated by the long-time level of $K_0(t) \approx K_T(t)$.[15]

In addition to η_{sf} we define the long-time modulus K_{Ts} in analogy with eq. (28), but with a different lower limit of time:

$$K_{Ts} = \mathrm{const}\int_{0.3\Delta t}^{\Delta t} K_T(t)\,(\Delta t - t)\,\mathrm{d}t \tag{29}$$

where const is normalization constant. Thus, K_{Ts} is a mean of $K_T(t)$ over the segment $[0.3\Delta t, \Delta t]$. As the function $K_0(t)$ mostly decreases with time, K_{Ts} is a bit lower than η_{sf} (as follows from eqs. (28), (29); note that there is no

---

[15] In the long-time limit, $K_0(t) \to$ const. If $K_0 = \mathrm{const}$, eq. (28) gives $\eta_{\mathrm{sf}} = K_0$, implying that $\eta_{\mathrm{sf}}(\Delta t \to \infty)$ is indeed dominated by the long-time level of $K_0(t)$.

difference between $K_0(t)$ and $K_T(t)$ in the long-time regime of eq. (29)). However, the difference between the 2 moduli is barely visible only around T_g where the plateau onset is comparable with $0.3\Delta t$ (cp. red and brown curves in Fig. 17). Above T_g the integration segment in eq. (29) (and, therefore, K_{Ts}) falls into the equilibrium plateau (cf. Fig. 12), while below T_g it belongs to the glassy plateau. We attempted to obtain the *equilibrium* isothermic compression modulus K_{Te} assuming that its T-dependence is smooth (featureless) around the glass transition (just like the T-dependencies of the affine compression modulus η_A or the shear modulus μ_A). To this end, it was postulated that $K_{Te} = K_{Ts}$ for $T \geq 0.29$, and a parabolic fit of $K_{Ts}(T)$ in the region $0.29 \leq T \leq 0.4$ was extrapolated to get K_{Te} at $T < 0.29$. Quite expectedly K_{Ts} exceeds the resultant equilibrium (genuine static) compression modulus K_{Te} below T_g, $K_{Ts} > K_{Te}$, since the regime of complete relaxation is inaccessible in the glassy state (cf. Fig. 17). The difference $K_{Ts} - K_{Te}$ is the magnitude of the terminal relaxation step of $K_T(t)$ occurring at $t \gg \Delta t$. It significantly increases on cooling in the glass-transition zone, but then appears to stay nearly constant at lower T's ($T < 0.24$). The relative non-equilibrium (glassy) contribution $\frac{K_{Ts}-K_{Te}}{\eta_A}$ amounts to about 4% at $T_g \approx 0.26$. This value can be compared with the analogous ratio for the shear modulus, $\mu_{sf}/\mu_A \sim 1.3\%$ at $T = T_g$ (note that the genuine *equilibrium shear* modulus is assumed to be identically zero both below and above T_g [2] [16]). Therefore T_g roughly corresponds to the onsets of both the quasi-static shear elasticity and a non-equilibrium contribution to the compression modulus.

Remarkably, the fluctuation compression modulus η_F always monotonically increases with temperature (cf. Fig. 17) in contrast to the shear-stress fluctuation modulus μ_F which shows a maximum near T_g (cf. Fig. 16(a)). The difference stems from their behavior above T_g: $\mu_F = \mu_A - \mu_{sf}$ decreases with T because μ_{sf} is negligible in this regime, while μ_A gets lower at higher temperature. By comparison, $\eta_F = \eta_A - \eta_{sf}$ increases with T both above and below T_g (for $T > T_f$) because the static modulus $\eta_{sf} \approx K_{Ts} \approx K_{Te}$ always decreases with T faster than η_A.

Fig. 17 also shows another quasi-static compression modulus, K_{vv}, defined using the volume-fluctuation formula [9,8,15,29]

$$K_{vv} = TV / \left\langle (V - \bar{V})^2 \right\rangle \tag{30}$$

where $V - \bar{V}$ is instantaneous deviation of the total system volume from its time-averaged value in the NPT ensemble (in this case we used both Nosé-Hoover thermostat and barostat). Eq. (30) is applicable if any relevant relaxation time (including those associated with thermostat and barostat) are either much shorter or much longer than Δt. This is true both above T_g (where all relaxation times are $\ll \Delta t$) and below T_g (where $\tau_\alpha \gg \Delta t$). In these cases $K_{vv} \simeq K_{Ts} \simeq \eta_{sf}$. Fig. 17 confirms this expectation: a small difference between K_{vv} and η_{sf} is only visible in the glass-transition zone near T_g.

The statistics of $V(t)$ deteriorates below T_g, so $K_{vv}(T)$ becomes noisy at $T < 0.2$. By contrast, the T-dependence of η_{sf} remains smooth in this region. The main

---

[16] Here we do not consider the non-ergodic regime below the putative ideal glass transition temperature.

reason for this difference is that in the case of η_{sf} (but not for K_{vv}) we applied the procedure described in Appendix F to compensate for the mean pressure variations between the configurations: $\eta_{sf} = \eta^*_{sf}$. The importance of the pressure correction for η_{sf} is also evident from Fig. 18 showing that $\delta\eta^0_{sf} \gg \delta\eta^*_{sf}$.

The quasi-static adiabatic modulus K_{As} was obtained based on the adiabatic relaxation modulus $K_A(t)$ (cf. Fig. 14) in analogy with K_{Ts} (cf. eq. (29) where $K_T(t)$ should be replaced with $K_A(t)$). It shows a monotonic and almost linear increase on cooling except a shoulder in the glass-transition zone (cf. Fig. 17). Again the difference $K_{As} - K_{Ae}$ (where K_{Ae} was obtained by linear extrapolation of $K_{As}(T)$ at $T > 0.3$ into the region $T < 0.3$) defines the magnitude of the terminal adiabatic relaxation step in the glassy regime ($T < T_g$). Just like the similar quantity $(K_{Ts} - K_{Te})$ for the isothermal relaxation, $K_{As} - K_{Ae}$ rapidly increases on cooling near T_g, but stays almost constant (increasing slightly) at lower T's. We also observe that $K_{As}(T)$ is always roughly in the middle between the quasi-static isothermic ($\eta_{sf} \approx K_{Ts}$) and instantaneous affine (η_A) moduli; all the 3 moduli seem to nearly merge at $T = 0$. The fact that $K_{As} = K_{Ts}$ at $T = 0$ is anticipated from eq. (D22) provided that the thermal pressure p_{Ts} is finite. On the other hand, we know that $\eta_A - K_{Ts} \approx \eta_A - \eta_{sf} = \eta_F$ (cf. eq. (26)) and that $\eta_F \geq 0$ by definition (cf. eq. (27); the inequality $\eta_F \geq 0$ at $T \to 0$ also comes from results of ref. [54]; an analogous inequality for μ_F is also well-known [55]). Thus, in the general case both η_F and μ_F must remain finite at $T = 0$, and therefore $\eta_A > \eta_{sf}$ and $\mu_A > \mu_{sf}$ at all temperatures. It appears however that η_F decreases very significantly at low temperatures (cf. Fig. 17), whereas a similar decrease of μ_F is not so pronounced (cf. Fig. 16(a)).

To calculate the standard deviations of compression moduli we determine η_A, η_F for each independent system. For example, the affine modulus η_A is obtained by time-averaging of the instantaneous modulus $\eta_A(t)$ defined in analogy with eq. (15)

$$\eta_A(t) = \frac{d+2}{d}\mu^{\rm or}_A(t) + 2p_0 - 2\rho T \tag{31}$$

where $\mu^{\rm or}_A(t)$ is specified in eq. (4):

$$\eta_A = \frac{1}{\Delta t}\int_0^{\Delta t} \eta_A(t)\mathrm{d}t \tag{32}$$

Similarly, the fluctuation modulus is defined as (cf. eq. (27))

$$\eta_F = \frac{V}{T}\frac{1}{\Delta t}\int_0^{\Delta t} (p(t) - \bar{p})^2\,\mathrm{d}t \tag{33}$$

Temperature dependencies of standard deviations for the affine and fluctuation compression moduli, $\delta\eta^0_A$, $\delta\eta^*_A$, $\delta\eta^0_F$, $\delta\eta^*_F$, are shown in Fig. 18(a). The pressure correction is obviously important for the affine modulus: $\delta\eta^0_A$ is always much higher than $\delta\eta^*_A$ (by a factor of 10 or more above T_g). By contrast, the pressure correction for η_F (just like for μ_F) appears to be insignificant near and below T_g: $\delta\eta^0_F \sim \delta\eta^*_F$ at $T \lesssim T_g$. The effect of pressure dispersion on $\delta\eta_F$ becomes detectable only well in the liquid regime, for $T > 0.4$. Turning to $\eta_{sf} = \eta_A - \eta_F$, we observe that $\delta\eta^0_{sf}$ is defined by $\delta\eta^0_A$ both above and below T_g outside the peak: $\delta\eta^0_{sf} \approx \delta\eta^0_A$ at $T > 0.32$ and $T < 0.22$. On the other hand, elimination of the pressure dispersion effect leads to a significant decrease of $\delta\eta^*_{sf}$ in the two regions,

cf. Fig. 18(b). Thus both η_{sf} and η_A strongly depend on the mean pressure, while such effect is much weaker for η_F.

The Gaussian approximation, $\delta\eta_F^{(\mathrm{G})}$, for $\delta\eta_F^*$ can be obtained as a straightforward generalization of the theory [10,17] for $\delta\mu_F^*$: the whole argument remains the same provided that the shear relaxation modulus $G(t)$ is replaced with the compression modulus $K_0(t)$. In other words, the variance $\left(\delta\eta_F^{(\mathrm{G})}\right)^2$ is defined by the r.h.s. of eq. 30 in ref. [10] with K_0 instead of G. Fig. 18(b) shows that the Gaussian approximation works very well for $T \geq 0.25$, where $\delta\eta_F^* \approx \delta\eta_F^{(\mathrm{G})}$. At lower T's the difference between $\delta\eta_F^*$ and $\delta\eta_F^{(\mathrm{G})}$ grows to more than 10%; it allows to obtain the structural non-ergodicity parameter $\delta\eta_F^{(\mathrm{ne})}$ [17,27]:

$$\left(\delta\eta_F^{(\mathrm{ne})}\right)^2 = (\delta\eta_F^*)^2 - \left(\delta\eta_F^{(\mathrm{G})}\right)^2 \tag{34}$$

The above equation leads to $\delta\eta_F^{(\mathrm{ne})}/\delta\eta_F^{(\mathrm{G})} \sim 0.5$ at $T \sim 0.2$. The corresponding shear non-ergodicity parameter, $\delta\mu_F^{(\mathrm{ne})}$ (cf. eq. (23)) is much larger: $\delta\mu_F^{(\mathrm{ne})}/\delta\mu_F^{(\mathrm{G})} \gtrsim 5$ at $0.15 \lesssim T \lesssim 0.2$.

Noteworthily, the shear and compression fluctuation moduli are comparable at low temperatures: $\eta_F \sim \mu_F \sim 15$. The higher ratio $\delta\mu_F^{(\mathrm{ne})}/\mu_F$ as compared to $\delta\eta_F^{(\mathrm{ne})}/\eta_F$ indicates that an order parameter related to μ_F would be more appropriate than η_F to study structural heterogeneities.

7. Conclusions

1. We performed MD and MC simulations of a two-dimensional system of polydisperse disks with LJ interactions using several methods to prepare quasi-equilibrated systems (cf. sect. 2): by slow cooling and tempering with MD or MC (methods SC-MD, SC-MC) and by tempering with MC involving particle swap moves followed by standard equilibration with local MC moves or MD (methods Sw-MC, Sw-MD). It is shown that above the glass transition temperature $T_g \approx 0.26$ the system properties (RDF, the structure factor $S(q)$, the MSD, the relaxation moduli) do not depend on the tempering (equilibration) approach. Remarkably, the glass transition can be easily detected based on the temperature behavior of either density ρ (cf. Fig. 1) or the affine shear modulus μ_A (cf. Fig. 6(a)) for systems prepared with different equilibration approaches: both $\rho(T)$ and $\mu_A(T)$ show a lower slope at $T < T_g$ for the preparation method SC-MD (continuous MD cooling) as compared to the Sw-MD and Sw-MC methods.

2. The systems equilibrated with particle swaps are thus denser and more rigid below T_g than slowly cooled systems. Moreover, the observed temperature dependencies of such static quantities as ρ [17], μ_A and the affine compression modulus η_A are smooth in the vicinity of T_g for the swapped systems (no change of slope near T_g, cf. Figs. 6(a), 17). These features indicate that the particle swap technique allowed for a nearly complete equilibration both above and below T_g in agreement with results of refs. [23,17].

3. The detected evolution of the Kirkwood RDF, $g(r)$, at low temperatures (cf. Fig. 2) points to a particle demixing (fractionation) process in the swap-based configurations at $T < T_f \approx 0.16$ (cf. Fig. 3). This tendency is also reflected in the behavior of the structure factor $S(q)$ showing an increase at low q's on

cooling towards T_f (cf. Fig. 4). The fractionation transition is also visible in the temperature dependence of the affine shear modulus μ_A obtained for the swap-based configurations (cf. Fig. 6(a)).

4. We demonstrate that the system dynamics below T_g significantly depend on the applied equilibration/tempering method: the particle self-diffusion is considerably slower for systems equilibrated using particle swaps (method Sw-MD), cf. Fig. 5, in spite of the fact that both ensembles show similar structure (with nearly the same RDF, cf. Fig. 2) for $T_f < T < T_g$. A dramatic effect of the preparation protocol is also reflected in the shear stress relaxation which shows a long-time plateau at low T's for swap-equilibrated systems, but a much faster decay with a transient shoulder for slowly cooled systems (cf. Fig. 8). It is therefore apparent that the less-equilibrated systems show much faster dynamics below T_g (cf. Fig. 10 and the discussion at the end of sect. 4).

5. The structural relaxation time τ_α of the swap-equilibrated system shows a super-Arrhenius temperature dependence (cf. the VFT law, eq. (8)). The VFT temperature T_0 (often associated with the Kauzmann or the ideal glass transition temperature [3]) turns out to be remarkably close to the fractionation temperature T_f.

6. It is shown that the shear-stress relaxation data obtained with MD and MC dynamics can be approximately superimposed by rescaling of the MC-time $t_{MC} \rightarrow t = t_{MC}/k$ (cf. Fig. 11). It turns out that the factor $k = k(T)$ shows a non-monotonic T-dependence with a maximum at $T \sim 0.3$ slightly above the glass-transition. However, the superposition gets imperfect in the glass-transition regime ($0.24 \leq T \leq 0.28$). Further simulations with larger ensembles may help to clarify the origin of this discrepancy. We argue (cf. discussion in sect. 4) that strictly speaking the two dynamics (MD and MC) are not equivalent even in the case of negligible inertia.

7. The shear-stress correlation function $C_\sigma(t)$ is not sensitive to the thermostatting mechanism since a shear deformation does not produce any temperature variation in the linear approximation (ΔT is proportional to the square of the shear rate). This feature is also reflected in the absence of cross-correlations between the shear stress and temperature or energy. By contrast, a normal stress or pressure do correlate with temperature and energy, and this sizeable effect leads to a dependence of the pressure correlation function $C_p(t)$ on the thermostatting method.

8. The shear relaxation modulus $G(t)$ was obtained based on shear stress fluctuations using the well-known FDT formula, eq. (2). The analogous relation defining the compression relaxation modulus $K_0(t)$ in terms of pressure fluctuations is given in eq. (16). We argue, however, that this relation provides the genuine isothermic compression modulus $K_T(t)$ only in the case of ideal thermostatting, or for long enough times, $t \gg \tau_T$, where τ_T is the thermostat-related temperature relaxation time. In the general case $K_T(t) \neq K_0(t)$ since $K_0(t)$ is a 'mixture' of isothermic and adiabatic responses (in particular, for $t \lesssim \tau_T$). We therefore arrived at the following challenge: to get all the response functions like $K_T(t)$ or the analogous adiabatic compression modulus $K_A(t)$ in the full time-range (to resolve all the relaxation processes in the physical system). In other words, the

goal was to predict the universal (thermostat-independent) [17] response functions of the very physical system based on correlation functions obtained for the extended thermostatted system. The relevant theory for the time-dependent heat capacity $c_v(t)$ was developed in ref. [13]. Its generalizations for the compression moduli (and the thermal pressure relaxation function $p_T(t)$) are presented in Appendices B, C (for $K_T(t)$) and Appendix D (for $K_A(t)$). The theory is based on the FDT relations between Laplace transforms of response and correlation functions. These relations are then converted into the real-time domain to get equations defining $K_T(t)$ and $K_A(t)$. This approach is valid for a rather wide range of 'decent' thermostats (cf. ref. [13]) including the NH thermostat used in our simulation studies. The relaxation moduli $K_T(t)$ and $K_A(t)$ for the pLJ system have been eventually obtained using eqs. (B10), (B30) and (D7), respectively. We anticipate that even more precise results can be obtained with eqs. (C12), (C15), (D19), (D20) that do not involve autocorrelations of the kinetic temperature often showing strong oscillations.

9. Using the general approach described above we calculated the isothermic ($K_T(t)$) and adiabatic ($K_A(t)$) relaxation functions at different temperatures and reveal that adiabatic moduli show much stronger short-time undershoots than $K_T(t)$ or $G(t)$ (cf. Figs. 7, 12 and 14). We also derived (cf. Appendix A) a simple approximate equation (A5) defining the adiabatic relaxation modulus $K_A(t)$ in terms of pressure, energy and temperature correlation functions and demonstrated numerically its validity for the pLJ model system. The approximation for $K_A(t)$ works amazingly well to $t \gtrsim 2$ (cf. Fig. 13).

10. The mean-square fluctuations (MSF) of shear stress and pressure along the trajectory are quantified by two fluctuation moduli, respectively, μ_F and η_F, which show qualitatively different temperature dependencies: while μ_F exhibits a clear maximum near T_g, η_F monotonically decreases on cooling (cf. Figs. 16(a) and 17). This means that the MSF of pressure, $\left\langle (p(t)-\bar{p})^2 \right\rangle$, decreases always faster than T, i.e., that $\left\langle (p(t)-\bar{p})^2 \right\rangle / T$ falls on cooling.

11. It is found that the instantaneous (affine) moduli for shear (μ_A) and compression (η_A) show a smooth temperature dependence around T_g for swapped configurations (method Sw-MD). By contrast we reveal a sharp increase of the quasi-static shear and compression moduli (μ_{sf} and $\eta_{sf} \approx K_{Ts}$, respectively) on cooling near T_g (cf. Fig. 17). A similar temperature behavior was found also for the quasi-static adiabatic compression modulus K_{As}. Remarkably, K_{As} stays roughly in the middle between η_A and K_{Ts}, and the 3 compression moduli (η_A, K_{Ts} and K_{As}) seem to nearly merge at zero temperature. Given that the fluctuation modulus $\eta_F \approx \eta_A - K_{Ts}$ is always positive for amorphous systems ($\eta_F = 0$ at $T = 0$ would imply that there is no stress relaxation at all, $K_0(t) = \text{const}$, which is impossible for systems with heterogeneous structure), we conclude that although the extrapolated η_F for the studied system does not vanish at $T = 0$, it decreases

---

[17] The basic idea is that the response functions must reflect the properties of a physical system as such, and therefore must be independent of its coupling to a thermostat. [13] For this reason the moduli like $\mu_A, \mu_F, \mu_{sf}, \eta_A, \eta_F, K_{Ts}, K_{As}$ are both ensemble- and thermostat-independent (as all these moduli are directly related to the response functions).

strongly at low temperatures.

12. We devise two procedures to improve the precision of the affine shear modulus μ_A and to reduce its standard deviation $\delta\mu_A$. They boil down to orientational averaging of μ_A by the coordinate frame rotations (cf. sect. 4) and to applying a linear regression to compensate for the mean pressure variations between the configurations (cf. Appendix F). Applied together these techniques lead to a dramatic reduction of $\delta\mu_A$: by a factor of 40 above T_g and a factor of 10 below T_g (cf. Fig. 15). It is also demonstrated that the pressure correction is important for the variance of the fluctuation shear modulus μ_F above T_g (cf. Fig. 16(c)). Turning to compression moduli, we found that while the standard deviations of the quasi-static and affine moduli ($\delta\eta_{sf}$ and $\delta\eta_A$) strongly depend on the mean pressure dispersion between the independent configurations, its effect is much weaker for $\delta\eta_F$ (cf. Fig. 18).

13. We predicted the height, h_T, of the terminal step for the isothermic relaxation modulus, $K_T(t)$, in the glassy regime, where the terminal process occurs in an inaccessible time range. The height h_T is obtained as the difference between the long-time plateau level (K_{Ts}) and the corresponding equilibrium compression modulus (K_{Te}) which was defined by an extrapolation of K_{Ts} from the liquid regime to lower temperatures ($T \lesssim T_g$). The analogous height of the terminal process for the adiabatic relaxation was obtained in a similar way as $h_A = K_{As} - K_{Ae}$. Well below T_g the isothermal step h_T is nearly constant and exceeds h_A for adiabatic relaxation by a factor of ~ 2.5 (cf. Fig. 17).

14. The assumption of Gaussian statistics for stress fluctuations works very well near and above T_g both for the shear stress and pressure. This concept leads to rather accurate quantitative predictions of the non-monotonic temperature dependencies for the standard deviations of both shear and compression fluctuation moduli, $\delta\mu_F^*$ and $\delta\eta_F^*$ (cf. Figures 16(b) and 18(b)). By contrast, both shear stress and pressure fluctuations become strongly non-Gaussian at low temperatures ($T \lesssim 0.2$).

15. We established that various shear moduli, μ_A, μ_F and μ_{sf}, are isotropic with the relative accuracy $\sim 0.1\%$ well below T_g. Around T_g the isotropy is less precise for μ_F and μ_{sf}: at $T \approx 0.24$ their relative angular variations rise to about 0.3% and 2%, respectively. This effect is apparently due to a stronger sensitivity of the shear modulus to variations of external parameters and its stronger dispersion within the ensemble near the glass transition. By contrast, the isotropy of the purely static affine modulus μ_A does not deteriorate near T_g (its accuracy gradually improves on heating and becomes $\sim 0.02\%$ at $T \approx 0.24$).

16. The compression relaxation moduli $K_T(t)$, $K_A(t)$ obtained using new FDT relations (cf. point 8 above) together with the shear relaxation modulus $G(t)$ and the time-dependent heat capacity $c_v(t)$ [13] largely define the linear viscoelastic properties of the system (as long as it is macroscopically isotropic and homogeneous, which is true for $T > T_f$). In particular, all the dynamical moduli and compliances like the Young modulus $E(t)$ or the creep compliance $J(t)$ (cf. refs. [33,34]) can be obtained on this basis. For example

$$J(s) = 1/G(s), \quad E_{T,A}(s) = \frac{G(s)d}{(d-1)/2 + (1/d)G(s)/K_{T,A}(s)} \tag{35}$$

where s indicates the s·Laplace transform defined in Appendix B, eq. (B8). A

simple way to obtain such and similar relations between the material functions [18] based on the analogous static relations is outlined at the end of Appendix D.

17. Our results could be pertinent for experimental systems of colloidal monolayers consisting of a binary mixture of superparamagnetic particles [42]. For such monolayers video-microscopy gives access to particle trajectories and allows for positional analysis as in 2D simulations [44]. Since in addition the interaction potential between the particles is known, shear and compression relaxation moduli can in principle be calculated. Such an analysis could complement prior studies of static strain fluctuations related to shear rigidity of the colloidal glass [41] and of spatio-temporal strain patterns that emerge in supercooled liquids [45].

8. The key results

I. Using the artificial MC dynamics involving swaps of particle diameters we managed to almost completely equilibrate the studied 2D pLJ model systems. Their equilibrium nature was carefully verified based on the following observations:

— The temperature dependence of density, $\rho(T)$, does not show any change of slope at the glass transition T_g (corresponding to solidification).

— Using swap MC moves also during the production runs we found that the shear stress correlation function rapidly decays to zero in this case indicating a complete stress relaxation during the tempering time.

— The same results are obtained on cooling from high T and on heating starting from quasi-crystalline configurations at $T = 0.01$. These configurations had been slowly heated and tempered using the Sw-MC method. At $T > 0.16$ they show only local clustering and quantitatively the same dynamical and static properties as their counterparts obtained on cooling from $T = 0.5$.

— The equilibrium FDT relation $\mu_0 = \mu_A$ is satisfied for the Sw-MC systems (cf. Fig. 6(b)).

II. The Sw-based systems at $T \lesssim T_g$, which can be considered as a thermodynamically equilibrium glass, show higher elastic moduli, much slower particle diffusion, and a more pronounced and longer plateau of the shear relaxation modulus $G(t)$, as compared to the SC-MC and SC-MD systems prepared by standard slow cooling. We thus not only confirmed a significant dependence of glass properties on its formation history, but also provided a tool to quantify the degree of deviation from equilibrium for an amorphous system.

The structure and properties of the Sw-equilibrated systems are likely to be similar to that of ultra-stable glasses obtained by vapour deposition, which are also supposed to be close to an equilibrium state [56]. Therefore, the Sw-systems we studied can serve as a simple model for vapour-deposited glasses.

III. An important step forward of the present manuscript beyond the prior work is the development of the linear response theory for the isothermic and adiabatic compression moduli (Appendices A to D). Together with the results for the shear relaxation modulus, this provides the general linear viscoelastic response

---

[18] These relations are useful in practice primarily in the regimes where inertial effects are not important.

of a system that is macroscopically homogeneous and isotropic. Small clusters of particles of similar size appear for Sw-based systems at $T = 0.2$, but all the systems remains macroscopically homogeneous and isotropic for $T > T_f \approx 0.16$. The developed theory is therefore applicable to all the systems we studied above the fractionation temperature.

IV. Both static shear and compression moduli (μ_{sf} and η_{sf}) strongly increase on cooling near T_g (cf. Figs. 16(a) and 17). Their behavior is sharp but continuous, so the system solidification occurs in a finite T-window ($0.23 \lesssim T \lesssim 0.28$) which can be read off from the peaks of standard deviations of the moduli, $\delta\mu^*_{sf}$ (Fig. 16(b)) and $\delta\eta^*_{sf}$ (Fig. 18(b)). These peaks are accurately reproduced with a theoretical approach assuming Gaussian statistics of stress fluctuations near and above T_g. The established temperature dependencies of the shear and bulk moduli, $\mu_{sf}(T)$ and $\eta_{sf}(T)$, are qualitatively similar to those obtained experimentally on colloidal monolayers of a binary mixture of superparamagnetic particles [42], albeit a much stronger increase of the bulk modulus near T_g was revealed for the experimental system.

Conflicts of interest

There are no conflicts of interest to declare.

Acknowledgements

A grant of computer time at the HPC computing cluster of the University of Strasbourg is gratefully acknowledged. We thank O. Benzerara and H. Meyer (all from Strasbourg) for assistance in some aspects of MD simulations and helpful discussions. L.K. was supported by a doctoral contract from the University of Strasbourg in the framework of the IRTG "Soft Matter Science".

APPENDIX A: General approach to calculate compression relaxation moduli

As explained in sections 5.2, 5.3 the isothermic and adiabatic pressure relaxation moduli, $K_T(t)$ and $K_A(t)$, cannot be obtained in the general case solely based on the pressure autocorrelation function $C_p(t)$ (so, generally, $K_T(t) \neq K_0(t)$, cf. sect. 5.2 and eq. (16)). However, as proposed in ref. [13] the response functions of thermostatted system can be (under certain conditions) expressed in terms of several correlation functions using appropriate FDT relations. A number of such relations eventually defining $K_T(t)$ and $K_A(t)$ are derived in Appendices B, C, D.

1. Isothermic modulus

Let us first consider the isothermic modulus, $K_T(t)$. It can be written as $K_T(t) = K_0(t) + \Delta K_T(t)$. The FDT expression for $\Delta K_T(t)$ is given in eq. (B30) in terms of the autocorrelation function of temperature, $C_T(t)$, and the thermal pressure response function $p_T(t)$ generalizing the thermodynamic derivative $\left(\frac{\partial p}{\partial T}\right)_{N,V}$ (cf. Appendix B, eq. (B20)). The function $p_T(t)$ can be calculated using another

FDT relation, eq. (B28), involving cross-correlation functions of pressure and energy, $C_{pE}(t)$, and of temperature and energy, $C_{TE}(t)$. Another way to obtain $K_T(t)$, which is more efficient numerically, is described in Appendix C.

While the correction $\Delta K_T(t)$ vanishes at $t \to \infty$, for finite times it accounts for the deformation-induced deviation of the instant kinetic temperature T from the thermostat (imposed) temperature. This deviation is rather small at $t = 0$ ($\Delta K_T(0) = -\frac{2}{d} T\rho$, cf. eq. (B32)), but it can significantly increase in time in the case of a weak system/thermostat coupling (large thermal mass Q for the NH thermostat). In our simulations this effect is avoided by using low Q's corresponding to a high Nosé frequency $\omega_Q \sim 100$ ($\omega_Q^2 = 2TNd/Q$), so that $\omega_Q \tau_f \sim 6$, where τ_f is the collision/vibration time. In this case, $\Delta K_T(t)$ remains always small and decays fast (during a short time ~ 0.2).

Thus, generally, the correction $\Delta K_T(t)$ significantly depends on the strength of the system/thermostat coupling. A similar effect was considered in ref. [13] for the dynamic heat capacity. For a strong coupling (a high Nosé frequency ω_Q) the correction time-range is short. However, the correction may become important if the system/thermostat coupling is too weak ($\omega_Q \tau_f \ll 1$) or too strong (for $\omega_Q \tau_f \gg 1$ in the case of a single NH thermostat).

2. Compression modulus

In this section we analyse the relaxation modulus for adiabatic compression, $K_A(t)$. As already mentioned, the canonic-affine deformation is adiabatic in nature, so the response at $t = 0$, $K_0(0)$, is equal to $K_A(0)$. However, the 2 functions are different for $t > 0$, and $K_A(t)$ normally exceeds $K_0(t)$.

Let us first consider the static limit, $t \to \infty$, assuming that the system can be eventually fully equilibrated after a perturbation. The following thermodynamic relation between adiabatic and isothermic moduli is valid in this regime:

$$K_A = \frac{c_p}{c_v} K_T \tag{A1}$$

where c_p, c_v are heat capacities (per particle) at constant pressure and volume, respectively. It leads to

$$K_A = K_T + \frac{T}{\rho} p_T^2 / c_v \tag{A2}$$

where

$$p_T = \left(\frac{\partial p}{\partial T} \right)_V = \alpha K_T \tag{A3}$$

is the thermal pressure, and $\alpha = \left(\frac{\partial \ln V}{\partial T} \right)_p$ is the thermal expansion coefficient.

In a glassy state the genuine equilibrium levels of p_T and c_v are not accessible, but they can be replaced by the corresponding long-time plateau values. It is tempting to consider p_T and c_v more generally as time-dependent functions, providing pressure and energy responses to a step-like T-increase (cf. eq. (B20) in Appendix B for $p_T(t)$ and ref. [13] for $c_v(t)$). In this spirit eq. (A2) can be empirically generalized as

$$K_A(t) \approx K_T(t) + \frac{T}{\rho} p_T(t)^2 / c_v(t) \tag{A4}$$

The above equation must be valid in the static limit ($t \to \infty$) and in the quasistatic glassy plateau regime where $t \ll \tau_\alpha$ (since the latter regime is essentially static as well, and the thermodynamic relations like eq. (A2) are valid not only at genuine equilibrium but also - albeit approximately - in a glassy state equilibrated within a metabasin [35,36,10]). Moreover, it is also correct at $t = 0$ where its r.h.s. is exactly equal to $K_A(0) = K_T(0) + \frac{2}{d} T\rho$. (Note that $p_T(0) = \rho$ and $c_v(0) = d/2$; cf. eq. (D27) in Appendix D.)

A rigorous approach allowing to calculate the adiabatic response is described in Appendix D. A number of relations between the Laplace-like s-transform of $K_A(t)$,

$$K_A(s) = s \int_0^\infty K_A(t) e^{-st} \mathrm{d}t$$

and similar transforms of correlation functions are established there. Some of these relations are then converted into the time-domain and expressed as equations which can be solved for $K_A(t)$, cf. eqs. (D5) and (D7). Remarkably, we also established an exact relation between the transformed response functions, eq. (D23), which is formally similar to eq. (A4) and can serve as a basis to justify its approximate validity. In a similar way, eq. (D5) generates the following approximate equation for the adiabatic relaxation modulus:

$$K_A(t) \approx K_0(t) + \frac{T}{\rho} p_{T0}(t)^2 / c_{v0}(t) \tag{A5}$$

It involves the functions $p_{T0}(t)$ and $c_{v0}(t)$ which are directly related to the correlation functions of energy and pressure (cf. eqs. (B18), (D4)), which were obtained by MD simulations.

APPENDIX B: FDT relations for isothermic compression relaxation modulus

1. Definition of the relaxation modulus

To obtain the isothermic bulk compression relaxation modulus $K_T(t)$ using FDT relations involving pressure and energy correlation functions we note first that the compression deformation, eq. (12), leads not only to a pressure increment

$$\Delta p(t) = \epsilon K_0(t) \tag{B1}$$

but also to a temperature variation:

$$\Delta T(t) = \epsilon \frac{T}{\rho} C_{Tp}(t), \tag{B2}$$

where

$$C_{Tp}(t) = \frac{N}{T^2} \langle \delta T(t + t') \delta p(t') \rangle \tag{B3}$$

Here and below $\langle ... \rangle$ mean both ensemble and gliding averaging as before, $\delta T(t) = T(t) - T_i$, $\delta p(t) = p(t) - \langle p \rangle$, and any non-linear terms (for $\epsilon \ll 1$) are omitted. An NVT_i ensemble is assumed by default (T_i is the temperature imposed by a thermostat). Eq. (B2) comes from the FDT [12,24,31].

In addition to the deformation, eq. (12), we consider 2 types of temperature perturbations: (i) a small jump-like velocity increase at $t = 0$:

$$v \to v(1 + \epsilon_v/d), \tag{B4}$$

and (ii) a small jump (ϵ_T) of the imposed temperature at $t = 0$:

$$T_i(t) = T_i - \epsilon_T \Theta(-t) \tag{B5}$$

where $\Theta(...)$ is the Heaviside function. By virtue of the FDT the T-perturbation (i) leads to the following responses (at $t > 0$):

$$\Delta p(t) = \epsilon_v T C_{pT}(t), \quad \Delta T(t) = \epsilon_v T C_T(t) \tag{B6}$$

where

$$C_T(t) = \frac{N}{T^2} \langle \delta T(t + t') \delta T(t') \rangle , \quad C_{pT}(t) = \frac{N}{T^2} \langle \delta p(t + t') \delta T(t') \rangle \tag{B7}$$

$C_{Tp}(t)$ is defined in a similar way; $C_{pT}(t) = C_{Tp}(t)$ is due to the time reversibility.

Combining eqs. (16), (17), (B1), (B2), (B3), (B6), (B7) and doing the following transform (labelled below as s·Laplace) for all response and correlation functions:

$$\Delta p(s) \equiv s \int \Delta p(t) e^{-st} \mathrm{d}t, \quad C_{pT}(s) \equiv s \int C_{pT}(t) e^{-st} \mathrm{d}t \tag{B8}$$

etc., we get the following responses to both a compression and a T-perturbation of type (i):

$$\Delta p(s) = \epsilon K_0(s) + \epsilon_v T C_{pT}(s), \quad \Delta T(s) = \epsilon \frac{T}{\rho} C_{Tp}(s) + \epsilon_v T C_T(s) \tag{B9}$$

To obtain the proper isothermic modulus K_T we must set $\Delta T(t) \equiv 0$. The latter condition cannot be satisfied with a constant ϵ_v. However, we may allow for a superposition of T-jumps (defined in eq. (B4)) occurring at any $t > 0$ (and not only at $t = 0$), which is equivalent to considering ϵ_v as a function of s. Then the condition $\Delta T(s) = 0$ leads to $\epsilon_v = -\epsilon C_{Tp}(s) / [\rho C_T(s)]$ and $\Delta p(s) = \epsilon K_T(s)$ with

$$K_T(s) = K_0(s) + \Delta K_T(s), \tag{B10}$$

$$\Delta K_T(s) = -\frac{T}{\rho} C_{pT}(s)^2 / C_T(s) \tag{B11}$$

Here and below the transforms defined in eqs. (B8) are indicated by s-variables only. The isothermic relaxation modulus, $K_T(t)$, can in principle be obtained by calculation of the Laplace transforms of $C_{pT}(t)$ and $C_T(t)$ correlation functions, and then by doing the inverse Laplace transform of $K_T(s)/s = \int_0^\infty K_T(t) e^{-st} \mathrm{d}t$. A more efficient alternative way is described below (in sect. 3).

2. Definition of the thermal pressure response $p_T(t)$ and general relations between its Laplace transform and the relaxation modulus

The T and p responses to a temperature perturbation of the second type (cf. eq. (B5)) are also related to the equilibrium correlation functions (as follows from the FDT [12,24,31,13]):

$$\Delta p(t) = \epsilon_T \left[C_{pE}(0) - C_{pE}(t)\right], \quad \Delta T(t) = \epsilon_T \left[C_{TE}(0) - C_{TE}(t)\right] \tag{B12}$$

where

$$C_{pE}(t) = T^{-2} \left\langle \delta p(t+t')\delta E(t') \right\rangle, \quad C_{TE}(t) = T^{-2} \left\langle \delta T(t+t')\delta E(t') \right\rangle \tag{B13}$$

Here the static correlations, $C_{TE}(0)$ and $p_{Ts0} \equiv C_{pE}(0)$, reflect the properties of the equilibrium canonic ensemble:

$$C_{TE}(0) = 1, \quad p_{Ts0} = p_{Ts} + C_{pE}(\infty) \tag{B14}$$

where

$$p_{Ts} \equiv \left(\frac{\partial p}{\partial T}\right)_{N,V} \tag{B15}$$

is the rate of change of the mean (equilibrium) pressure with temperature (thermal pressure), and $C_{pE}(\infty)$ is the long-time limit of $C_{pE}(t)$. Note that generally $C_{pE}(\infty) \neq 0$ in a glassy state.

Combining the above equations with eqs. (16), (17), (B1), (B2) we find s-transforms of the responses to both a compression and a T-perturbation of type (ii):

$$\Delta p(s) = \epsilon K_0(s) + \epsilon_T p_{T0}(s), \quad \Delta T(s) = \epsilon \frac{T}{\rho} C_{Tp}(s) + \epsilon_T \left[1 - C_{TE}(s)\right] \tag{B16}$$

where

$$p_{T0}(s) \equiv p_{Ts0} - C_{pE}(s) \tag{B17}$$

In the time-domain the latter equation becomes:

$$p_{T0}(t) \equiv C_{pE}(0) - C_{pE}(t) \tag{B18}$$

Using the same trick as before we find that the isothermic condition $\Delta T(t) \equiv 0$ (at $\epsilon = \text{const}$) leads to: $\epsilon_T = -\epsilon \frac{T}{\rho} C_{Tp}(s) / \left[1 - C_{TE}(s)\right]$ hence

$$K_T(s) = K_0(s) - \frac{T}{\rho} C_{Tp}(s) p_{T0}(s) / \left[1 - C_{TE}(s)\right] \tag{B19}$$

The time-dependent function $p_T(t)$ generalizing the thermodynamic constant p_{Ts} can be defined via the pressure increment Δp at time t after a step-like increase (by ΔT_0) of the ensemble-averaged temperature at $t = 0$:

$$p_T(t) = \Delta p(t) / \Delta T_0 \tag{B20}$$

Obviously $p_T(t=0)=\rho$. [19] Demanding that $\Delta T(t)=\Delta T_0\Theta(t)$ and using eqs. (B16) with $\epsilon=0$ and $\epsilon_T=\epsilon_T(s)$ we get

$$p_T(s)=\frac{p_{T0}(s)}{1-C_{TE}(s)} \tag{B21}$$

Applying the same operation to eqs. (B9) we obtain

$$p_T(s)=C_{pT}(s)/C_T(s) \tag{B22}$$

As the response functions (like $p_T(t)$) must be universal (independent of how the T-perturbation was created, cf. ref. [13]), eqs. (B21), (B22) define the same function and lead to an exact relation between pressure/energy correlation functions (valid in the thermodynamic limit $N\to\infty$):

$$C_T(s)\left[p_{Ts0}-C_{pE}(s)\right]=C_{pT}(s)\left[1-C_{TE}(s)\right] \tag{B23}$$

This relation is akin to eq. 19 of ref. [13] which reads

$$C_T(s)\left[c_{vs0}-C_E(s)\right]=C_{TE}(s)\left[1-C_{TE}(s)\right] \tag{B24}$$

where

$$C_E(t)=\langle\delta E(t+t')\delta E(t')\rangle\,/\left(NT^2\right) \tag{B25}$$

and

$$c_{vs0}=C_E(t=0) \tag{B26}$$

Eq. (B23) also ensures that the two results for $K_T(s)$ obtained above (eqs. (B11), (B19)) are equivalent, thus supporting the idea of universality of the isothermic modulus $K_T(t)$.

Finally, we note that eqs. (B19), (B21), (B22) lead to

$$\Delta K_T(s)=-\frac{T}{\rho}C_T(s)p_T(s)^2=-\frac{T}{\rho}C_{pT}(s)p_T(s) \tag{B27}$$

It shows that once $p_T(t)$ is known, the relaxation modulus $K_T(t)$ can be readily calculated by convolutions.

3. Equations defining $K_T(t)$.

In the previous sections we established the relations between Laplace transforms of response functions $K_T(t)$, $p_T(t)$ and of equilibrium correlation functions which can be easily calculated using thermostatted simulations. However, in order to obtain the response functions one would have to do direct and inverse Laplace transforms which may pose a formidable problem given that some of these functions may show

---

[19] Note that $p_T(t)$ is related to the relaxation coefficient of volumetric thermal expansion whose s·Laplace transform is equal to $p_T(s)/K_T(s)$.

significant oscillations. A way to bypass this problem was outlined in ref. [13] where the time-dependent heat capacity was calculated using similar relations. The basic idea is to transform the relevant relations into the time domain (to get rid of Laplace transforms), and to use the least oscillating correlation functions. The first part of this program is outlined below, the second part is clarified in the Appendix C.

Eq. (B27) connects the Laplace transforms of the isothermic modulus $K_T(t)$ and of the thermal pressure response function $p_T(t)$. To obtain the latter function we recall eqs. (B21), (B17) leading to

$$p_T(s)\,[1 - C_{TE}(s)] = p_{Ts0} - C_{pE}(s)$$

and note that the above equation is equivalent to the following relation between the time-dependent functions:

$$\int_0^t p_T(t-t')\frac{\mathrm{d}}{\mathrm{d}t'}C_{TE}(t')\mathrm{d}t' = C_{pE}(t) - p_{Ts0} \tag{B28}$$

This equation can be easily solved for $p_T(t)$ in the iterative manner. [20] The solution is unique and stable. Its stability follows from the following property of $C_{TE}(s)$: there are no roots of $1 - C_{TE}(s)$ with $\Re(s) > 0$. It can be proved using eq. (B24) and the approach detailed in the Appendix C of ref. [13].

Finally we get using the second eq. (B27) and the obtained $p_T(t)$:

$$\Delta K_T(t) = -TC_{pT}(t) - \frac{T}{\rho}\int_0^t C_{pT}(t-t')\mathrm{d}p_T(t') \tag{B29}$$

Alternatively, the isothermic modulus can be found based on the first eq. (B27):

$$\Delta K_T(t) = -\rho TC_T(t) - \frac{T}{\rho}\int_0^t C_T(t-t')\mathrm{d}p_{T2}(t') \tag{B30}$$

where

$$p_{T2}(t) \equiv \rho p_T(t) + \int_0^t p_T(t-t')\mathrm{d}p_T(t') \tag{B31}$$

Note that at $t = 0$: $p_T(0) = \rho$, $p_{T2}(0) = \rho^2$ and $C_T(0) = 2/d$, so (on recalling eq. (B10))

$$K_T(0) = K_0(0) - \frac{2}{d}T\rho \tag{B32}$$

The second term in the last equation is typically rather small for supercooled liquids.

---

[20] More precisely, the time-variable is first discretized with step δt: $t_i = i\delta t$, and the functions $p_T(t)$, $C_{TE}(t)$ are approximated on each segment $(t_i - \delta t < t < t_i)$ by their constant mean values $p_T^{(i)}$, $C_{TE}^{(i)}$, $i = 1, 2...$ Then eq. (B28) is applied at $t = t_1, t_2, ...$ to get one-by-one the values $p_T^{(1)}$, $p_T^{(2)}$,... .

APPENDIX C: Isothermic compression modulus in terms of correlations of potential energy and excess pressure

The function $C_{TE}(t)$ shows significant oscillations at short t. Besides, $1-C_{TE}=0$ at $t=0$ ($s\to\infty$). Both these features lead to a poor precision of $p_T(t)$ obtained from eqs. (B21), (B28) at short t. For better precision it is beneficial to use variables that are coupled weaker to the instantaneous temperature. Such more useful variables are the potential energy U and the excess pressure p_{ex} instead of total energy E and total pressure p:

$$U = E - TNd/2, \quad p_{ex} = p - \rho T$$

Here $TNd/2 = K$ is the kinetic energy, $\rho T = p_{id}$ is the ideal-gas pressure due to momenta of the particles (p_{ex} is due to their interactions).

The relevant correlation functions of U and p_{ex} are (cf. eqs. (B7), (B13), (B25)):

$$C_U(t) = \langle \delta U(t+t')\delta U(t')\rangle \,/\, \left(NT^2\right), \;\; C_{UE}(t) = \langle \delta U(t+t')\delta E(t')\rangle \,/\, \left(NT^2\right),$$

$$C_{p_{ex}}(t) = \frac{N}{T^2}\,\langle \delta p_{ex}(t+t')\delta p_{ex}(t')\rangle$$

$$C_{Tp_{ex}}(t) = \frac{N}{T^2}\,\langle \delta T(t+t')\delta p_{ex}(t')\rangle = C_{p_{ex}T}(t) \tag{C1}$$

The function $C_{p_{ex}}(t)$ defines the response of p_{ex} after a small compression

$$x \to (1-\epsilon/d)x \tag{C2}$$

which does not affect the particle velocities (hence this transformation in the phase space is not canonical). The relevant FDT relations are:

$$\Delta p_{ex}(t) = \epsilon\left[\frac{T}{\rho}C_{p_{ex}}(t) + K^{ex}_{Ts0}\right] \tag{C3}$$

and

$$\Delta T(t) = \epsilon\frac{T}{\rho}C_{Tp_{ex}}(t) \tag{C4}$$

where $K^{ex}_{Ts0} \equiv \eta^{ex}_A - \frac{T}{\rho}C_{p_{ex}}(t=0)$ and $\eta^{ex}_A = \eta_A - \frac{d+2}{d}\rho T$ is the excess part of the affine compression modulus (cf. eq. (13)).

Next, turning to the T-perturbation of the first type, eq. (B4), we find

$$\Delta p_{ex}(t) = \epsilon_v T C_{p_{ex}T}(t), \quad \Delta T(t) = \epsilon_v T C_T(t) \tag{C5}$$

The analogous FDT relations associated with the second T-perturbation, eq. (B5), are:

$$\Delta p_{ex}(t) = \epsilon_T\left[C_{p_{ex}E}(0) - C_{p_{ex}E}(t)\right], \quad \Delta T(t) = \epsilon_T\left[C_{TE}(0) - C_{TE}(t)\right] \tag{C6}$$

where (cp. eq. (B13))

$$C_{p_{ex}E}(t) = T^{-2}\,\langle \delta p_{ex}(t+t')\delta E(t')\rangle \tag{C7}$$

The isothermal excess modulus $K_T^{ex}(t)$ (defining excess pressure response to a small compression at constant T) and the excess thermal pressure coefficient $p_T^{ex}(t)$ can be obtained using the above equations following the approach described in Appendix B. In particular, we get

$$p_T^{ex}(s) = \frac{p_{Ts0}^{ex} - C_{p_{ex}E}(s)}{1 - C_{TE}(s)} = C_{p_{ex}T}(s)/C_T(s) \tag{C8}$$

where $p_{Ts0}^{ex} = C_{p_{ex}E}(t=0)$, leading to

$$C_T(s)\,[p_{Ts0}^{ex} - C_{p_{ex}E}(s)] = C_{p_{ex}T}(s)\,[1 - C_{TE}(s)] \tag{C9}$$

The latter equation is equivalent to eq. (B23) since $C_{pE}(s) = C_{p_{ex}E}(s) + \rho C_{TE}(s) +$ const and $C_{pT}(s) = C_{p_{ex}T}(s) + \rho C_T(s)$ as follows from $p = p_{ex} + \rho T$. In a similar way we get the excess compression modulus:

$$K_T^{ex}(s) = \frac{T}{\rho} C_{p_{ex}}(s) + K_{Ts0}^{ex} - \frac{T}{\rho} C_{p_{ex}T}(s) p_T^{ex}(s) \tag{C10}$$

Taking into account that obviously $K_T(t) = K_T^{ex}(t) + \rho T$, we arrive at

$$K_T(s) = \rho T + K_{Ts0}^{ex} + \frac{T}{\rho} C_{p_{ex}}(s) - \frac{T}{\rho} C_{p_{ex}T}(s) p_T^{ex}(s) \tag{C11}$$

In the time domain it reads (on using $p_T^{ex}(t=0) = 0$)

$$K_T(t) = \rho T + K_{Ts0}^{ex} + \frac{T}{\rho}\left[C_{p_{ex}}(t) - \int_0^t C_{p_{ex}T}(t-t')\mathrm{d}p_T^{ex}(t')\right] \tag{C12}$$

where $\mathrm{d}p_T^{ex}(t') = \frac{\mathrm{d}p_T^{ex}(t')}{\mathrm{d}t'}\mathrm{d}t'$.

It remains therefore to obtain $p_T^{ex}(t)$. Using eqs. (C8) we get

$$p_T^{ex}(s) = \frac{p_{Ts0}^{ex} - C_{p_{ex}U}(s)}{1 - C_{TU}(s)} \tag{C13}$$

where $C_{p_{ex}U}(s)$, $C_{TU}(s)$ are the s-transforms of

$$C_{p_{ex}U}(t) = T^{-2}\,\langle \delta p_{ex}(t+t')\delta U(t')\rangle\,, \quad C_{TU}(t) = T^{-2}\,\langle \delta T(t+t')\delta U(t')\rangle \tag{C14}$$

The corresponding equation for $p_T^{ex}(t)$ is

$$p_T^{ex}(t) = p_{Ts0}^{ex} - C_{p_{ex}U}(t) + \int_0^t C_{TU}(t-t')\mathrm{d}p_T^{ex}(t') \tag{C15}$$

This equation is similar to eq. 48 of ref. [13]. It can be solved iteratively starting from $t = 0$; it has a unique and stable solution (cf. ref. [13] for details). Note that $p_T^{ex} = 0$ and $C_{p_{ex}U} = p_{Ts0}^{ex}$ at $t = 0$ (corresponding to $s \to \infty$) as follows from the first eq. (C6). Eq. (C15) also defines the full response function $p_T(t)$ due to the obvious relation

$$p_T(t) = p_T^{ex}(t) + \rho$$

An advantage of eqs. (C15) and (C12) defining the relaxation isothermic bulk compression modulus over eqs. (B28), (B29) is that the correlation functions (like $C_{p_{ex}U}(t)$, $C_{TU}(t)$) involved in eqs. (C15), (C12) show much weaker oscillations than those (like $C_{pE}(t)$, $C_{TE}(t)$) involved in eqs. (B28), (B29). This feature results in a higher numerical precision of the eventually evaluated time-dependent response functions.

APPENDIX D: FDT relations for adiabatic compression relaxation modulus

The adiabatic condition means that no heat is transferred into (or out of) the system. It therefore implies that the initial deformation (ϵ-compression at $t = 0$) must be a canonical affine transformation of the phase space given in eq. (12), and that the energy E is conserved afterwards:

$$E = \text{const}\,, \quad t > 0 \tag{D1}$$

since no work is done by the system ($V = \text{const}$). In the case of a thermostatted system (in particular, with the Nose-Hoover dynamics we consider) there is permanent heat exchange between the system and the thermostat, so the condition (D1) must be maintained by additional compensating heat transfers due to, for example, the T_i-perturbations defined in eq. (B5). Let us therefore focus on the pressure p and the energy E responses. Considering now 2 perturbations defined in eqs. (12) and eq. (B5), respectively, we get in analogy with eqs. (B16): [21]

$$\Delta p(s) = \epsilon K_0(s) + \epsilon_T p_{T0}(s), \quad \Delta E(s) = \epsilon VT\left[C_{Ep}(s) - p_{Ts0}\right] + \epsilon_T N c_{v0}(s) \tag{D2}$$

where $p_{T0}(s)$ is defined in eq. (B17), $p_{Ts0} = C_{Ep}(t = 0)$ and

$$c_{v0}(s) \equiv c_{vs0} - C_E(s) \tag{D3}$$

(cf. eqs. (B14), (B26)). Upon conversion into the time-domain eq. (D3) becomes

$$c_{v0}(t) = C_E(0) - C_E(t) \tag{D4}$$

The condition (D1) implies that $\Delta E(t) = 0$ at $t > 0$, hence $\Delta E(s) = 0$. The functions $\epsilon_T = \epsilon_T(s)$ and $K_A(s) \equiv \Delta p(s)/\epsilon$ are then obtained using eqs. (D2) for $\epsilon = \text{const}$ and $\Delta E(s) = 0$:

$$\epsilon_T = \epsilon \frac{T}{\rho} \frac{p_{T0}(s)}{c_{vs0} - C_E(s)}$$

$$K_A(s) = K_0(s) + \Delta K(s), \quad \Delta K(s) \equiv \frac{T}{\rho} p_{T0}(s)^2 / c_{v0}(s) \tag{D5}$$

Converting the above equations into the time domain we get

$$K_A(t) = \frac{T}{\rho} C_p(t) + K_{Ts0} + \Delta K(t) \tag{D6}$$

where $K_{Ts0} = \eta_A - \frac{T}{\rho} C_p(t = 0)$ and the function $\Delta K(t)$ is defined by the following equation

$$\int_0^t \Delta K(t - t')\mathrm{d}c_{v0}(t') = \frac{T}{\rho} \int_0^t p_{T0}(t - t')\mathrm{d}p_{T0}(t') \tag{D7}$$

---

[21] Here by $\Delta E(t)$ we mean $E(t) - E(t = 0^+)$.

where $c_{v0}(t)$ and $p_{T0}(t)$ are defined in eqs. (D4), (B18), respectively. Thus, the adiabatic relaxation modulus $K_A(t)$ can be easily obtained by solving eq. (D7) for $\Delta K(t)$ using the same numerical approach as described below eq. (B28).

The adiabatic modulus $K_A(t)$ can be also obtained based on correlation functions involving excess pressure p_{ex} and potential energy U (in analogy with the isothermic modulus $K_T(t)$, cf. Appendix C). To this end one could use the approach detailed in Appendix C based on new FDT relations. However, we take a slightly different route: instead of considering new FDT relations we simply use the already established eqs. (D5) and transform them in order to get rid of correlation functions of variables that explicitly depend on T. This is achieved using the general relation

$$p_{T0}(s)/c_{v0}(s) = p_T(s)/c_v(s), \tag{D8}$$

and trivial relations coming from $E = U + NdT/2$ and $p = p_{ex} + \rho T$:

$$C_E(s) = C_{UE}(s) + \frac{d}{2} C_{TE}(s), \quad C_{pE}(s) = C_{p_{ex}E}(s) + \rho C_{TE}(s) + \text{const} \tag{D9}$$

Here $p_{T0}(s)$, $c_{v0}(s)$ and $p_T(s)$ are defined in eqs. (B17), (D3), (B21), and $c_v(s)$ is the s·Laplace transform of the time-dependent isochoric heat capacity, $c_v(t)$, obtained in ref. [13] (cf. eq. 13 there):

$$c_v(s) = c_{v0}(s) / \left[1 - C_{TE}(s)\right] \tag{D10}$$

On using eq. (B24) one finds

$$\left[c_{vs0} - d/2 - C_U(s)\right] C_T(s) = C_{TU}(s) \left[1 - C_{TU}(s)\right] \tag{D11}$$

so

$$c_v(s) = \frac{c_{vs0} - C_{EU}(s)}{1 - C_{TU}(s)} \tag{D12}$$

Similarly we get on using either eq. (C9) or (B23):

$$\left[p^{ex}_{Ts0} - C_{p_{ex}U}(s)\right] C_T(s) = C_{p_{ex}T}(s) \left[1 - C_{TU}(s)\right] \tag{D13}$$

leading to (in view of eq. (B22))

$$p_T(s) = \frac{p_{Ts0} - C_{pU}(s)}{1 - C_{TU}(s)} \tag{D14}$$

and

$$\frac{p_{T0}(s)}{c_{v0}(s)} = \frac{p_{Ts0} - C_{pU}(s)}{c_{vs0} - C_{EU}(s)} \tag{D15}$$

Another useful relation comes from eqs. (D13), (D11):

$$\left[p^{ex}_{Ts0} - C_{p_{ex}U}(s)\right] C_{TU}(s) = C_{p_{ex}T}(s) \left[c_{vs0} - d/2 - C_U(s)\right] \tag{D16}$$

The above relations allow to exclude the temperature correlation function $C_T(s)$ from the adiabatic modulus defined in eqs. (D5)

$$K_A(s) = K_0(s) + \frac{T}{\rho}\frac{p_{T0}(s)^2}{c_{v0}(s)} = K_{Ts0} + \frac{T}{\rho}\left[C_p(s) + p_{T0}(s)\frac{p_{Ts0} - C_{pU}(s)}{c_{vs0} - C_{EU}(s)}\right]$$

The result is

$$K_A(s) = K^{ex}_{Ts0} + \frac{2+d}{d}\rho T + \frac{T}{\rho}C_{p_{ex}}(s) + \frac{T}{\rho}h(s) \tag{D17}$$

where

$$h(s) = \frac{\left[p^{ex}_{Ts0} - C_{p_{ex}U}(s)\right]\left[p^{ex}_{Ts0} + 2\rho - C_{p_{ex}E}(s)\right] - \frac{2}{d}\rho^2\left[c_{vs0} - \frac{d}{2} - C_U(s)\right]}{c_{vs0} - C_{EU}(s)} \tag{D18}$$

The adiabatic relaxation modulus $K_A(t)$ can be deduced from eq. (D17):

$$K_A(t) = K^{ex}_{Ts0} + \frac{2+d}{d}\rho T + \frac{T}{\rho}C_{p_{ex}}(t) + \frac{T}{\rho}h(t) \tag{D19}$$

where the function $h(t)$ is defined by equation

$$\int_0^t \left[c_{vs0} - C_{EU}(t-t')\right]\mathrm{d}h(t') = \frac{2}{d}\rho^2\left(C_U(t) - c_{vs0}\right) + \left(p^{ex}_{Ts0} + \rho\right)^2 - \tag{D20}$$

$$-\left(p^{ex}_{Ts0} + 2\rho\right)C_{p_{ex}U}(t) + \int_0^t C_{p_{ex}E}(t-t')\mathrm{d}C_{p_{ex}U}(t')$$

with $h(t=0) = 0$, as follows from eq. (D18) and the general relation $h(t=0) = h(s \to \infty)$.

Eq. (D20) can be solved in the same way as eq. (D7). Although eq. (D20) seems to be more complicated, it can provide better numerical precision since the function $c_{v0}(t) = c_{vs0} - C_E(t)$ involved in eq. (D7) generally shows stronger short-time oscillations than the function $C_{EU}(t-t')$ in the l.h.s. of eq. (D20). In the case of strong system/thermostat coupling (for example, for the Nosé-Hoover thermostat with low enough thermal mass Q) the T-fluctuations relax fast (during a short time $\sim \tau_N = \sqrt{2}/\omega_Q$), so all correlations involving T vanish for $t \gg \tau_N$. In this regime, the relevant correlations involve only p_{ex} and U, so eq. (D17) can be simplified as

$$K_A(s) \simeq K^{ex}_{Ts0} + \rho T + \frac{T}{\rho}\left[C_{p_{ex}}(s) + \frac{\left(p^{ex}_{Ts0} + \rho - C_{p_{ex}U}(s)\right)^2}{c_{vs0} - C_U(s)}\right] \tag{D21}$$

Setting $s = 0$ (corresponding to the static limit $t \to \infty$) we get the static adiabatic modulus K_{As}:

$$K_{As} = K_{Ts} + \frac{T}{\rho}\frac{p^2_{Ts}}{c_{vs}} \tag{D22}$$

in agreement with the general thermodynamic relation between adiabatic and isothermic compression moduli. [12]

Finally, note a simple relation between K_A and K_T:

$$K_A(s) = K_T(s) + \frac{T}{\rho}\frac{p_T(s)^2}{c_v(s)} \tag{D23}$$

which can be transformed as

$$K_A(s) = K_T(s) + \frac{T}{\rho} p_T(s) \frac{p_{Ts0} - C_{pU}(s)}{c_{vs0} - C_{EU}(s)} \tag{D24}$$

and used to calculate $K_A(t)$ once the functions $K_T(t)$ and $p_T(t)$ are known. A similar equation for the isobaric heat capacity $c_p(s)$ reads:

$$c_p(s) = c_v(s) + \frac{T}{\rho} \frac{p_T(s)^2}{K_T(s)} \tag{D25}$$

Both eqs. (D23), (D25) can be proved using the general relations derived above. Again, eq. (D25) has exactly the same form as the corresponding static relation [12]:

$$c_{ps} = c_{vs} + \frac{T}{\rho} \frac{p_{Ts}^2}{K_{Ts}} \tag{D26}$$

Taking $s \to \infty$ in eq. (D23) leads to a simple relations between instantaneous moduli (at $t = 0$):

$$K_A(0) = K_T(0) + \frac{T}{\rho} \frac{p_T(0)^2}{c_v(0)} = K_T(0) + \frac{2}{d} \rho T \tag{D27}$$

where we took into account that $p_T(0) = \rho$ (since instantaneous pressure response to a T-jump involves solely the ideal-gas pressure) and $c_v(0) = d/2$ (for a similar reason).

Eqs. (D23), (D25) have exactly the same structure as the classical thermodynamic relations for the corresponding static quantities (cf. eqs. (D22), (D26)). This feature can be in fact more general: any equilibrium relation between thermodynamic derivatives generates an analogous relation between the corresponding dynamical response functions (in the s·Laplace representation). There is no general proof of this statement, but we can provide a few hints pointing to its validity: (i) The examples given above show that the relations between response functions do not depend explicitly on the Laplace parameter s (generally, this is an assumption which can be easily checked). (ii) The $s \to 0$ limit of a response function can be reduced to a thermodynamic derivative. (iii) All static relations between the thermodynamic derivatives coming from differentiation rules (like the chain rule) have their dynamical analogs based on the Boltzmann superposition principle. (iv) All symmetry relations between cross-derivatives (like $\frac{\partial p}{\partial T}\Big|_V = \frac{\partial S}{\partial V}\Big|_T$) have their dynamical counterparts (symmetry relations between linear response functions) which follow from the time-reversibility of the dynamics being akin to the Onsager's principle of symmetry for kinetic coefficients. [30]

APPENDIX E: Impulsive correction to μ_A

The orientation-averaged instantaneous affine shear modulus μ_A^{or} is defined in eq. (4). A straightforward way to employ it is to use analytical expressions for $u'(s)$ and $u''(s)$ valid for $s < s_{cut}$. This way yields $\mu_A^{or(0)} \neq \mu_A^{or}$. The problem is that the potential $u(s)$ shows a kink at $s = s_{cut}$ leading to a singular contribution,

$-u'(s_{cut})\delta(s-s_{cut})$, in $u''(s) \equiv \mathrm{d}^2u/\mathrm{d}s^2$. This contribution gives rise to the so-called impulsive correction [5,8,10]:

$$\mu_A^{or} = \mu_A^{or(0)} + \Delta\mu_A$$

In the present study $\Delta\mu_A$ was calculated directly by approximating the δ-function as

$$f_\Delta(s) = \Delta^{-1}\left[4 - 6\left(s_{cut} - s\right)/\Delta\right]\Theta(s_{cut} - s)\Theta(\Delta + s - s_{cut}) \qquad \text{(E1)}$$

where $\Theta(.)$ is the Heaviside function, and the width $\Delta = 0.025$ was chosen to satisfy 2 conditions: $\Delta \ll 1$ and $s_{cut}\rho N\Delta \gg 1$. Eq. (E1) comes from the condition that $\delta(s - s_{cut})$ is approximated by a function which must be nonzero in the interval $s_{cut} - \Delta < s < s_{cut}$ whose center differs from the position of the original δ-function. The resulting impulsive correction is negative:

$$\Delta\mu_A = -\frac{u'(s_{cut})}{Vd(d+2)}\sum_l s^2 f_\Delta(s) \qquad \text{(E2)}$$

APPENDIX F: How to reduce the effect of pressure fluctuations on a variable X

The method described below is applicable to any macroscopic variable X including $X = \mu_A$ and $X = \eta_A$. A pressure dispersion is inevitable even in the ensembles aimed to keep a constant pressure. As explained in sect. 2 the volume of each configuration was quenched after the equilibration stage (tempering in the NPT ensemble), so that the m independent systems have slightly different volumes and their time-averaged pressures,

$$\bar{p} = \frac{1}{\Delta t}\int_0^{\Delta t} p(t)\mathrm{d}t$$

obtained from the NVT production runs for each system, deviate from the imposed pressure p_0. These deviations result in quenched shifts of the chosen variable X for all the configurations (unless X is totally pressure-independent). To compensate for this effect we used a linear regression approach: both X and $\bar{p}$ have been measured for each system, and then X was replaced by $X^* = X + \alpha(p_0 - \bar{p})$, where the coefficient $\alpha = \langle X\left(\bar{p} - p_{av}\right)\rangle / \left\langle\left(\bar{p} - p_{av}\right)^2\right\rangle$ and $p_{av} = \langle\bar{p}\rangle$ is the mean pressure averaged over the m-ensemble. This way we obtain a set of m values of X^* whose ensemble-average $\langle X^*\rangle = \langle X\rangle + \alpha\left(p_0 - p_{av}\right)$ corresponds to $p = p_0$. At the same time the standard deviation of the X^*-set gets minimized.

REFERENCES

[1] R. B. Bird, R. C. Armstrong and O. Hassager, *Dynamics of Polymeric Liquids: Fluid Mechanics*, Wiley, NY, 1987.

[2] L. Klochko, J. Baschnagel, J. P. Wittmer and A. N. Semenov, *Soft Matter*, 2018, **14**, 6835.

[3] A. Cavagna, *Phys. Rep.*, 2009, **476**, 51.

[4] J. Zhao, S. L. Simon and G. B. McKenna, *Nature Comm.,* 2013, **4**, 1783.

[5] I. Kriuchevskyi, J. P. Wittmer, H. Meyer, O. Benzerara and J. Baschnagel, *Phys. Rev. E*, 2018, **97**, 012502.

[6] I. Kriuchevskyi, J. P. Wittmer, H. Meyer, and J. Baschnagel, *Phys. Rev. Lett.*, 2017, **119**, 147802.

[7] I. Kriuchevskyi, J. Wittmer, O. Benzerara, H. Meyer and J. Baschnagel, *Eur. Phys. J. E*, 2017, **40**, 43.

[8] H. Xu, J. P. Wittmer, P. Polińska and J. Baschnagel, *Phys. Rev. E*, 2012, **86**, 046705.

[9] J. P. Wittmer, H. Xu, P. Polińska, F. Weysser and J. Baschnagel, *J. Chem. Phys.*, 2013, **138**, 12A533.

[10] L. Klochko, J. Baschnagel, J. P. Wittmer and A. N. Semenov, *J. Chem. Phys.*, 2019, **151**, 054504.

[11] M. P. Allen and D. J. Tildesley, *Computer Simulation of Liquids*, Oxford University Press, Oxford, 2017.

[12] L. D. Landau and E. M. Lifshitz, *Statistical Physics*, Pergamon Press, Oxford, 1998.

[13] L. Klochko, J. Baschnagel, J. P. Wittmer and A. N. Semenov, *J. Chem. Phys.*, 2021, **154**, DOI: 10.1063/5.0046697.

[14] J. P. Wittmer, H. Xu, O. Benzerara and J. Baschnagel, *Mol. Phys.*, 2015, **113**, 2881.

[15] J. P. Wittmer, H. Xu, P. Polińska, F. Weysser and J. Baschnagel, *J. Chem. Phys.*, 2013, **138**, 191101.

[16] L. Klochko, J. Baschnagel, J. P. Wittmer, O. Benzerara, C. Ruscher and A. N. Semenov, *Phys. Rev. E*, 2020**,** **102**, 042611.

[17] G. George, L. Klochko, A. N. Semenov, J. Baschnagel and J. P. Wittmer, *Eur. Phys. J. E*, 2021, **44**, 13.

[18] H. Eslami, P. Sedaghat and F. Müller-Plathe, *Phys. Chem. Chem. Phys.*, 2018, **20**, 27059.

[19] J. Russo and H. Tanaka, *Proc. Natl. Acad. Sci. U.S.A.*, 2015, **112**, 6920.

[20] E. Flenner and G. Szamel, *Nat. Commun.*, 2015, **6**, 7392.

[21] J. P. Wittmer, A. Tanguy, J.-L. Barrat and L. Lewis, *Europhys. Lett.*, 2002, **57**, 423.

[22] A. Tanguy, J. P. Wittmer, F. Leonforte and J.-L. Barrat, *Phys. Rev. B*, 2002, **66**, 174205.

[23] A. Ninarello, L. Berthier and D. Coslovich, *Phys. Rev. X*, 2017, **7**, 021039.

[24] J. P. Hansen and I. R. McDonald, *Theory of Simple Liquids*, Academic Press, NY, 2006.

[25] S. C. Plimpton, *Comput. Phys.*, 1995, **117**, 1. https://lammps.sandia.gov/doc/Manual.html

[26] F. Varnik, *Molecular Dynamics Simulations on the Glass Transition in Macromolecular Films*, PhD thesis, Johannes Gutenberg University, Mainz, 2001.

[27] G. George, L. Klochko, A. N. Semenov, J. Baschnagel, and J. P. Wittmer, *Eur. Phys. J. E*, 2021, **44**, 54.
[28] J. S. Rowlinson, *Liquids and Liquid Mixtures*, Butterworths, London, 1959.
[29] H. B. Callen, *Thermodynamics and an Introduction to Thermostatistics*, Wiley, New York, 1985.
[30] Onsager, L. Reciprocal relations in irreversible processes. II, *Phys. Rev.*, 1931, **38**, 2265-2279.
[31] D. Forster, *Hydrodynamic Fluctuations, Broken Symmetry, and Correlation Fluctuations*, Benjamin Cummings, London, 1983.
[32] E. B. Tadmor and R. E. Miller, *Modeling Materials*, Cambridge University Press, Cambridge, 2011.
[33] J. D. Ferry, *Viscoelastic Properties of Polymers*, John Wiley and Sons, New York, 1980.
[34] L. D. Landau and E. M. Lifshitz, *Theory of Elasticity*, Pergamon Press, New York, 1959.
[35] P. G. Debenedetti and F. H. Stillinger, *Nature*, 2001, **410**, 259.
[36] H. Yoshino, *J. Chem. Phys.*, 2012, *136*, 214108.
[37] J.-L. Barrat, J.-N.Roux, J.-P. Hansen and M.L.Klein, *Europhys. Lett.*, 1988, **7**, 707.
[38] X. Wang, S. Ramirez-Hinestrosa, J. Dobnikar and D. Frenkel, *Phys. Chem. Chem. Phys.*, 2019, **22**, 10624.
[39] D. Frenkel and B. Smit, *Understanding Molecular Simulation*, Academic Press, London, 2002.
[40] C. Ruscher, S. Ciarella, C. Luo, L. M. C. Janssen, J. Farago and J. Baschnagel, *J. Phys.: Condens. Matter*, 2021, **33**, 064001.
[41] C. L. Klix, F. Ebert, F. Weysser, M. Fuchs, G. Maret and P. Keim, *Phys. Rev. Lett.*, 2012, **109**, 178301.
[42] C. L. Klix, G. Maret and P. Keim, *Phys. Rev. X*, 2015, **5**, 041033.
[43] H. Yoshino and F. Zamponi, *Phys. Rev. E*, 2014, **90**, 022302.
[44] F. Ebert, P. Dillmann, G. Maret and P. Keim, *Rev. Sci. Inst.*, 2009, **80**, 083902.
[45] B. Illing, S. Fritschi, D. Hajnal, C. Klix, P. Keim and M. Fuchs, *Phys. Rev. Lett.*, 2016, **117**, 208002.
[46] A. Lemaître, *Phys. Rev. Lett.*, 2014, **113**, 245702.
[47] S. Fritschi and M. Fuchs, *J. Phys.: Condens. Matter*, 2018, **30**, 024003.
[48] E. Flenner and G. Szamel, *Proc. Natl. Acad. Sci. USA*, 2019, **116**, 2015.
[49] L. Berthier and W. Kob, *J. Phys.: Condens. Matter*, 2007, **19**, 205130.
[50] D. Coslovich, A. Ninarello and L. Berthier, *SciPost Phys.*, 2019, **7**, 077.
[51] R. Zwanzig and R. D. Mountain, *J. Chem. Phys.*, 1965, **43**, 4464.
[52] C. Ruscher, A. N. Semenov, J. Baschnagel and J. Farago, *J. Chem. Phys.*, 2017, **146**, 144502.
[53] J. L. Lebowitz, J. K. Percus and L. Verlet, *Phys. Rev.*, 1967, **153**, 250.
[54] J. F. Lutsko, *J. Appl. Phys.*, 1989, **65**, 2991.
[55] I. Procaccia, C. Rainone, C. A. B. Z. Shor and M. Singh, *Phys. Rev. E*, 2016, **93**, 063003.
[56] M. D. Ediger, *J. Chem. Phys.*, 2017, **147**, 210901.

FIGURE CAPTIONS

FIG. 1. Number density ρ of the pLJ model at normal pressure $P = 2$ as a function of temperature T. The old data (open circles) from ref. [9], obtained from a continuous cooling process using local MC moves only (quench method SC-MC), reveal two distinct linear slopes which were used to determine a glass transition temperature $T_g \approx 0.26$. The data obtained with the SC-MD method with cooling rate $\Gamma = 10^{-5}$ (filled rhombs) show a similar behavior. Using in addition swap moves (quench method Sw-MC or Sw-MD) much higher densities have been achieved (boxes) below T_g.

FIG. 2. The radial distribution functions $g(r)$ for $T = 0.4$, 0.325, 0.26, 0.19, 0.16, 0.15 (from bottom to top: the curves are shifted vertically with step 0.5 for clarity). Black curves correspond to configurations equilibrated by particle swaps (method Sw-MD); color curves (blue, brown, magenta, blue, red, magenta) to systems prepared by slow cooling with MD (method SC-MD).

FIG. 3. Configuration snapshots for $T = 0.10$, 0.15, 0.16, 0.2, 0.26 and 0.4 (from left to right) obtained with the Sw-MC equilibration method. The color code ranges from black (smallest beads) to red (largest beads). The configurations are homogeneous, isotropic and liquid-like above the demixing temperature $T_f \approx 0.16$. Below T_f we observe demixing (segregation) of beads of different diameters and, as a result, hexagonal clusters of alike beads. The main part of this work is focused on temperatures $T > T_f$. Note that even at $T = 0.2$ small clusters of particles of similar size are formed, but the system remains homogeneous and isotropic beyond the size of these clusters.

FIG. 4. (a) The static structure factor $S(q)$ for swap-equilibrated configurations (using method Sw-MD) at $T = 0.5$ (blue curve), 0.4 (black), 0.325 (red), 0.26 (brown), 0.19 (green), 0.16 (magenta). (b) The structure factor $S(q)$ for a broader range of temperatures obtained for swapped configurations (obtained with method Sw-MC) using only local MC moves for the production runs. Main panel: Double logarithmic representation. Inset: Linear representation focusing on wavevectors q around the first maximum.

FIG. 5. The particle MSD, $h_0(t)$, at different temperatures $T = 0.4$ (black curve), 0.35 (green), 0.3 (blue), 0.26 (magenta), 0.24 (black), 0.23 (red), 0.21 (brown); T decreases from top to bottom. The solid lines and crosses ($\times$) correspond to 'swapped' (Sw-MD) and slowly-cooled (SC-MD) configurations, respectively. At $T > T_g$ both data sets overlap completely. The straight dashed line indicates the slope corresponding to Fickian diffusion ($h_0 \propto t$).

FIG. 6. (a) Temperature dependence of the affine modulus μ_A for the 'swapped' configurations obtained with method Sw-MD (black solid line) and for the 'cooled' systems, method SC-MD (red solid line). The brown dashed line is tangential to the black solid line at $T = 0.2 \div 0.3$. The vertical dashed lines indicate $T_f = 0.16$ and $T_g = 0.26$. For 'swapped' configurations $\mu_A = \mu_A^{\mathrm{or}*}$ was calculated as explained in section 4 and Appendix F. All the results are obtained with MD production runs. (b) The affine shear modulus $\mu_{A,bare}$ (triangles) and the rescaled second moment of the shear stress, $\mu_0 = (T/\rho)\, C_\sigma(0)$

(circles), obtained either using only local MC moves (open symbols) or also with additional particle swap moves during production runs (filled symbols). The two static averages are obtained using MC dynamics for systems equilibrated by both local and particle swap moves (method Sw-MC). We show here $\mu_{A,bare}$ without the impulsive correction $\Delta\mu_A \sim -0.3$ (cf. eq. (E2)) instead of $\mu_A = \mu_{A,bare} + \Delta\mu_A$.

FIG. 7. The shear relaxation modulus $G(t)$ for 'swapped' configurations (method Sw-MD) at $T = 0.4$, 0.35, 0.3, 0.28, 0.27, 0.26, 0.25, 0.24, 0.23, 0.22, 0.21, 0.19, 0.18, 0.17, 0.16, 0.15 (from bottom to top). The non-monotonic behavior of $G(t)$ at long times, $t \gtrsim \Delta t/2$ (at some temperatures) is a trivial effect of insufficient statistics.

FIG. 8. The shear relaxation modulus $G(t)$ for (a) $T = 0.4$, 0.35, 0.3, 0.28, 0.27, 0.26, 0.25, 0.24 (from bottom to top), (b) $T = 0.24$, 0.21, 0.17, 0.16 (from bottom to top). In both parts red curves correspond to 'cooled' configurations (obtained with method SC-MD), black curves to 'swapped' configurations (method Sw-MD).

FIG. 9. The log-log dependence of $kG(t)$ vs. t/τ_α for $T = 0.4$, 0.35, 0.3, 0.28, 0.27, 0.26, 0.25, 0.24, 0.23 (curves from right to left) for systems equilibrated with method Sw-MD (using particle swaps). The shift-factor $k = k(T)$ increases from 1 to 1.35 (at $T = 0.28$) and then decreases back to 1. The T-dependence of the terminal relaxation time $\tau_\alpha = \tau_\alpha(T)$ is shown by rhombs in Fig. 10.

FIG. 10. T-dependence of the α-relaxation time τ_α for 'cooled' (SC-MD, crosses) and 'swap-based' (Sw-MD, rhombs) configurations. The solid curve represents the fit with the VFT law, eq. (8). The horizontal line corresponds to the total sampling time $\Delta t = 10^5$. The vertical line indicates T_g.

FIG. 11. $G(t)$ for swap-equilibrated configurations based on stress-correlations obtained with MD (black curves for Sw-MD) and MC dynamics (red curves for Sw-MC [17]) for temperatures (a) $T = 0.4$, 0.35, 0.30; (b) $T = 0.3$, 0.28, 0.27, 0.26, 0.25, 0.24, 0.21, 0.20 (curves from bottom to top). The time for MC curves was set to $t = t_{MC}/k$, where t_{MC} is the number of MC time-steps and $k = k(T)$: $k(0.4) = 488$, $k(0.35) = 546$, $k(0.3) = 588$, $k(0.28) = 556$, $k(0.27) = 500$, $k(0.26) = 476$, $k(0.25) = 385$, and $k = 294$ for $T \leq 0.24$.

FIG. 12. Time dependence of the isothermic bulk compression relaxation modulus, $K_T(t)$, obtained using FDT relations as described in the text, for 'swapped' configurations (method Sw-MD) at $T = 0.4$, 0.35, 0.3, 0.28, 0.27, 0.26, 0.25, 0.24, 0.23, 0.22, 0.21, 0.19, 0.18, 0.17, 0.16, 0.15 (from bottom to top).

FIG. 13. Time dependence of the adiabatic bulk compression relaxation modulus, $K_A(t)$, obtained using the FDT relations as described in the text, for 'swapped' configurations (method Sw-MD) at $T = 0.4$, 0.35, 0.3, 0.27, 0.25, 0.23, 0.21, 0.19 (from bottom to top). Black curves are based on the 'exact' eq. (D7); red curves correspond to the approximation, eq. (A5).

FIG. 14. Time dependence of the adiabatic bulk compression relaxation modulus, $K_A(t)$, obtained using the FDT relation, eq. (D7), as described in the text, for 'swapped' configurations (method Sw-MD) at $T = 0.4$, 0.35, 0.3, 0.28, 0.27,

0.26, 0.25, 0.24, 0.23, 0.22, 0.21, 0.19, 0.18, 0.17, 0.16, 0.15 (from bottom to top).

FIG. 15. T-dependencies of standard deviations for the affine shear moduli: $\delta\mu_A^0$ (no orientational averaging, no pressure correction: red curve with rhombs), $\delta\mu_A^{\rm or}$ with orientational averaging (brown), $\delta\mu_A^*$ with pressure correction (blue), $\delta\mu_A^{\rm or*}$ with both orientational averaging and pressure correction (black). Vertical dashed lines indicate T_f and T_g.

FIG. 16. T-dependencies of: (a) The quasi-static modulus $\mu_{sf}^{\rm or*}$ (red curve) and fluctuation modulus $\mu_F^{\rm or*}$ (black) for the pLJ systems equilibrated by particle swaps (method Sw-MD). The vertical dashed lines show $T_f = 0.16$ and $T_g = 0.26$. (b) The standard deviations $\delta\mu_{sf}^*$ (red curve), $\delta\mu_F^*$ (brown), $\delta\mu_{sf}^{\rm or*}$ (blue), $\delta\mu_F^{\rm or*}$ (magenta) as a function of T together with $\delta\mu_F^{(G)}$ (black curve), the Gaussian approximation for $\delta\mu_F^*$. Note that $\delta\mu_{sf}^* \approx \delta\mu_F^*$ and $\delta\mu_{sf}^{\rm or*} \approx \delta\mu_F^{\rm or*}$ in the peak region. (c) The standard deviations $\delta\mu_F^0$ (red curve), $\delta\mu_{sf}^0$ (brown), $\delta\mu_F^*$ (black with 'x'), $\delta\mu_{sf}^*$ (blue), $\delta\mu_F^{(G)}$ (magenta), and $\delta\mu_A^0$ (black). In all the cases the sampling time is $\Delta t = 10^5$.

FIG. 17. Temperature dependencies of (quasi-)static compression moduli for systems prepared with method Sw-MD: the affine modulus $\eta_A = \eta_A^*$ (the upper black curve), its linear extrapolation from $T > T_f$ to $T < T_f$ (black with long dashes), the fluctuation modulus $\eta_F = \eta_F^*$ (magenta curve with '+'), the quasi-static moduli: $\eta_{sf} = \eta_{sf}^*$ (red curve), K_{vv} based on volume fluctuation formula, eq. (30) (blue curve), K_{Ts} (brown curve), K_{Te} (black with crosses), K_{As} (magenta), K_{Ae} (black with short dashes). Note that η_A^*, η_F^* and η_{sf}^* were calculated for the prescribed pressure ($= p_0$) using eq. (15) and the procedure to compensate for the mean pressure deviations among the independent configurations described in Appendix F. K_{Ts} and K_{As} correspond to long-time plateau levels of isothermic and adiabatic relaxation moduli, $K_T(t)$ and $K_A(t)$, respectively. K_{Te} and K_{Ae} are equilibrium moduli obtained by extrapolation to low temperatures ($T \lesssim T_g$) of the liquid branches of $K_{Ts}(T)$ and $K_{As}(T)$, respectively, as described in the text. The vertical dashed lines indicate T_f and T_g.

FIG. 18. Temperature dependencies of standard deviations of compression moduli (obtained using Sw-MD method): (a) $\delta\eta_A^*$ (blue curve), $\delta\eta_A^0$ (red), $\delta\eta_F^*$ (black), $\delta\eta_F^0$ (magenta with '×'), $\delta\eta_{sf}^0$ (brown with '+'). (b) $\delta\eta_F^*$ (black), $\delta\eta_F^{\rm (G)}$ (red), $\delta\eta_{sf}^*$ (blue), $\delta\eta_{sf}^0$ (brown with '+'), $\delta\eta_F^0$ (magenta with '×'). Vertical lines indicate T_f and T_g.

Fig. 1.

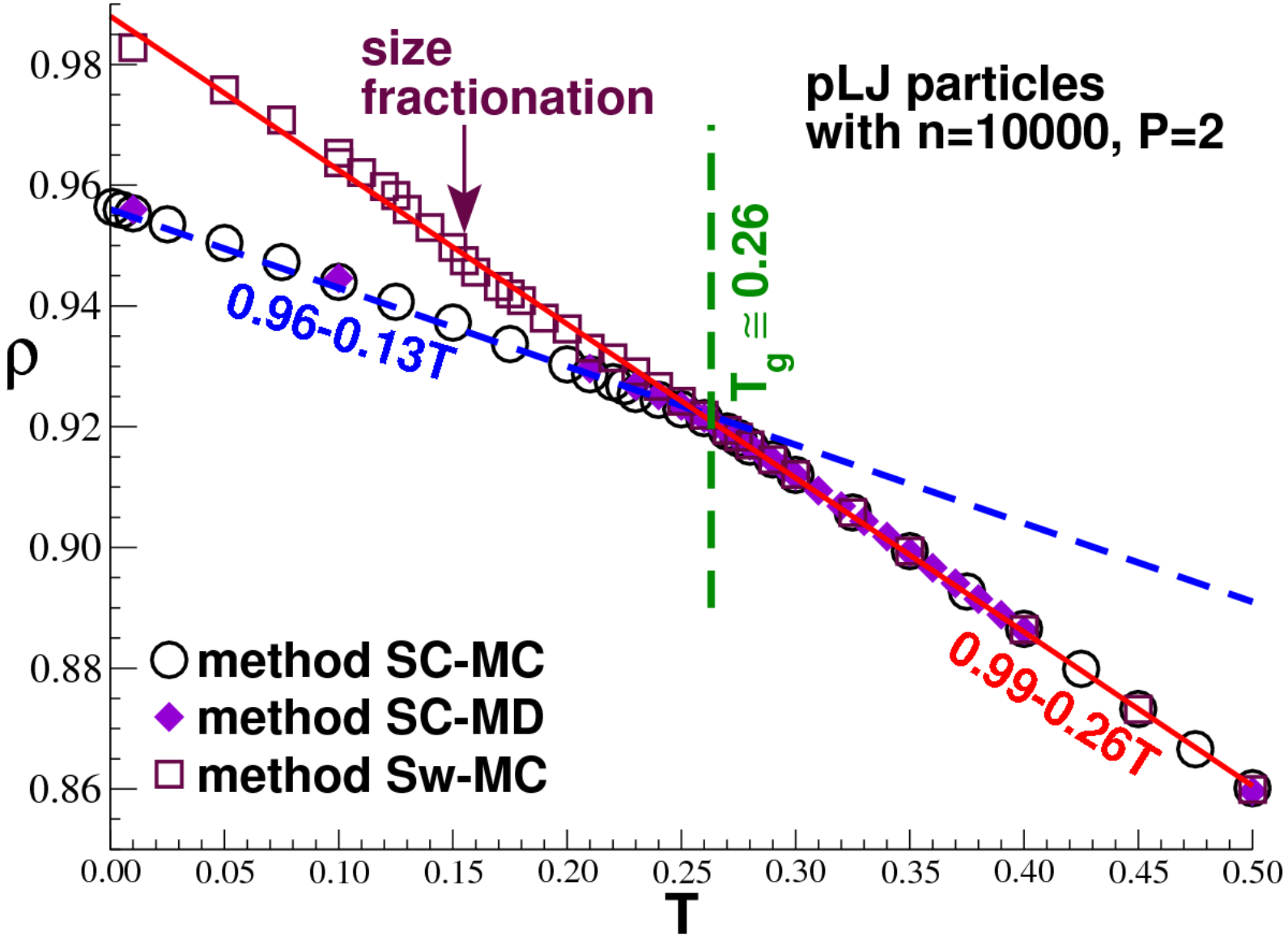
size
fractionation
pLJ particles
with n=10000, P=2
$T_g \approx 0.26$
0.96-0.13T
0.99-0.26T
method SC-MC
method SC-MD
method Sw-MC
ρ
T
0.98
0.96
0.94
0.92
0.90
0.88
0.86
0.00
0.05
0.10
0.15
0.20
0.25
0.30
0.35
0.40
0.45
0.50

Fig. 2.

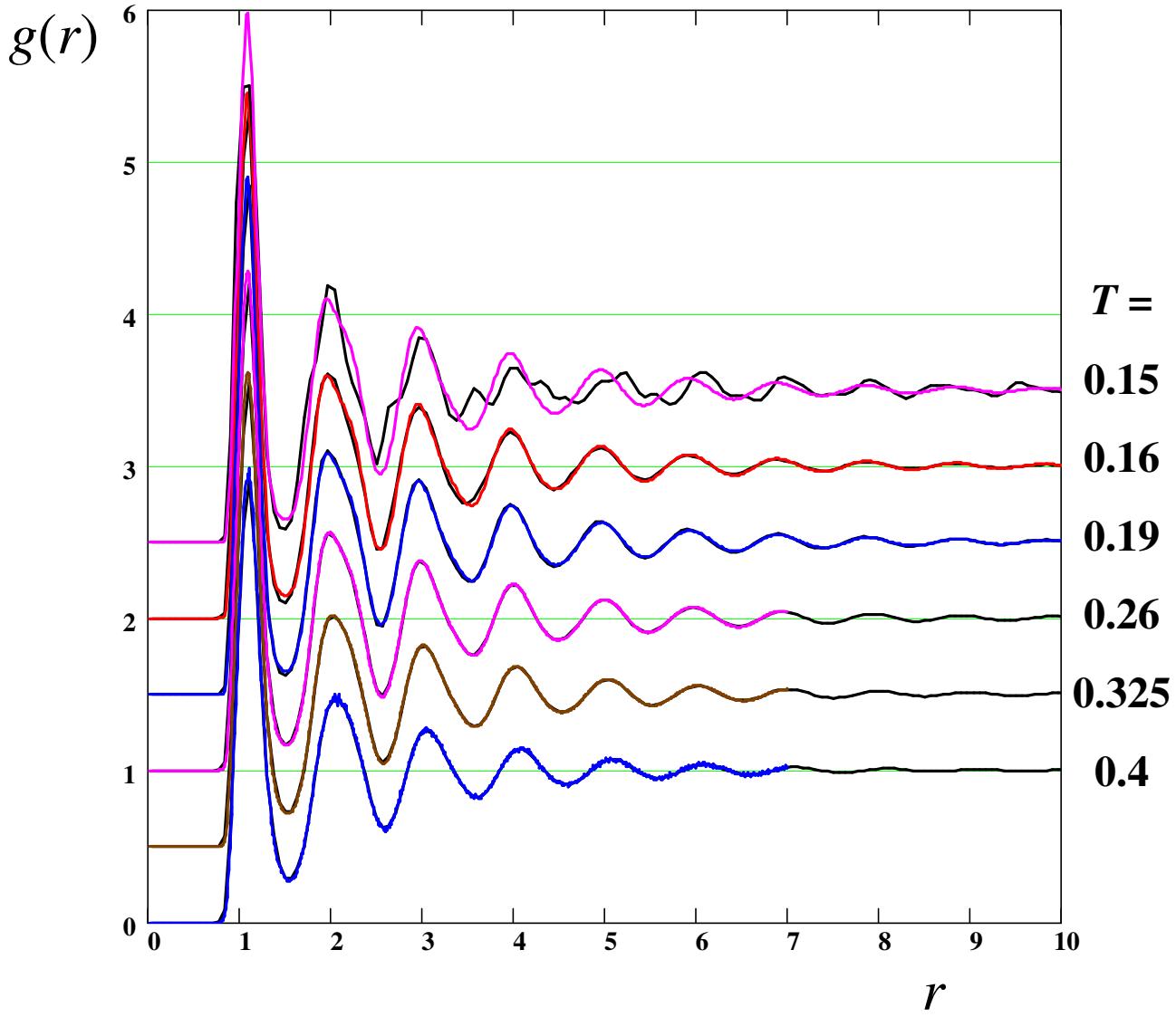

Fig. 3.

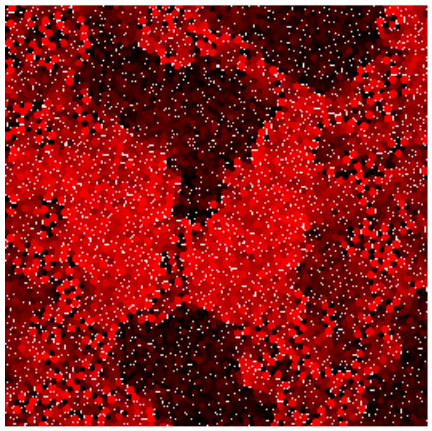

T=0.1

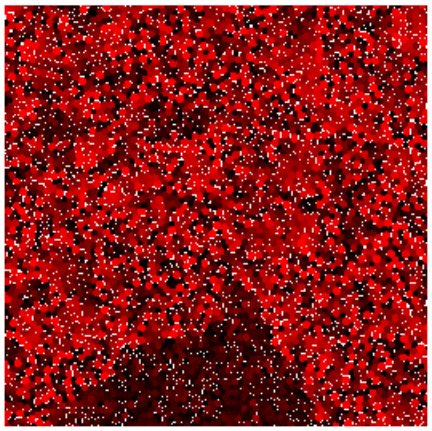

T=0.15

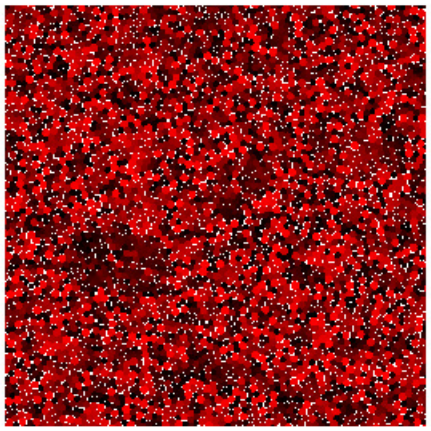

T=0.16

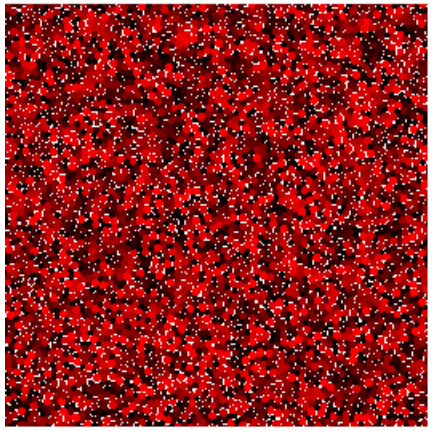

T=0.2

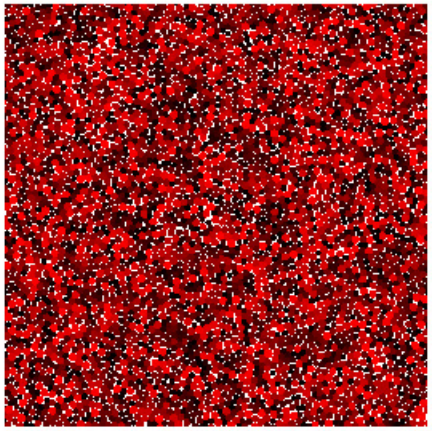

T=0.26

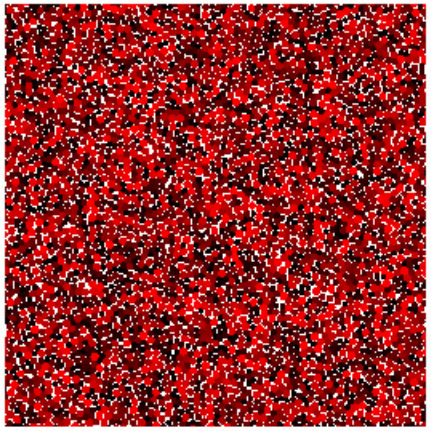

T=0.4

Fig. 4 (a).

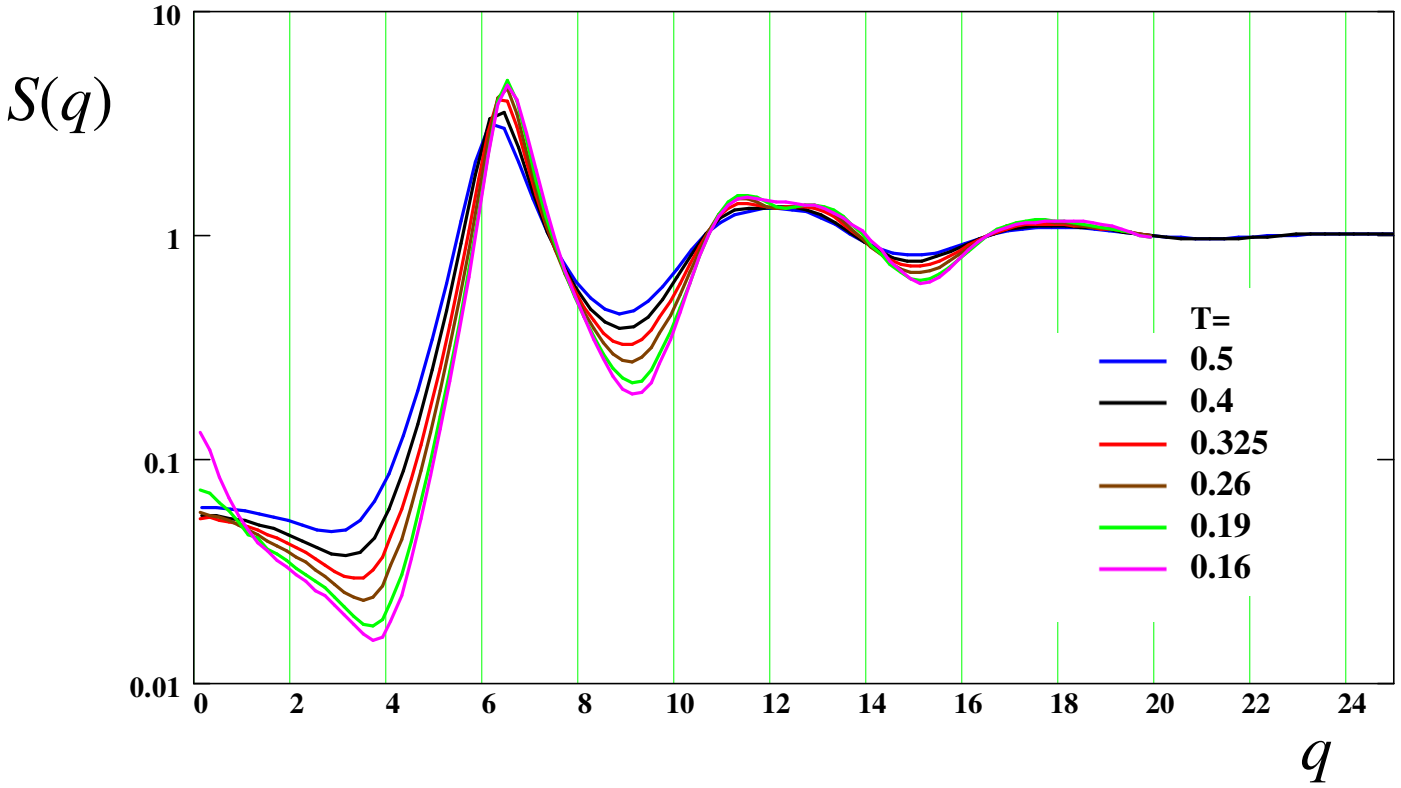
S(q)
10
1
0.1
0.01
0
2
4
6
8
10
12
14
16
18
20
22
24
q
T=
0.5
0.4
0.325
0.26
0.19
0.16

Fig. 4 (b).

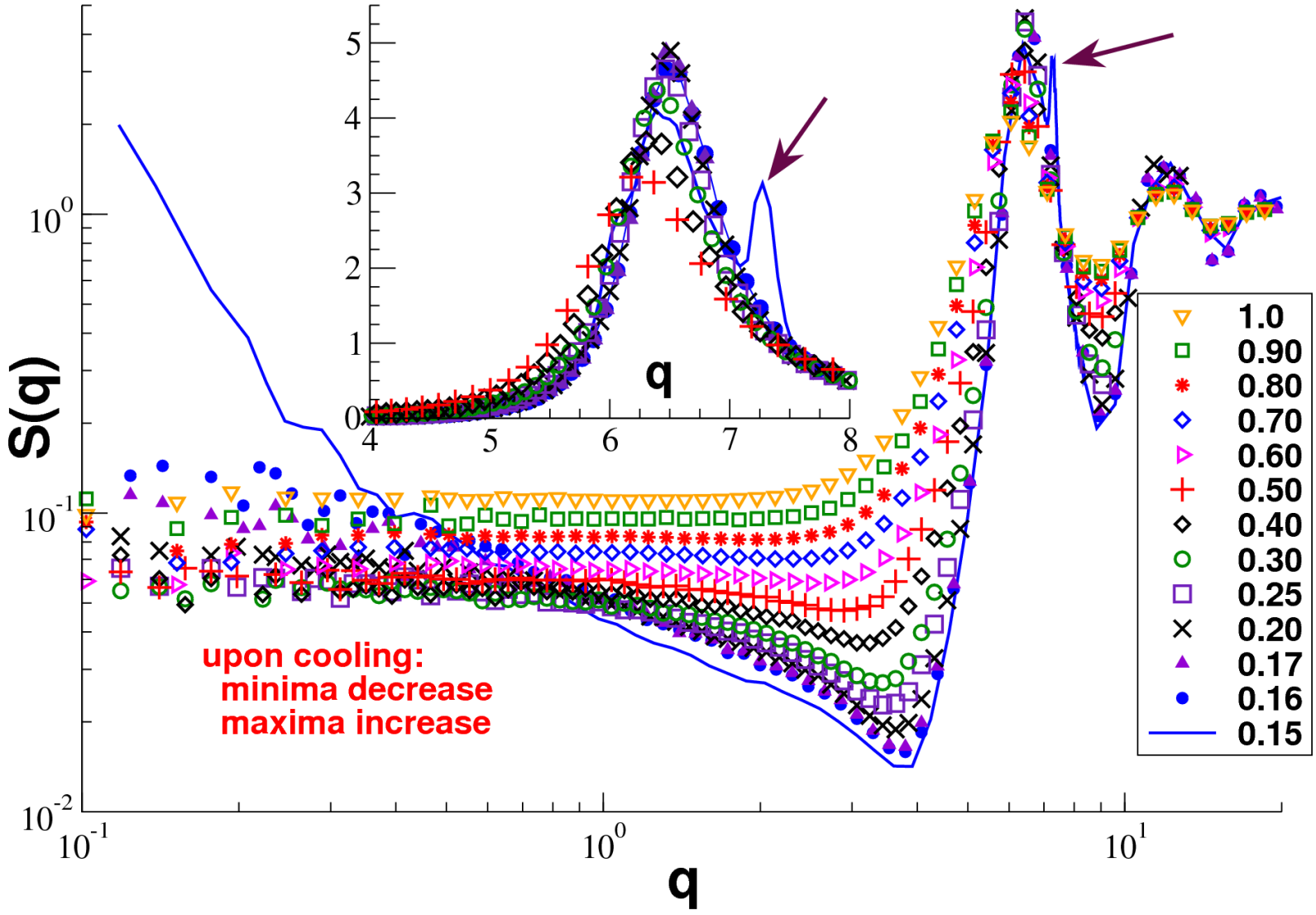
S(q)
q
upon cooling:
minima decrease
maxima increase
1.0
0.90
0.80
0.70
0.60
0.50
0.40
0.30
0.25
0.20
0.17
0.16
0.15

Fig. 5.

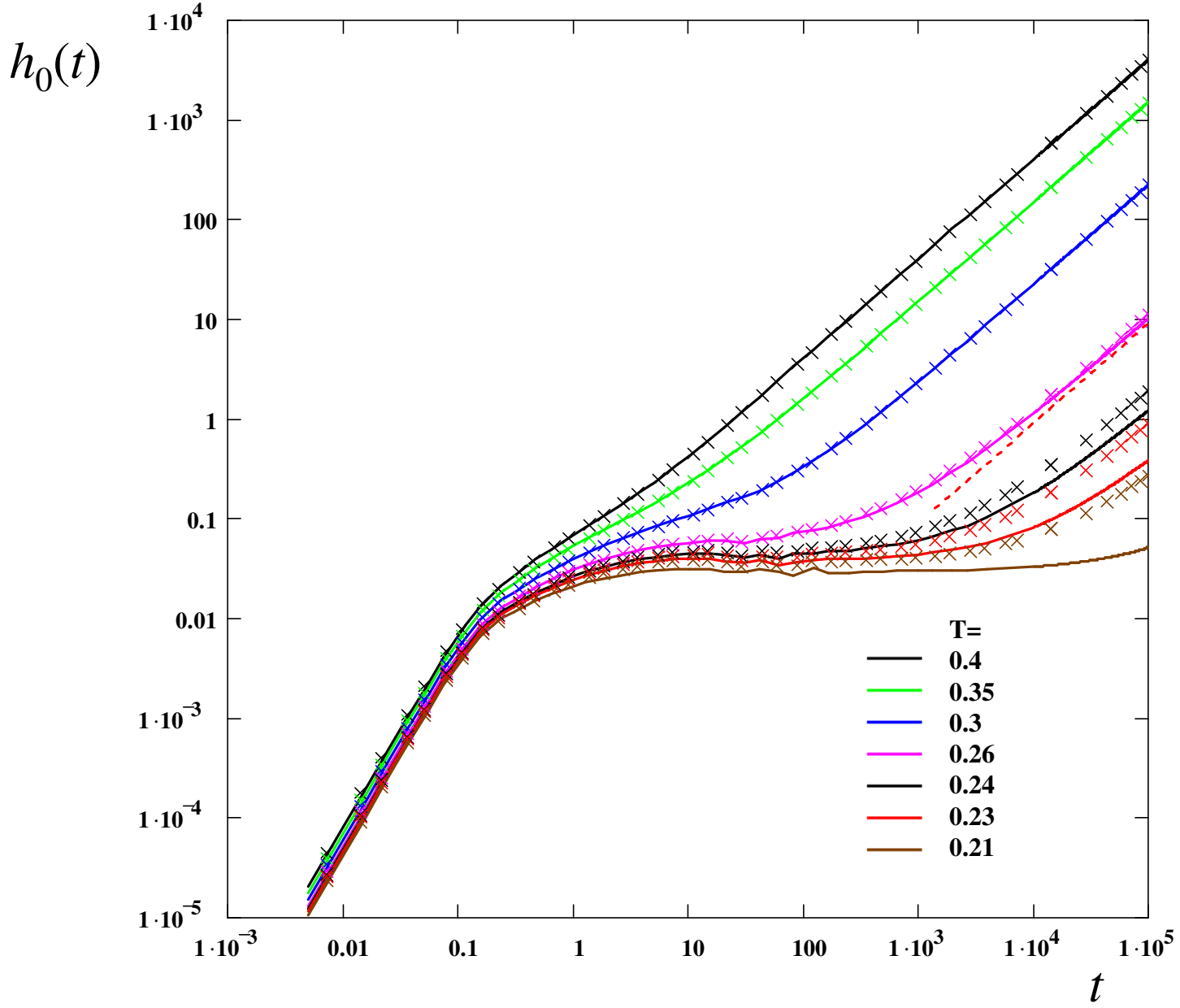
$h_0(t)$
$1\cdot10^{4}$
$1\cdot10^{3}$
100
10
1
0.1
0.01
$1\cdot10^{-3}$
$1\cdot10^{-4}$
$1\cdot10^{-5}$
$1\cdot10^{-3}$
0.01
0.1
1
10
100
$1\cdot10^{3}$
$1\cdot10^{4}$
$1\cdot10^{5}$
t
T=
0.4
0.35
0.3
0.26
0.24
0.23
0.21

Fig. 6 (a).

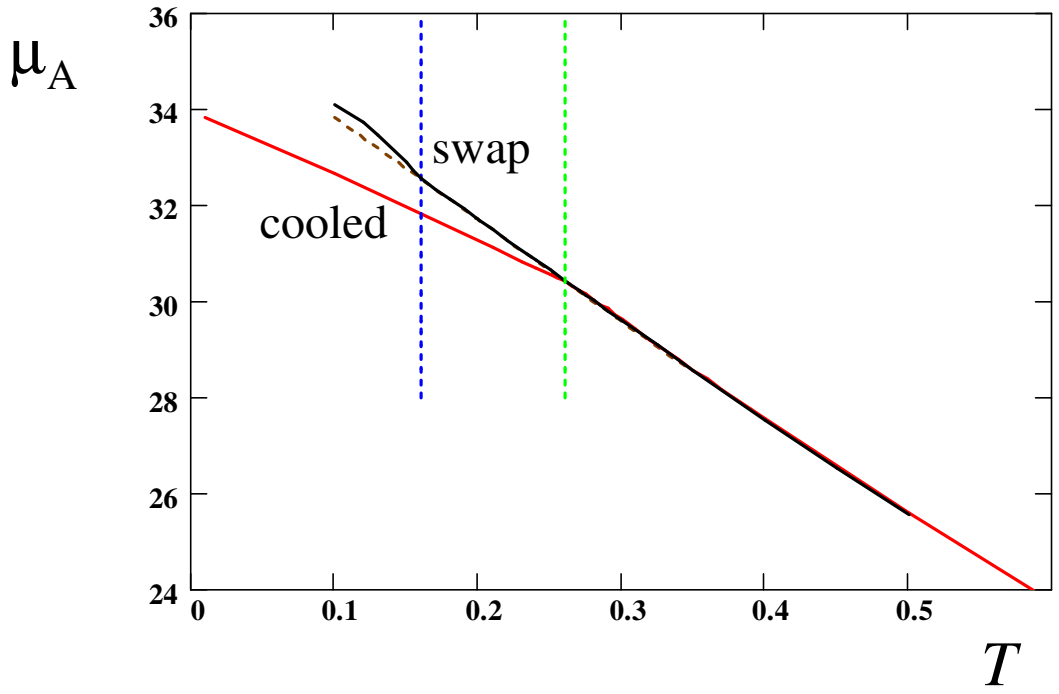

Fig. 6 (b).

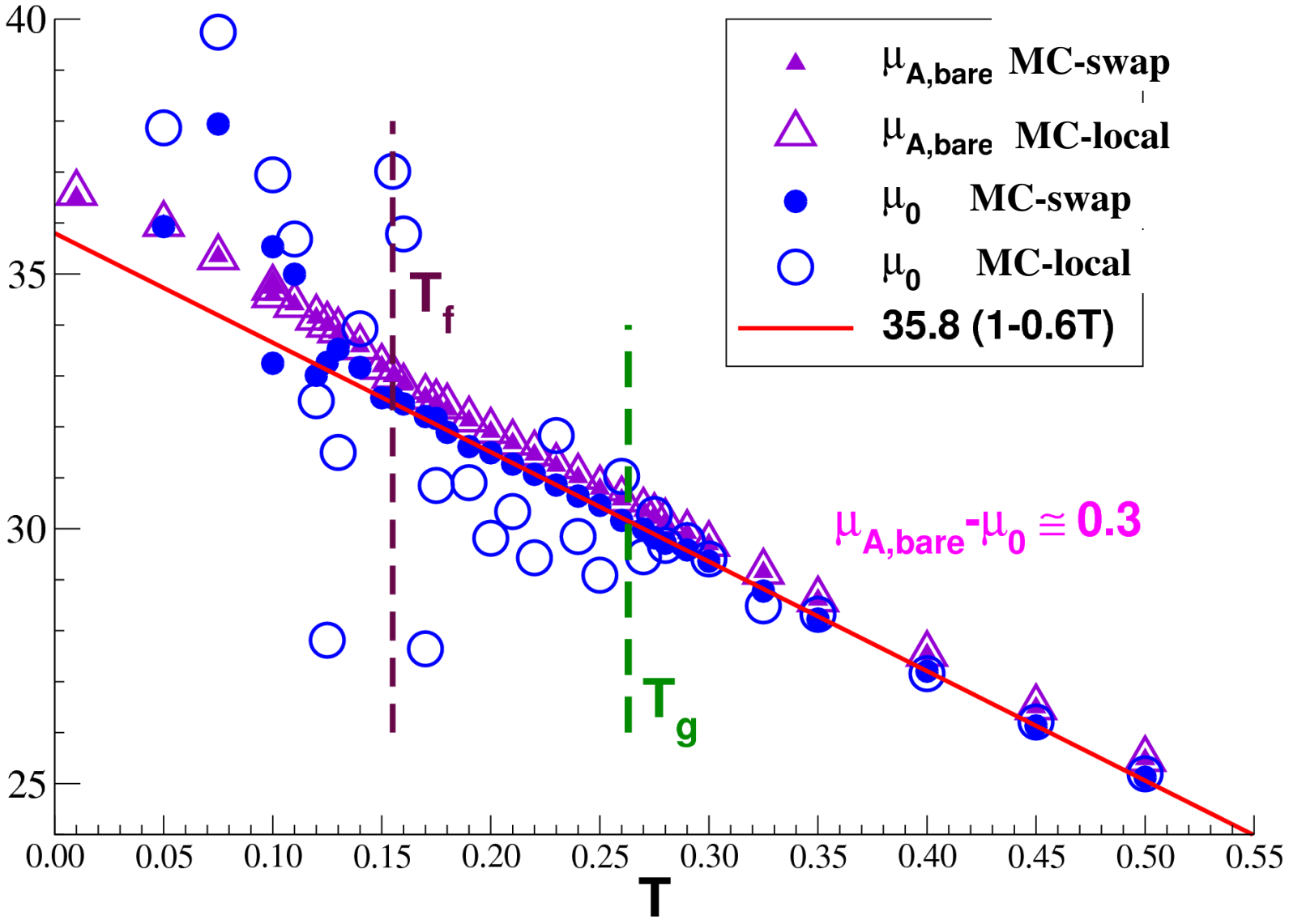
40
35
30
25
0.00
0.05
0.10
0.15
0.20
0.25
0.30
0.35
0.40
0.45
0.50
0.55
T
T_f
T_g
$\mu_{A,bare}$ MC-swap
$\mu_{A,bare}$ MC-local
μ_0 MC-swap
μ_0 MC-local
35.8 (1-0.6T)
$\mu_{A,bare}-\mu_0 \cong 0.3$

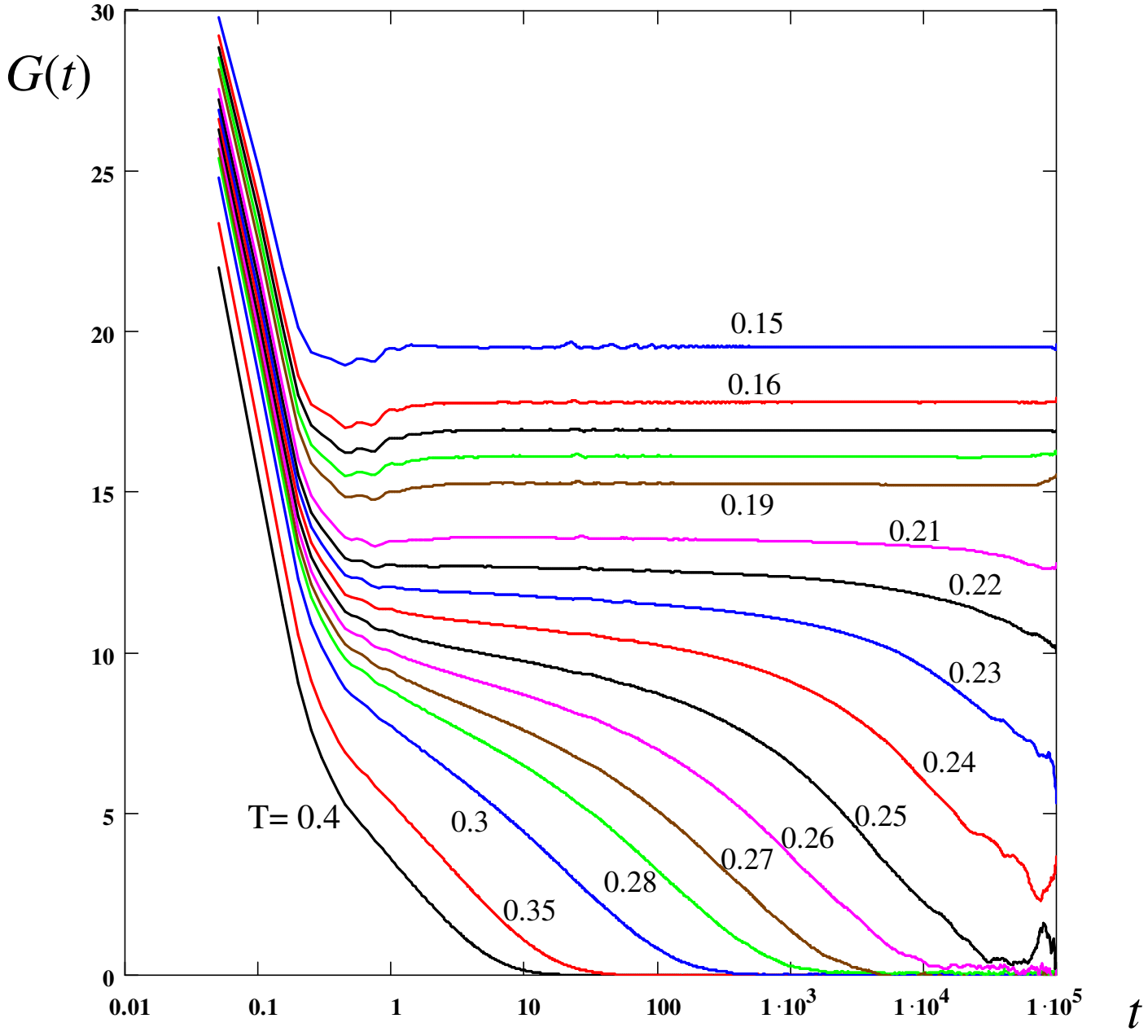
G(t)
30
25
20
15
10
5
0
0.01
0.1
1
10
100
1·10^3
1·10^4
1·10^5
t
0.15
0.16
0.19
0.21
0.22
0.23
0.24
0.25
0.26
0.27
0.28
0.3
0.35
T= 0.4

Fig. 7.

Fig. 8 (a).

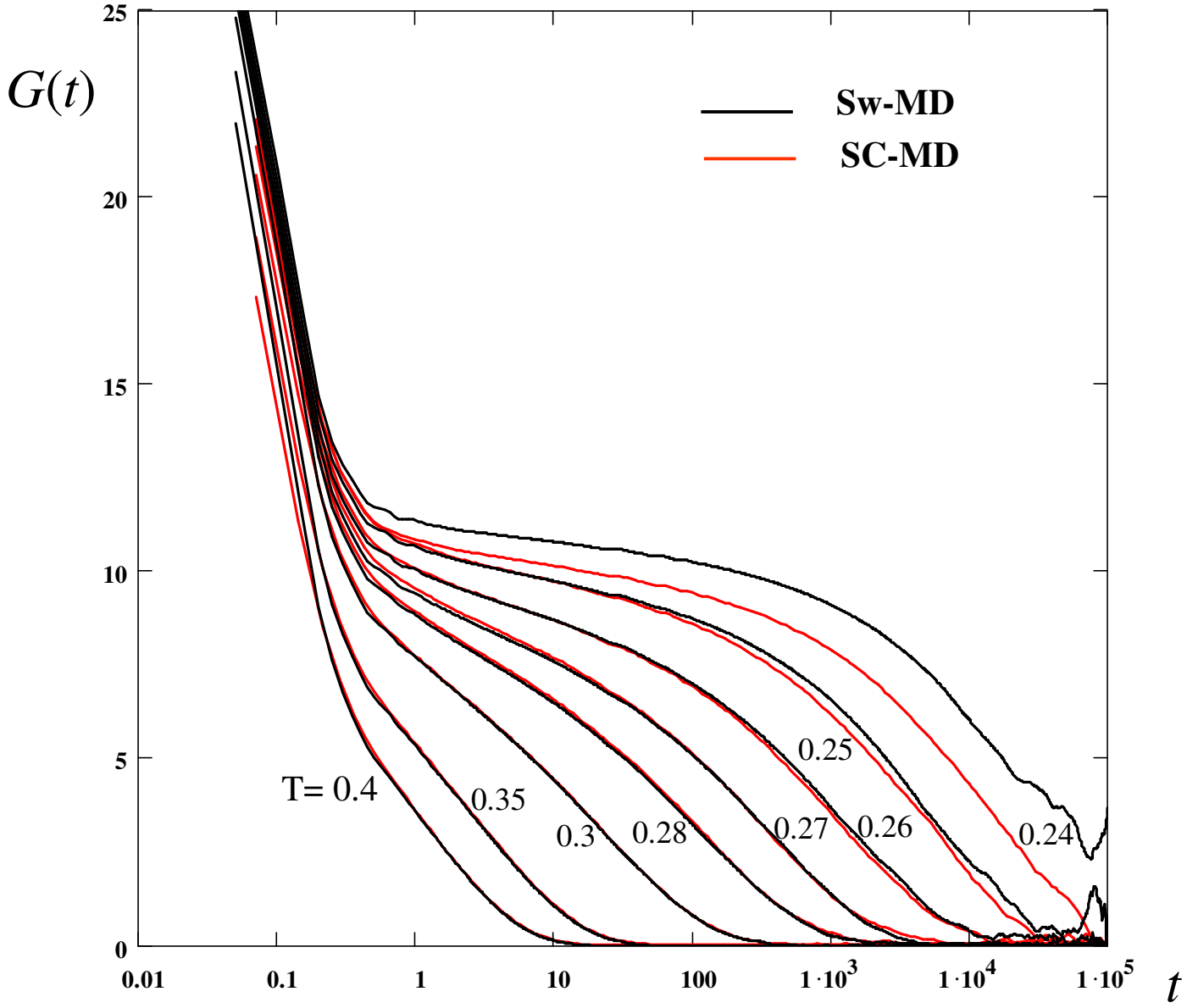
G(t)
Sw-MD
SC-MD
T= 0.4
0.35
0.3
0.28
0.27
0.26
0.25
0.24
25
20
15
10
5
0
0.01
0.1
1
10
100
1·10^3
1·10^4
1·10^5
t

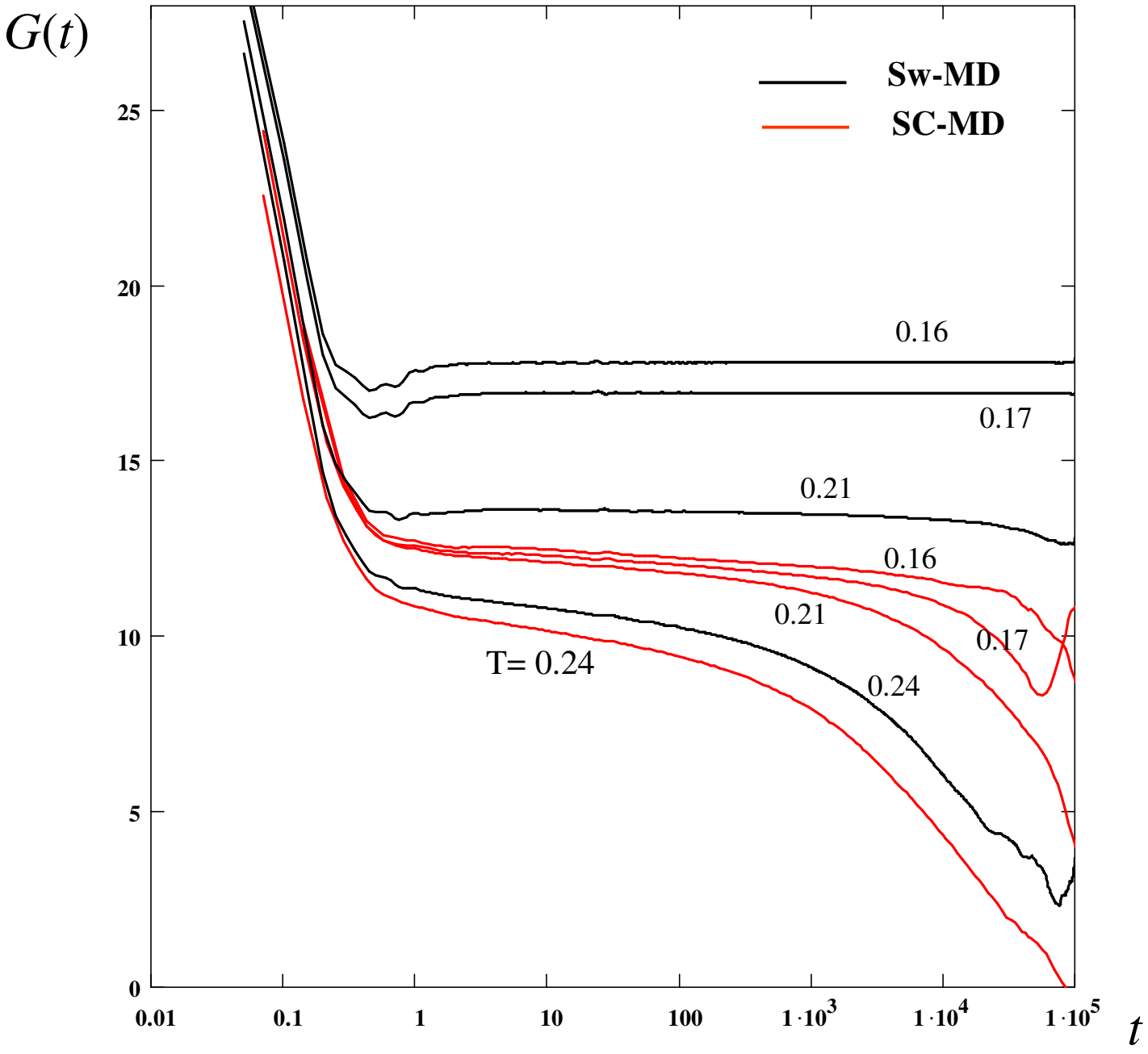
G(t)
Sw-MD
SC-MD
0.16
0.17
0.21
0.16
0.21
0.17
T= 0.24
0.24
25
20
15
10
5
0
0.01
0.1
1
10
100
1·10^3
1·10^4
1·10^5
t

Fig. 8 (b).

Fig. 9.

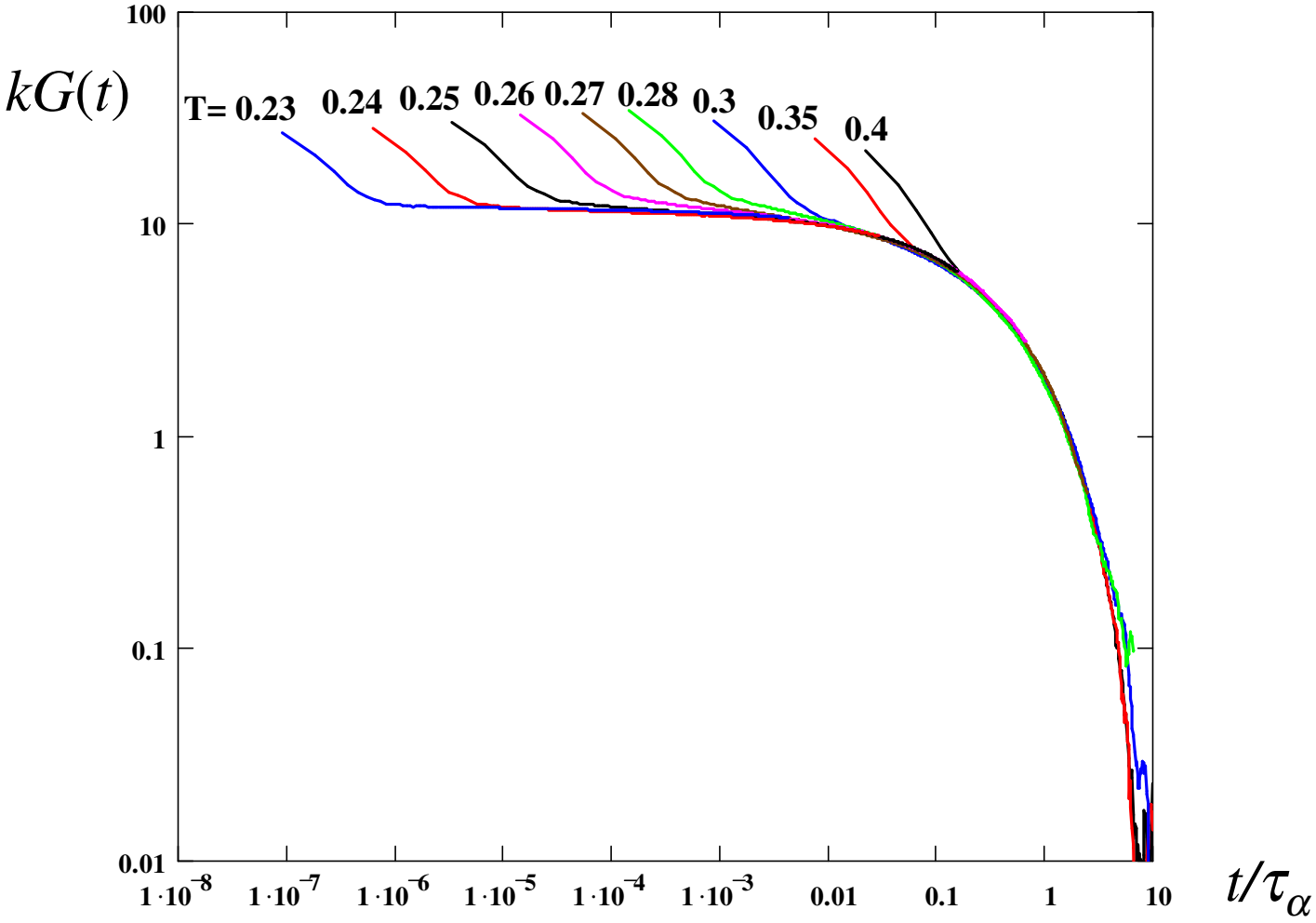
100
10
1
0.1
0.01
kG(t)
T= 0.23
0.24
0.25
0.26
0.27
0.28
0.3
0.35
0.4
1·10^-8
1·10^-7
1·10^-6
1·10^-5
1·10^-4
1·10^-3
0.01
0.1
1
10
t/τ_α

Fig. 10.

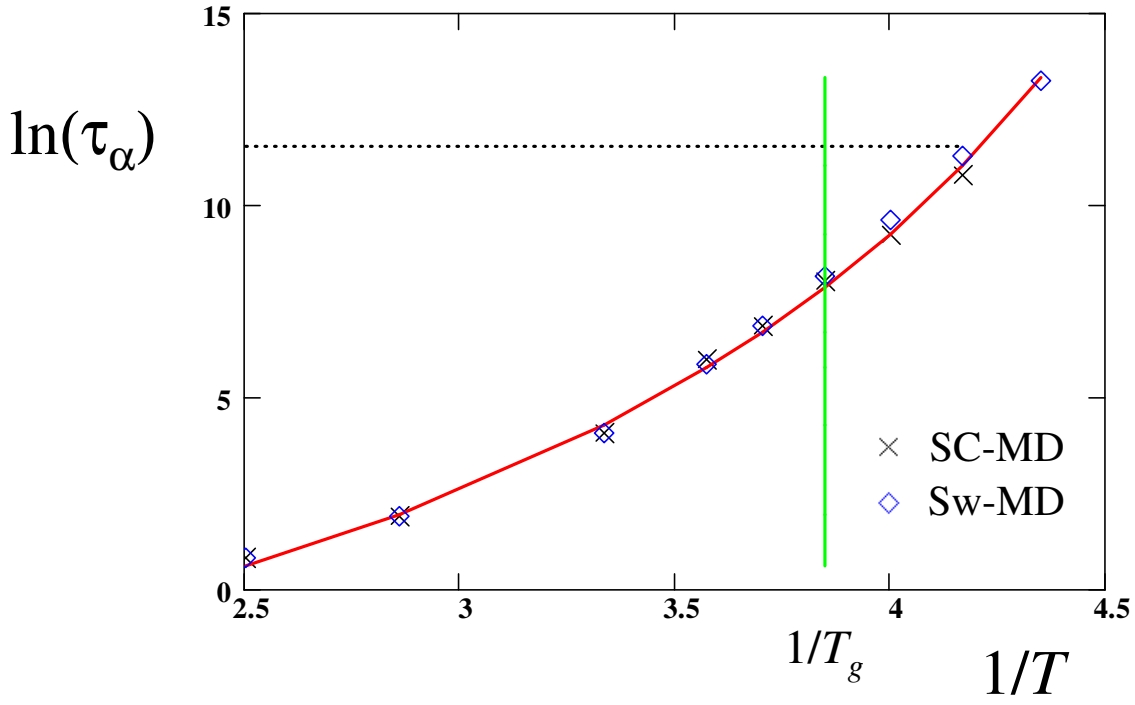

Fig. 11 (a).

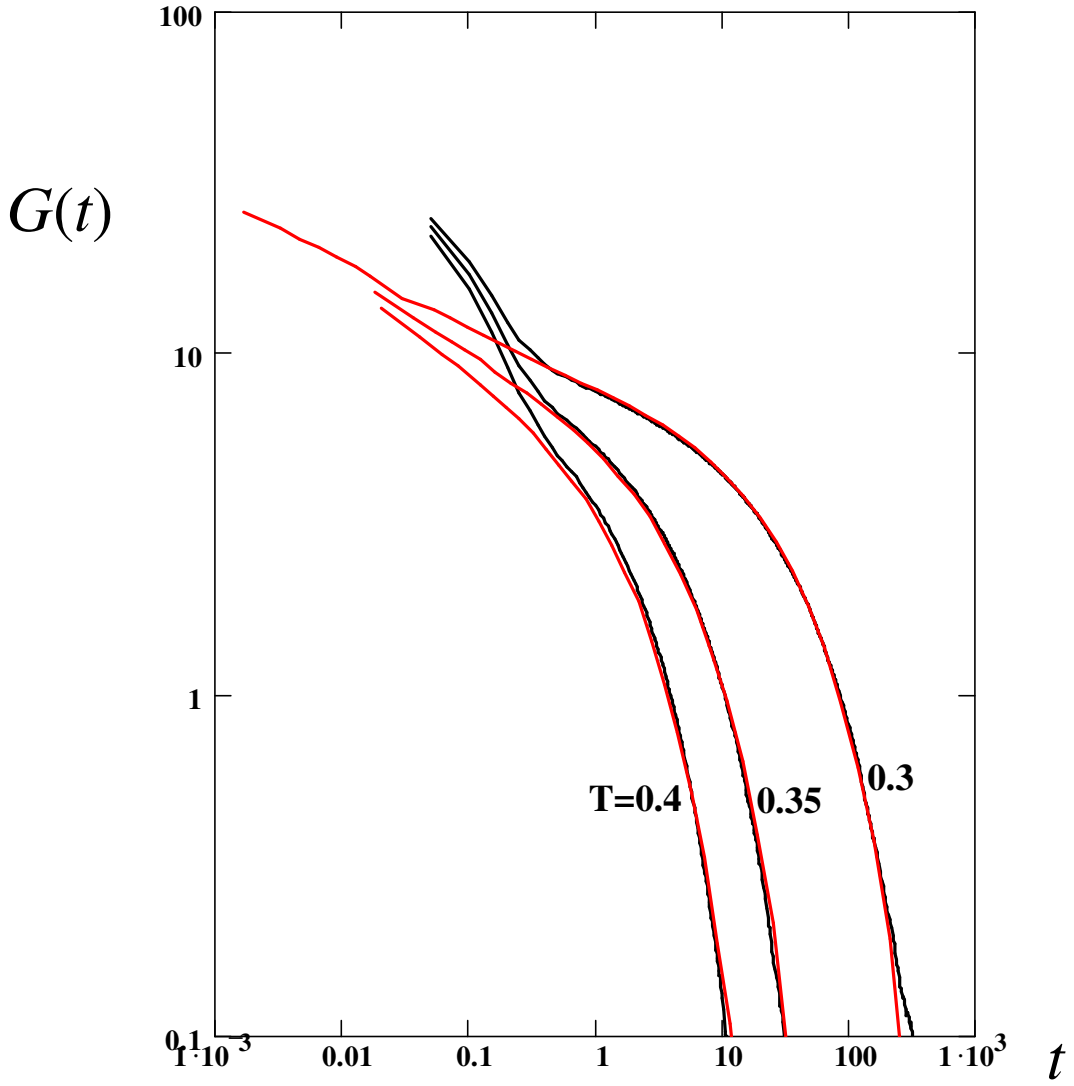

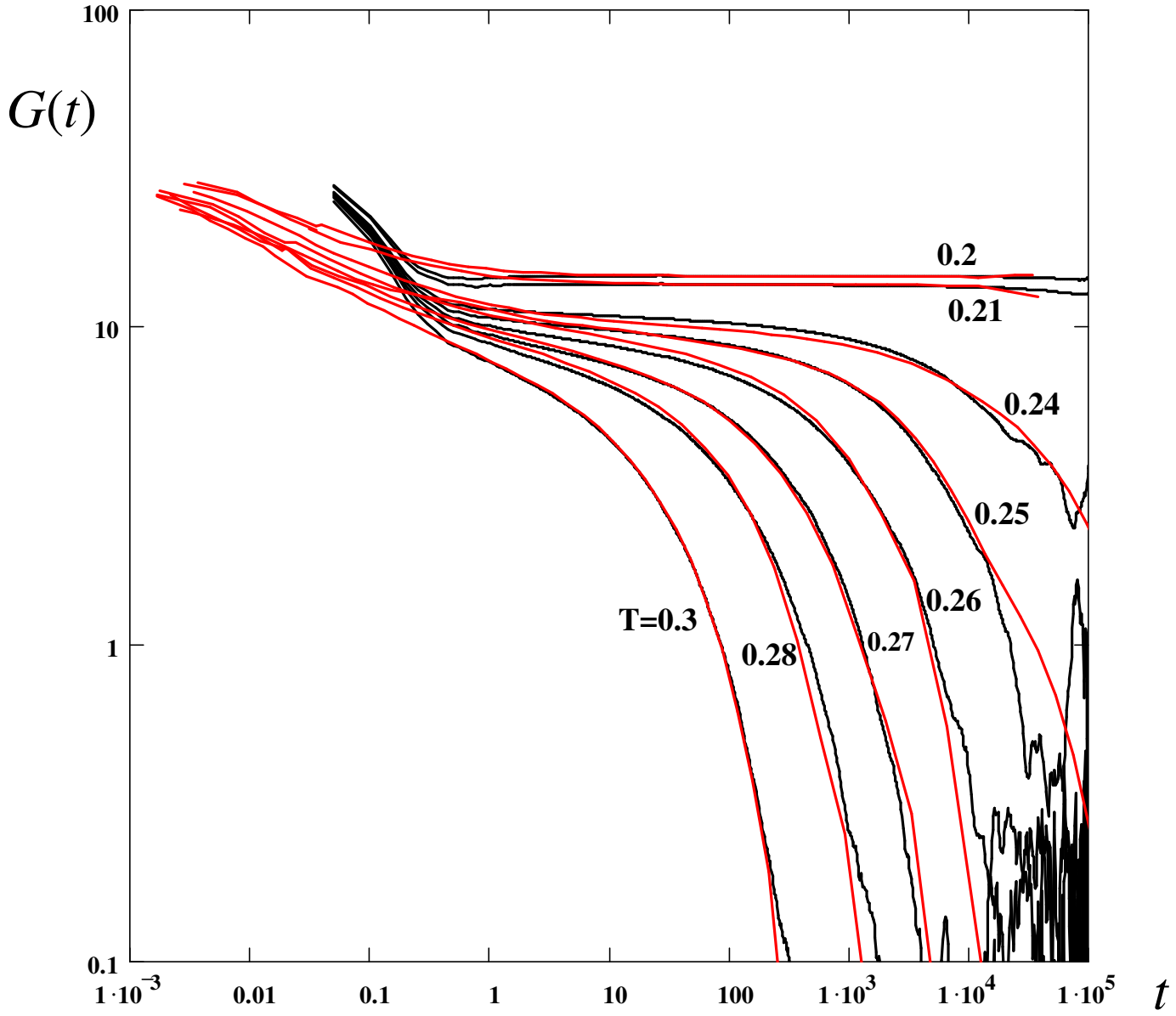
100
10
1
0.1
G(t)
1·10^-3
0.01
0.1
1
10
100
1·10^3
1·10^4
1·10^5
t
0.2
0.21
0.24
0.25
0.26
0.27
0.28
T=0.3

Fig. 11 (b).

Fig. 12.

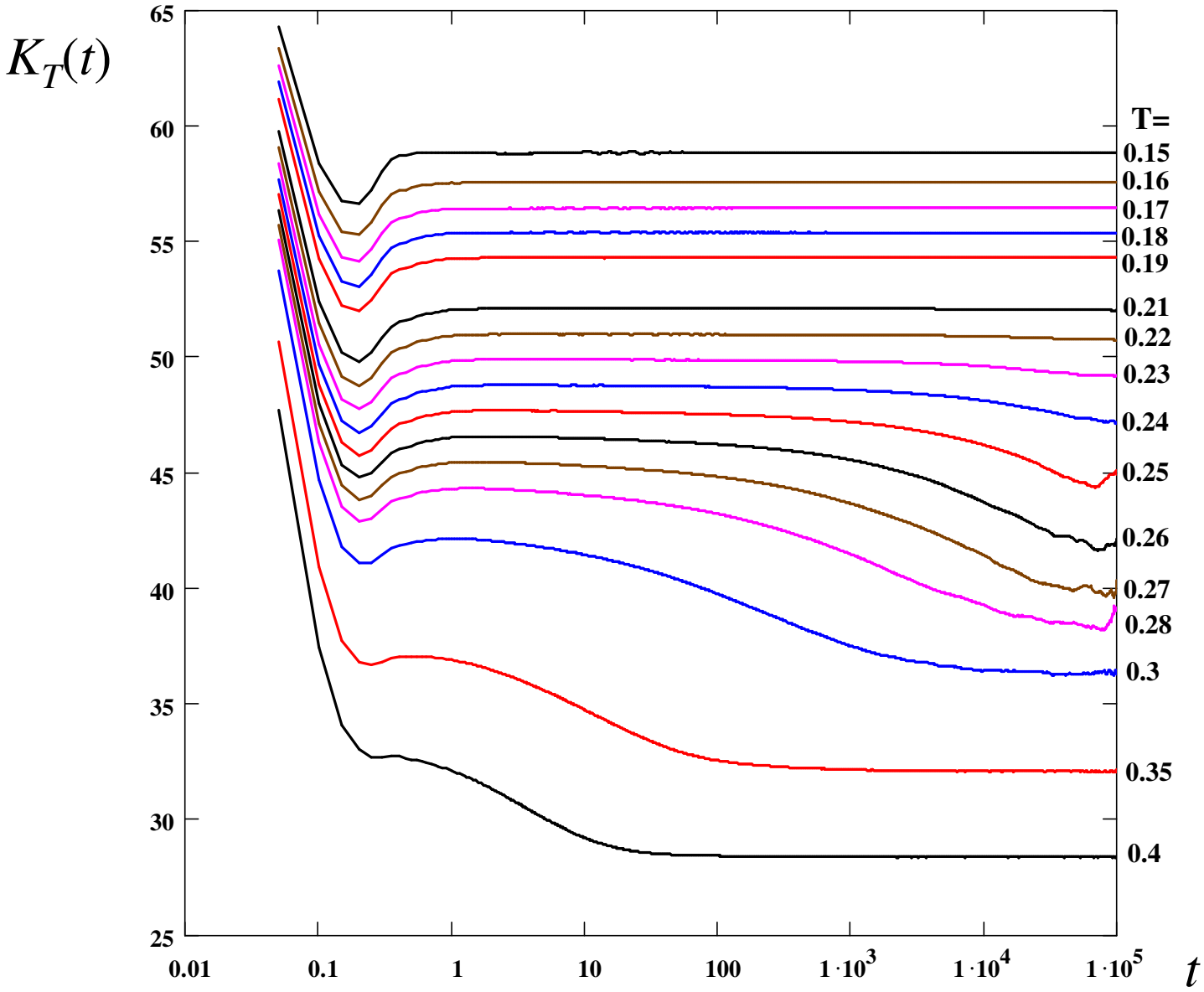
$K_T(t)$
65
60
55
50
45
40
35
30
25
0.01
0.1
1
10
100
$1 \cdot 10^3$
$1 \cdot 10^4$
$1 \cdot 10^5$
t
T=
0.15
0.16
0.17
0.18
0.19
0.21
0.22
0.23
0.24
0.25
0.26
0.27
0.28
0.3
0.35
0.4

Fig. 13.

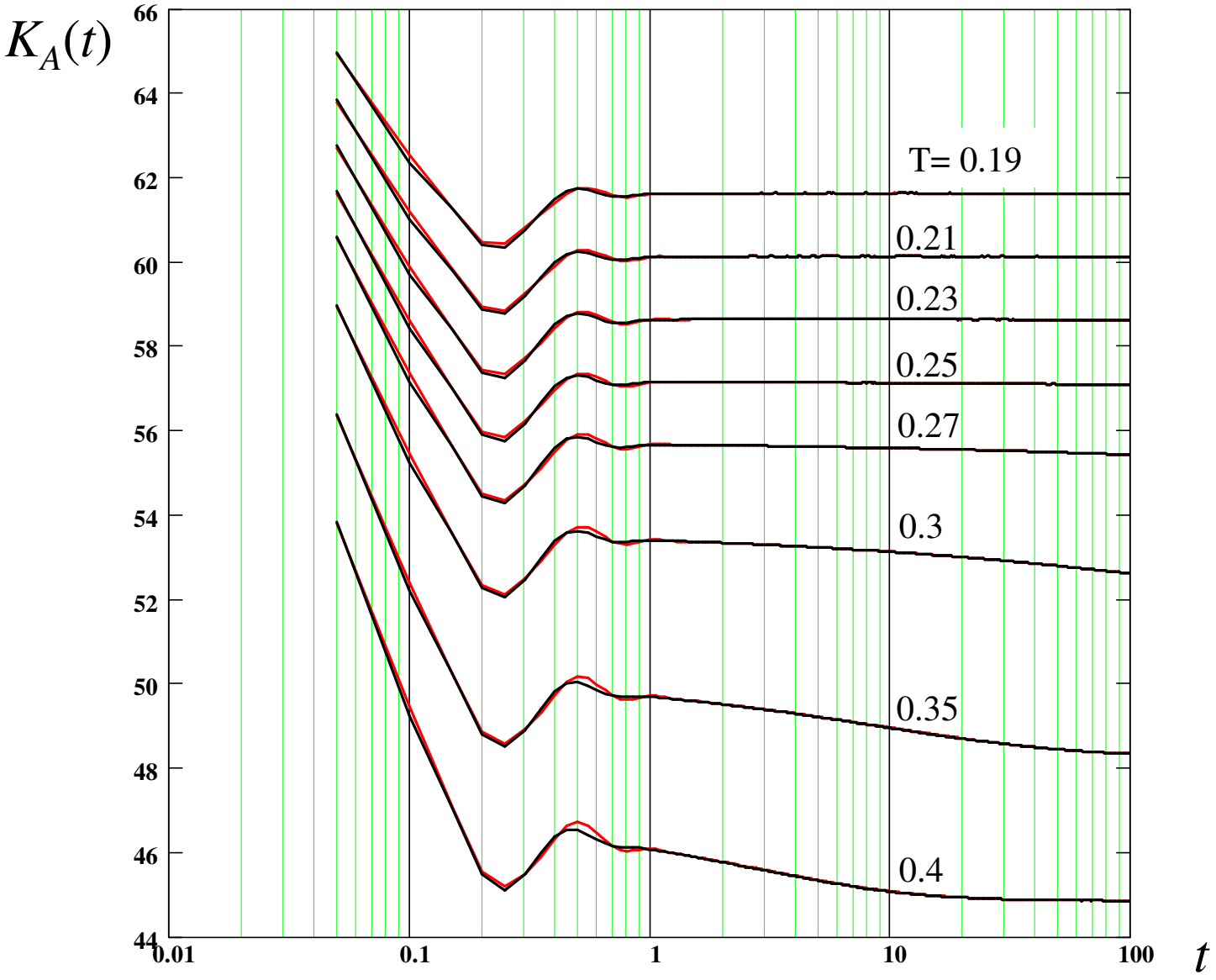
$K_A(t)$
66
64
62
60
58
56
54
52
50
48
46
44
0.01
0.1
1
10
100
t
T= 0.19
0.21
0.23
0.25
0.27
0.3
0.35
0.4

Fig. 14.

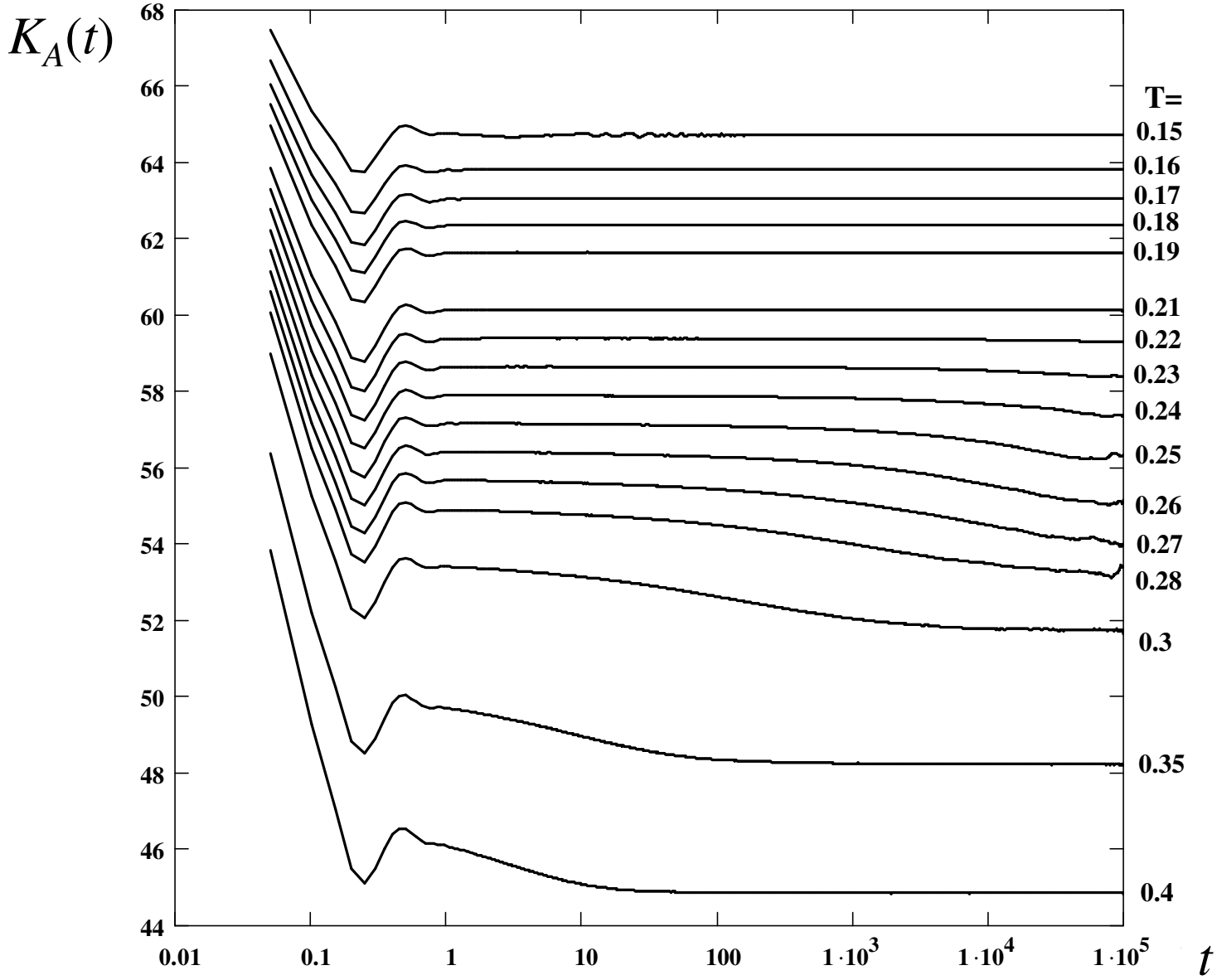
$K_A(t)$
68
66
64
62
60
58
56
54
52
50
48
46
44
0.01
0.1
1
10
100
$1 \cdot 10^3$
$1 \cdot 10^4$
$1 \cdot 10^5$
t
T=
0.15
0.16
0.17
0.18
0.19
0.21
0.22
0.23
0.24
0.25
0.26
0.27
0.28
0.3
0.35
0.4

Fig. 15.

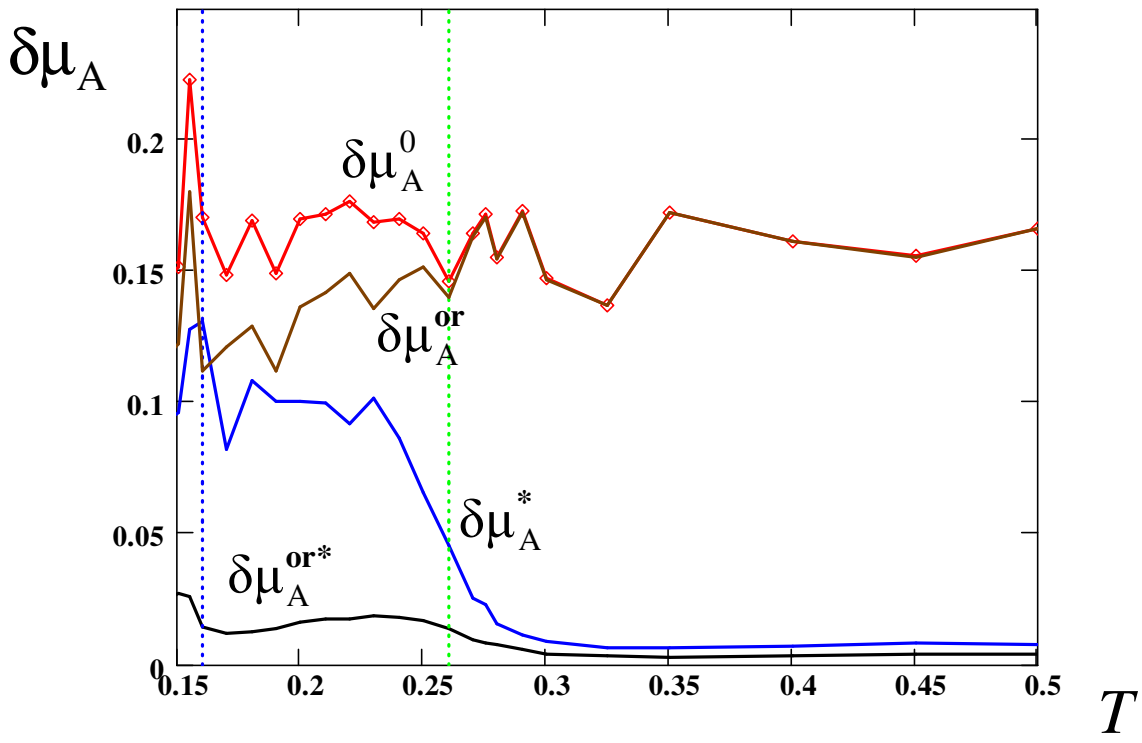
δμA
0.2
0.15
0.1
0.05
0
0.15
0.2
0.25
0.3
0.35
0.4
0.45
0.5
T
δμA0
δμAor
δμA*
δμAor*

Fig. 16 (a).

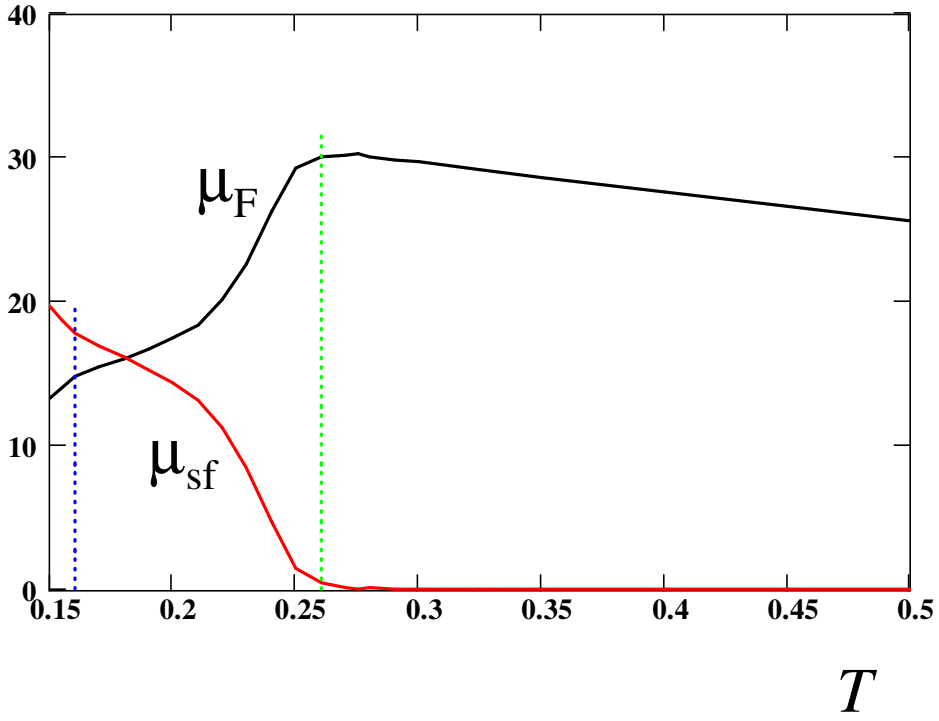

Fig. 16 (b).

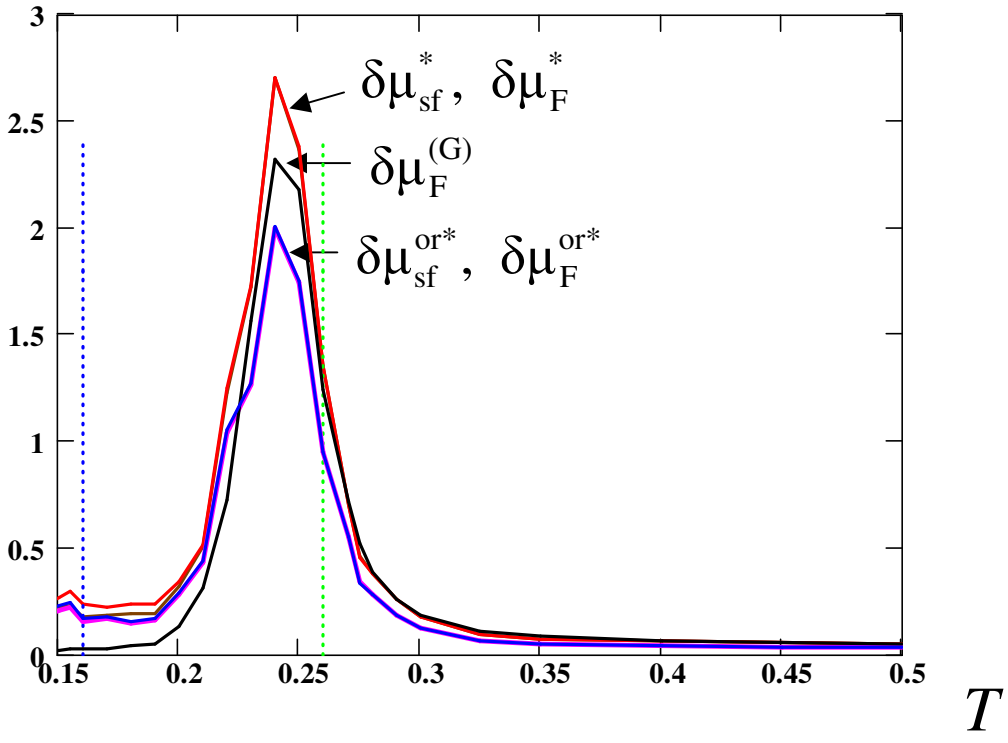
3
2.5
2
1.5
1
0.5
0
0.15
0.2
0.25
0.3
0.35
0.4
0.45
0.5
$\delta\mu_{sf}^{*}$, $\delta\mu_{F}^{*}$
$\delta\mu_{F}^{(G)}$
$\delta\mu_{sf}^{or*}$, $\delta\mu_{F}^{or*}$
T

Fig. 16 (c).

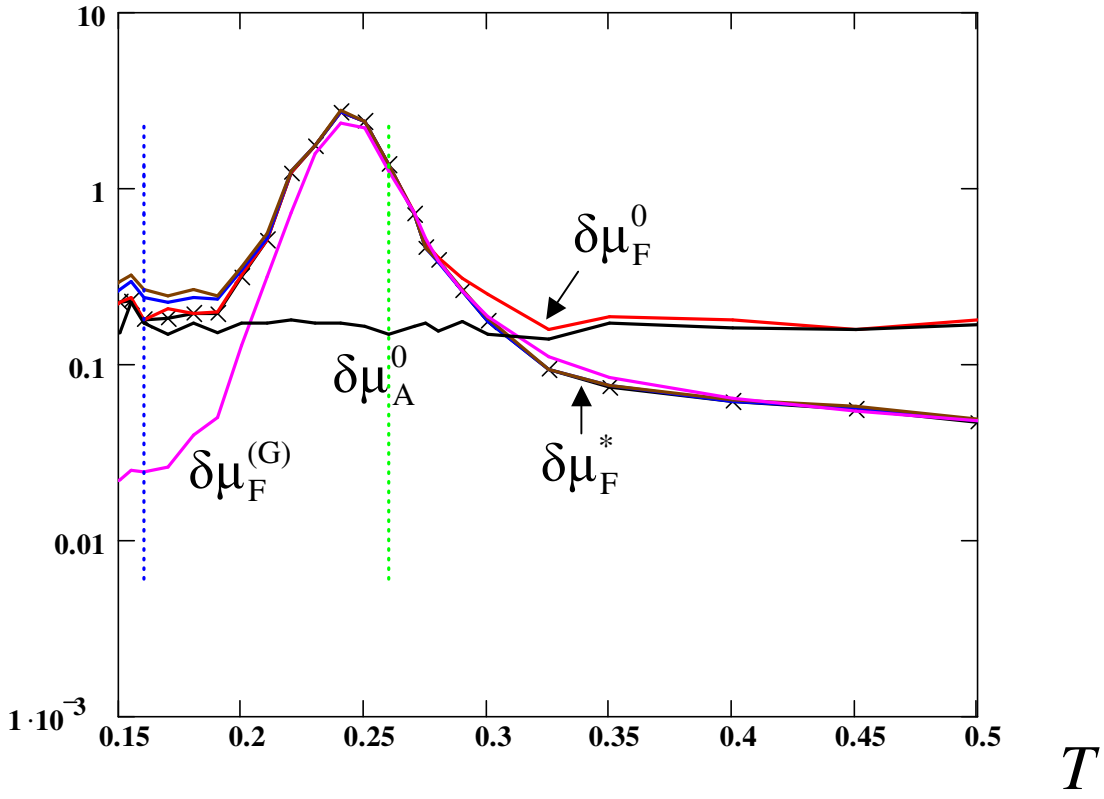

Fig. 17.

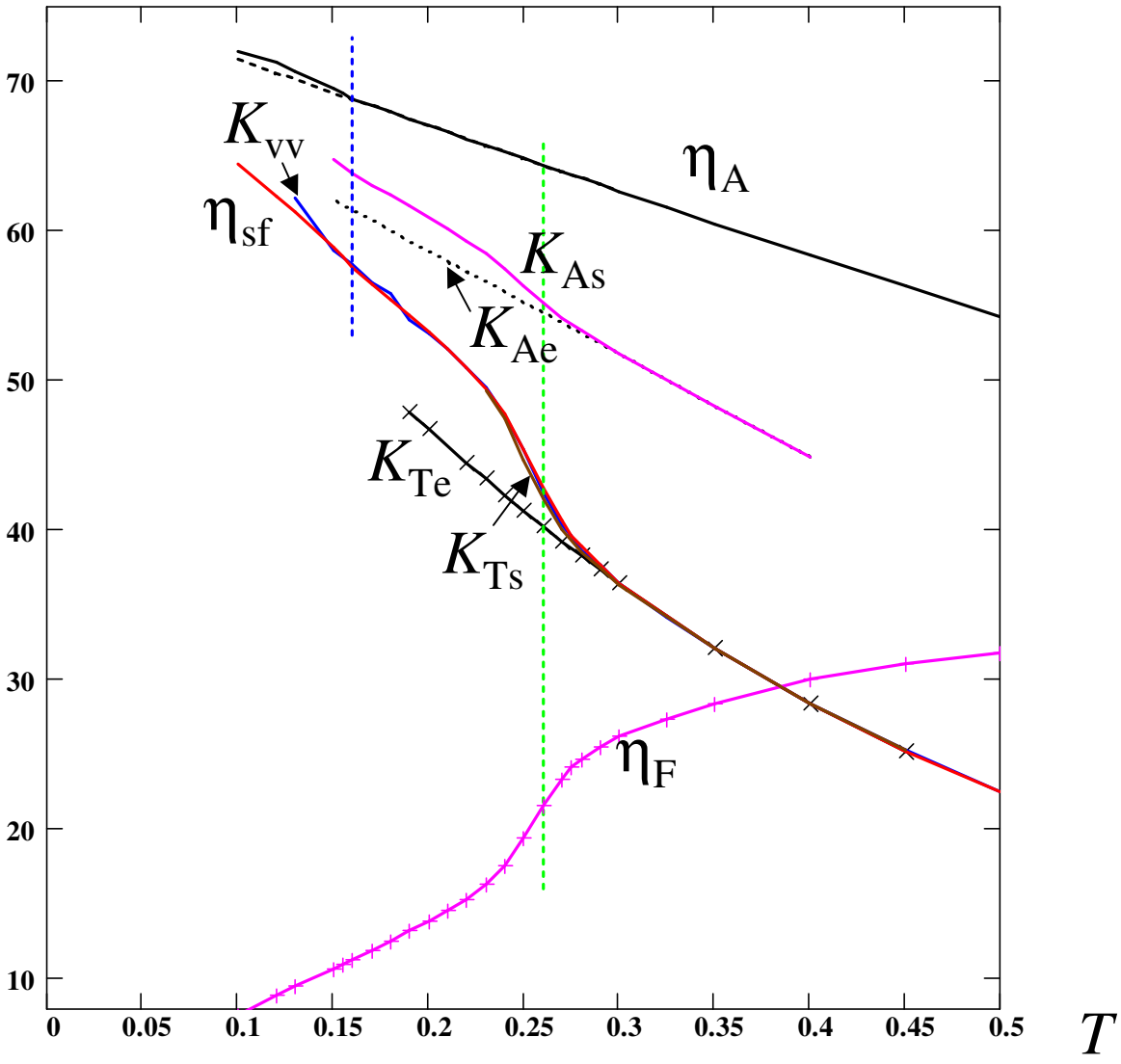
70
60
50
40
30
20
10
0
0.05
0.1
0.15
0.2
0.25
0.3
0.35
0.4
0.45
0.5
T
K_{vv}
η_{sf}
η_A
K_{As}
K_{Ae}
K_{Te}
K_{Ts}
η_F

Fig. 18 (a).

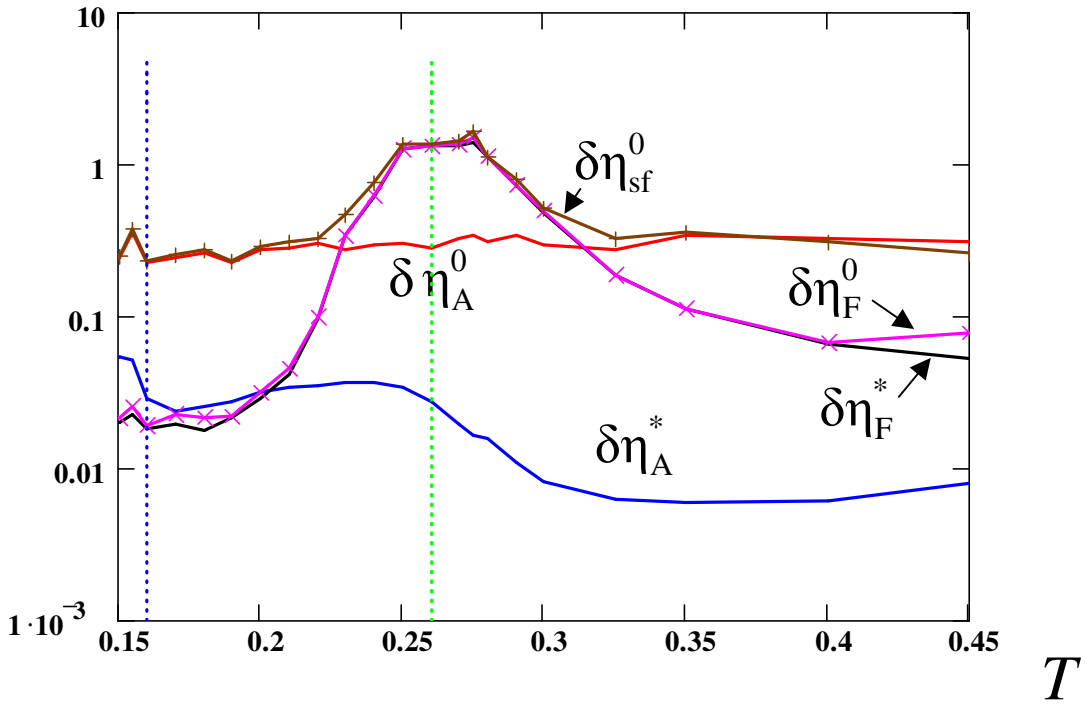
10
1
0.1
0.01
1·10^-3
0.15
0.2
0.25
0.3
0.35
0.4
0.45
T
δη^0_sf
δη^0_A
δη^0_F
δη^*_F
δη^*_A

Fig. 18 (b).

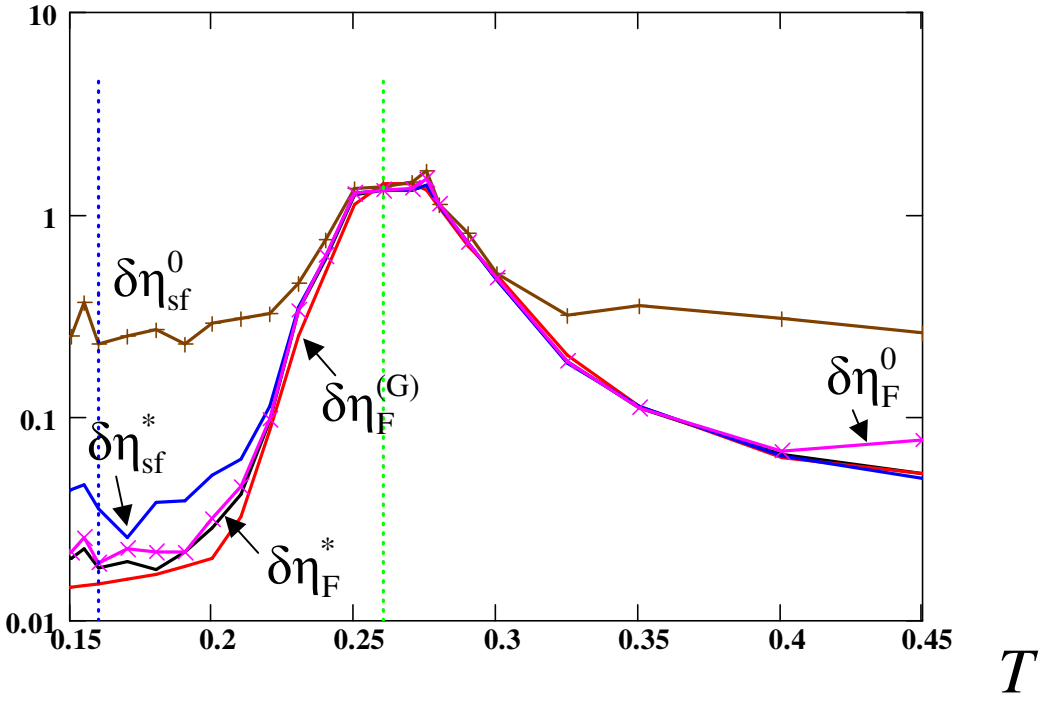
10
1
0.1
0.01
0.15
0.2
0.25
0.3
0.35
0.4
0.45
$\delta\eta_{sf}^{0}$
$\delta\eta_{F}^{(G)}$
$\delta\eta_{F}^{0}$
$\delta\eta_{sf}^{*}$
$\delta\eta_{F}^{*}$
T